AD-A121 970 DEVELOPMENT OF AN AUTOMATED GEAR TOOTH CONTOUR MEASURING DEVICE(U) AERODYNE RESEARCH INC BILLERICA MA A R OUELLETTE 12 APR 82 DAAK50-81-C-0022 1/2

UNCLASSIFIED F/G 13/9 NL

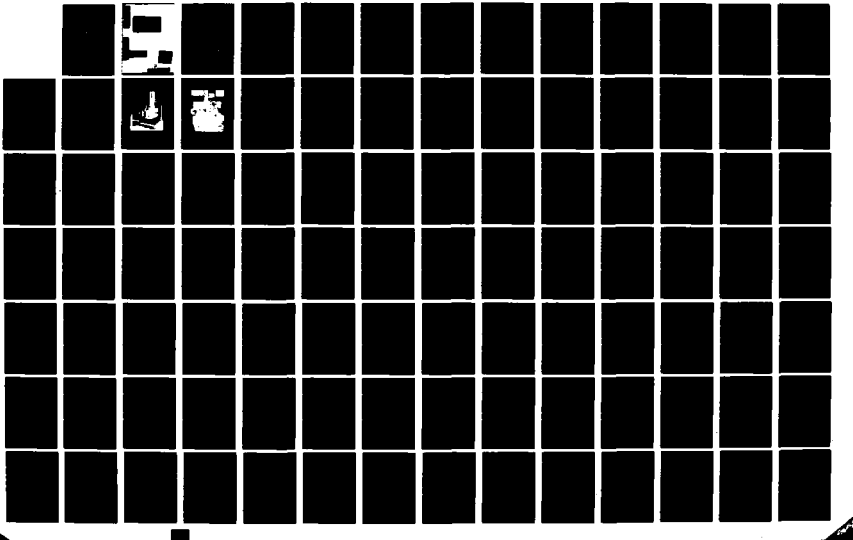

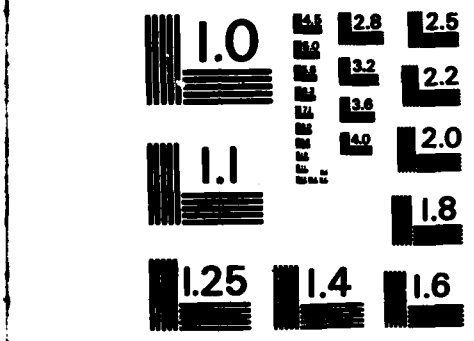

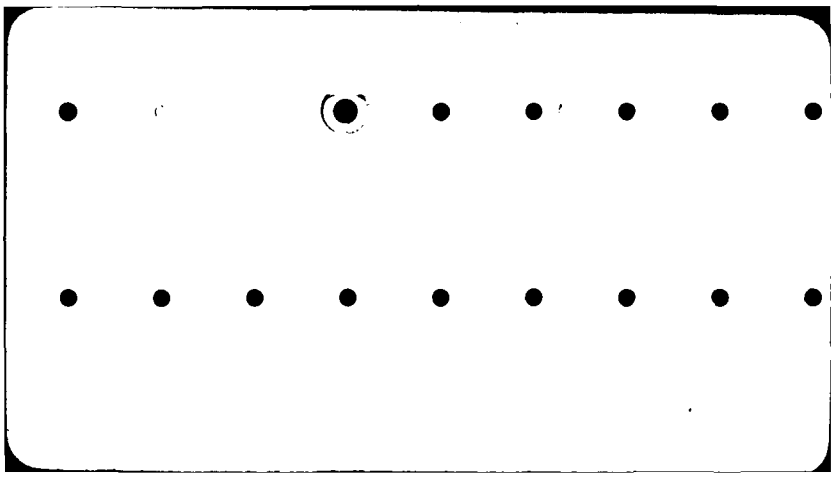

(11)

REPORT DAAK50-81-C-0022

ADVANCED DEVELOPMENT DIVISION

DEVELOPMENT OF AN AUTOMATED GEAR TOOTH CONTOUR MEASURING DEVICE

PHASE I

Alfred R. Ouellette
Aerodyne Research, Inc.
45 Manning Road
Billerica, MA 01821

12 April 1982

Final Report - Phase I Development

Prepared for

U. S. ARMY MATERIALS AND MECHANICS
RESEARCH CENTER
Arsenal Street
Watertown, MA 02172

U. S. ARMY AVIATION RESEARCH AND
DEVELOPMENT COMMAND
4300 Goodfellow Boulevard
St. Louis, MO 63120

Unclassified

SECURITY CLASSIFICATION OF THIS PAGE (When Data Entered)

REPORT DOCUMENTATION PAGE		READ INSTRUCTIONS BEFORE COMPLETING FORM
1. REPORT NUMBER DAAK50-81-C-0022	2. GOVT ACCESSION NO. AD-A121 970	3. RECIPIENT'S CATALOG NUMBER
4. TITLE (and Subtitle) Development of an Automated Gear Tooth Contour Measuring Device - Phase I		5. TYPE OF REPORT & PERIOD COVERED Final Report - Phase I Development 6. PERFORMING ORG. REPORT NUMBER
7. AUTHOR(s) Alfred R. Ouellette		8. CONTRACT OR GRANT NUMBER(s) DAAK50-81-C-0022
9. PERFORMING ORGANIZATION NAME AND ADDRESS Aerodyne Research, Inc. 45 Manning Road Billerica, MA 01821		10. PROGRAM ELEMENT, PROJECT, TASK AREA & WORK UNIT NUMBERS Item 0002 (A002)
11. CONTROLLING OFFICE NAME AND ADDRESS U.S.Army Materials and Mechanics Research Center Arsenal Street Watertown, MA 02172		12. REPORT DATE April 12, 1982 13. NUMBER OF PAGES 109
14. MONITORING AGENCY NAME & ADDRESS (if different from Controlling Office) U.S.Army Aviation Research & Development Command 43 Goodfellow Boulevard St. Louis, MO 63120		15. SECURITY CLASS. (of this report) Unclassified 15a. DECLASSIFICATION/DOWNGRADING SCHEDULE

16. DISTRIBUTION STATEMENT (of this Report)

Approved for public release; distribution unlimited.

17. DISTRIBUTION STATEMENT (of the abstract entered in Block 20, if different from Report)

18. SUPPLEMENTARY NOTES

This submission is the final Phase I report incorporating draft corrections.

19. KEY WORDS (Continue on reverse side if necessary and identify by block number)

Mensuration
Coordinate Measuring Machine
Noncontact Optic Probe
Spur Gear
Surface Wear Assessment

20. ABSTRACT (Continue on reverse side if necessary and identify by block number)

This report covers the Phase I development work intended to demonstrate the feasibility of measuring gear size parameters by noncontacting means to within an absolute accuracy range of ± 10 to ± 30 microinches. The work completed in this phase involved two major state-of-the-art developments: a Coordinate Measuring Machine and a Noncontact Optic Probe. The machine accuracy was shown to be better than the lower limit of the tolerance range as an environmentally compensated measuring system and, under stabilized conditions, can perform measuring cycles lasting more

DD FORM 1 JAN 73 1473 EDITION OF 1 NOV 65 IS OBSOLETE
S/N 0102-LF-014-6601

Unclassified
SECURITY CLASSIFICATION OF THIS PAGE (When Data Entered)

TABLE OF CONTENTS

TABLE OF CONTENTS (Continued)

LIST OF ILLUSTRATIONS

LIST OF ILLUSTRATIONS (Continued)

LIST OF TABLES

SUMMARY

This report covers the Phase I development work for an Automated Gear Tooth Contour Measuring Device (AGTCMD). Phase I is a manually operated machine designed to demonstrate feasibility of measurement to an absolute accuracy of ± 10 to ± 30 microinches using a noncontacting optical probe. The Phase II work, when funded, will provide a fully automated system capable of rapid measurement and wear assessment of spur gears ranging in sizes from 2 inches to 12 inches pitch diameter.

The Phase I testing demonstrated state-of-the-art performance as an environmentally compensated coordinate measuring machine wherein precision and absolute accuracy was shown to be better than the desired tolerance of ± 10 microinches. The noncontacting optic probe, also a state-of-the-art development, showed the sensitivity needed to meet the program goals.

For the x-y coordinate measuring machine, errors associated with scale accuracy, vibration, structural rigidity, geometry and thermal effects were first defined analytically, and then correlated with the test data. Thermal stability tests were performed to show effects of machine warm-up from a cold start, effects of ambient temperature and atmospheric pressure changes, effects of human body heat, stabilized and transient operating conditions and the benefits of fluid filling the machine structure. Repeatability tests were done for simple mechanical positioning precision and for part mensuration in the environmentally compensated mode. To evaluate absolute accuracy performance as an environmentally compensated system, gauge blocks were measured in an uncontrolled room at varying temperatures around 12° F higher than the metrological standard.

Unlike the coordinate measuring machine, the noncontacting optic probe did not attain an operational status in Phase I. Rather, it functioned as a breadboard device which gave sufficient test data to show feasibility of meeting the desired goals and provided solutions to identified performance problems. It clearly demonstrated performance better than currently available optic probes.

1. INTRODUCTION

This Final Report covers the Phase I development of an Automated Gear Tooth Contour Measuring Device (AGTCMD) under Contract No. DAAK50-81-C-0022 issued by the U. S. Army Aviation Research and Development Command.

The developmental work for the AGTCMD is to be carried out in two phases. Phase I is for proof-of-concept and involves development of a nonautomated breadboard machine. Phase II, which may be funded after the Government's evaluation of Phase I work, involves a continuation of the development for a fully-automated system.

Aerodyne Research, Inc. submitted Proposal No. ARI-P-1358(A) on 12 January 1981 and a contract was awarded to commence work on 15 July 1981.

The fully developed AGTCMD is designed to provide an automated noncontact method for rapid measurement of the contour and dimensional parameters of spur gears ranging in sizes from 2 inches to 12 inches in pitch diameter, with face widths from 1/2 to 3 inches and circular pitch greater than 0.3 inches. In addition to size measurement, the AGTCMD is required to assess tooth wear damage manifested by surface pitting, scoring or spalling. It is desired that the machine be relatively light and portable. The sensor used for measurement is a noncontact, optical type of probe. The desired mensuration accuracy is ± 10 microinches for the smaller gear sizes up to ± 30 microinches for the larger gear sizes. The tolerance along the gear axis (gear width) is ± 100 microinches.

The above stated goals for system performance says that the AGTCMD development program endeavors to advance the state-of-the-art in two major areas:

a. Mensuration accuracy as an environmentally-compensated Coordinate Measuring Machine (CMM).

b. Sensitivity and probing versatility of a noncontacting probe.

1.1 COORDINATE MEASURING MACHINE

The results of a survey of Coordinate Measuring Machines was published in March 1981[1]. It includes a listing of 16 manufacturers with a tabulation of "Accuracy

(1) Coordinate Measuring Mac[illegible]es ... "[illegible]nters for Productivity and Profit," Machine and Tool Blue Book, March [illegible]; F[illegible]hcock Publishing Co.

Claimed" for each. In general, the values given are valid only at a reference temperature of 20° C and do not include the repeatability of the electronic contact probes. For the majority of the listings, an accuracy of ± 300 to ± 400 microinches is given for their smaller machines. Repeatability is from ± 100 to ± 200 microinches. Those manufacturers claiming better accuracy are Leitz, Inc. with a basic system inaccuracy of ± 47 microinches plus ± 25 microinches per inch. Repeatability is ± 20 microinches. The Moore Special Tool Company claims the highest accuracy at 35 microinches over a full x-y travel of 11 x 18 inches, with a repeatability of ± 5 microinches. One role seen by Moore for their Universal Measuring Machine is that of a referee when a disagreement exists for parts measured by Coordinate Measuring Machines(2). Moore acknowledges that their machines do not provide the level of productivity (speed of of operation) given by the CMM. There are also comments made by competitive manufacturers of CMM that published accuracy statements are misleading for one reason or another and that much confusion exists regarding accuracy performance of CCM.

The author is in agreement with the above assessment and is hopeful that matter presented in this report offers some clarification. It is therefore appropriate to begin with some basic definitions of terms relating to mensuration performance of CMM. These terms are resolution, repeatability, accuracy and absolute accuracy.

a. Machine Resolution

Machine resolution, for the AGTCMD, is the length or angular division represented by the digital readout of the display console.

b. Repeatability

Repeatability or precision is the tolerance range over which the machine reproduces consecutive measurements, independent of "true" measurement. While resolution and repeatability are generally independent of accuracy, it should be noted that the useful accuracy of the machine cannot be better than the resolution value or repeatability range.

(2) Moore, Wayne R., "Foundations of Mechanical Accuracy," The Moore Special Tool Company, 1970.

c. Machine Accuracy

Machine accuracy is the error in measurement of the "true" size of the part in its current state.

d. Absolute Accuracy

Absolute accuracy is the error in measurement of the true size of the part referenced to a "basic" temperature of 68° F. This distinction may seem to be obvious, but becomes increasingly complex with the level of accuracy demanded and it is seldom given the recognition that is needed. It follows, from the definition given, that absolute accuracy is the only meaningful concept for microinch level part mensuration. An absolute accuracy error is no more acceptable than an accuracy error or precision error since, in the final analysis, the part is unknowingly measured incorrectly.

Thermal effect is an interactive phenomenon between the machine and the part to be measured. It involves more than recording the part's temperature and compensating for its thermal expansion. Thermal changes can affect machine accuracy as well as absolute accuracy. Machine accuracy is degraded by linear expansion of the machine scale but mostly by structural thermal gradients that cause distortion which magnify the measurement error. Thermal effects will be discussed more in Section 3.4.

Another aspect loosely treated in the CMM literature is the machine accuracy over the range of part measuring capacity. This consideration relates to structural deflection, straightness of travel and pitch, roll and yaw of the slides. These effects are named geometric errors and are analyzed in Section 3.3.

1.2 NONCONTACTING PROBES

To the extent of the writer's knowledge, the CMM listed in the survey use electronic contacting probes. These can range from single axis, unidirectional probes to three-axis bidirectional probes. By way of definitions, a common machine shop indicator is a single-axis, unidirectional probe. It responds only to motion along one

axis, on one side of the contact ball. If this indicator were single axis bidirectional, it would respond to motion on both sides of the ball and a size measurement would have to compensate for the diameter of the contact ball. It follows that the multiaxis probe would have this bidirectional capability in each of the axes. These definitions of probe versatility are given because it helps to place the AGTCMD probe development in perspective. The application requires a two-axis, bidirectional, noncontacting probe capable of both measuring size and accessing surface defects along three axes. Additionally, the probe must have a long, small diameter configuration which allows entry into a variety of gear tooth sizes.

Currently available noncontacting optic probes are single-axis, unidirectional with spot sizes restricted to size measurement only. Two of the known manufacturers of these optical sensors are Selcom and Autech. They are most commonly used for measuring part thickness. A single gauging probe measures part thickness with reference to the part mounting surface or two sensors are used to measure thickness in a differential mode. Here, the sensors are calibrated on a gauge of known thickness, and the part size is then determined by algebraic summation of the two sensor readings. The published resolution of the Selcom unit is 0.025% of measuring range or 75 microinches limiting. The accuracy is given at ± 150 microinches for the smallest range. The Autech catalog data gives a best resolution of 100 microinches and repeatability of ± 200 microinches. The goal for the AGTCMD probe performance is a resolution of 5 microinches and repeatability of ± 10 microinches.

In light of the above assessment of available noncontact optic probes, it should be appreciated that development of the AGTCMD probe seeks multistep advancement in the state-of-the-art.

Section 4 of this report presents the results of performance testing of the Phase I system followed by the Conclusions in Section 5 and Recommendations in Section 6.

2. GENERAL SYSTEM DESCRIPTION

2.1 PHASE I SYSTEM

The Phase I system is a nonautomated prototype of the final system. It has been designed so that the majority of the elements will be usable in the final system. It comprises two basic modules: a stand-alone, electronic/digital readout console and a portable measuring machine. These modules are shown in the photograph of Figure 2.1. Included in the machine module is the noncontact optic probe. The breadboard model of the device is the vertical assembly attached to the bridge of the machine, as seen in Figure 2.1. The close-up view of Figure 2.2 shows the probe rod and spindle assembly.

Figures 2.3 and 2.4 show diagrams of the front and side view of the Phase I machine. It has an x-y interferometer which monitors the position of the x-y table slides. The optic probe is fixed to the bridge and the table-mounted gear moves relative to the probe. This configuration is highly beneficial in terms of minimizing the geometric machine errors resulting from slide motion inaccuracy. This aspect will be discussed in detail in Section 3.3. The probe rod, which is a long, small diameter lens, is collet-mounted in a precision spindle. The angular position of the probe is determined by a rotary encoder having a resolution of one thousandth of a degree. The probe has an electrical surface contact signalling feature to prevent damage from overtravel. The principle of noncontact sensing is described in Section 3.6.

The automated version of the machine will have D.C. servo drives on five axes: x, y and z motion; (β) probe angular positoning, and (θ) gear tooth indexing from a rotary table. For Phase I, the machine is manually positioned in the x-y axis by lead screw hand cranks. The crank assembly for each axis consists of two cranks. One is for course positioning and moves the stage 0.1 inches per revolution. The fine crank, engaged via a worm gear, gives a stage displacement of 833 microinches per revolution. The fine crank thus facilitates stage positioning down to one microinch. With training and care, one can position to about 6 microinches with the course crank.

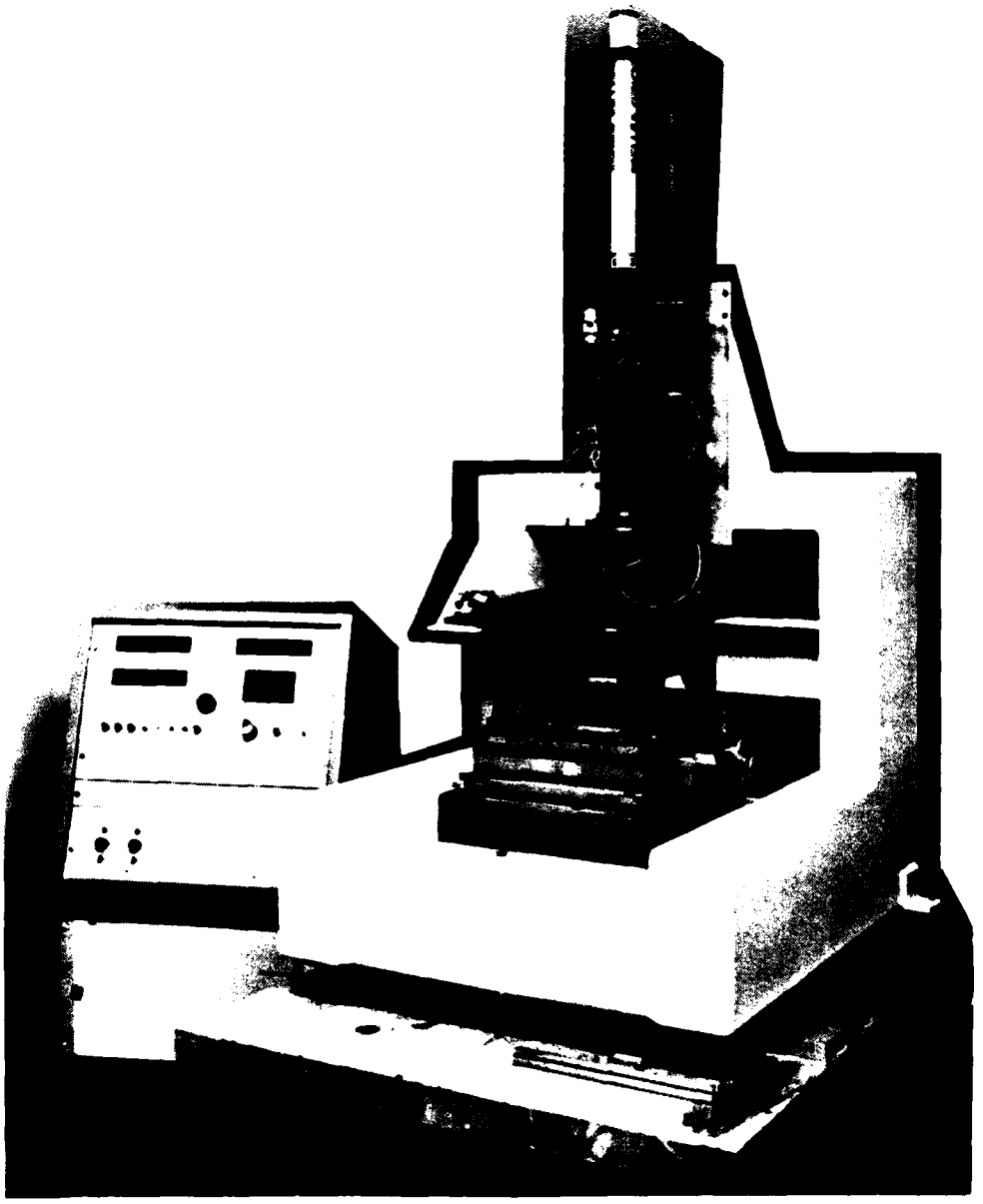

Figure 2.1 Phase I AGTCMD

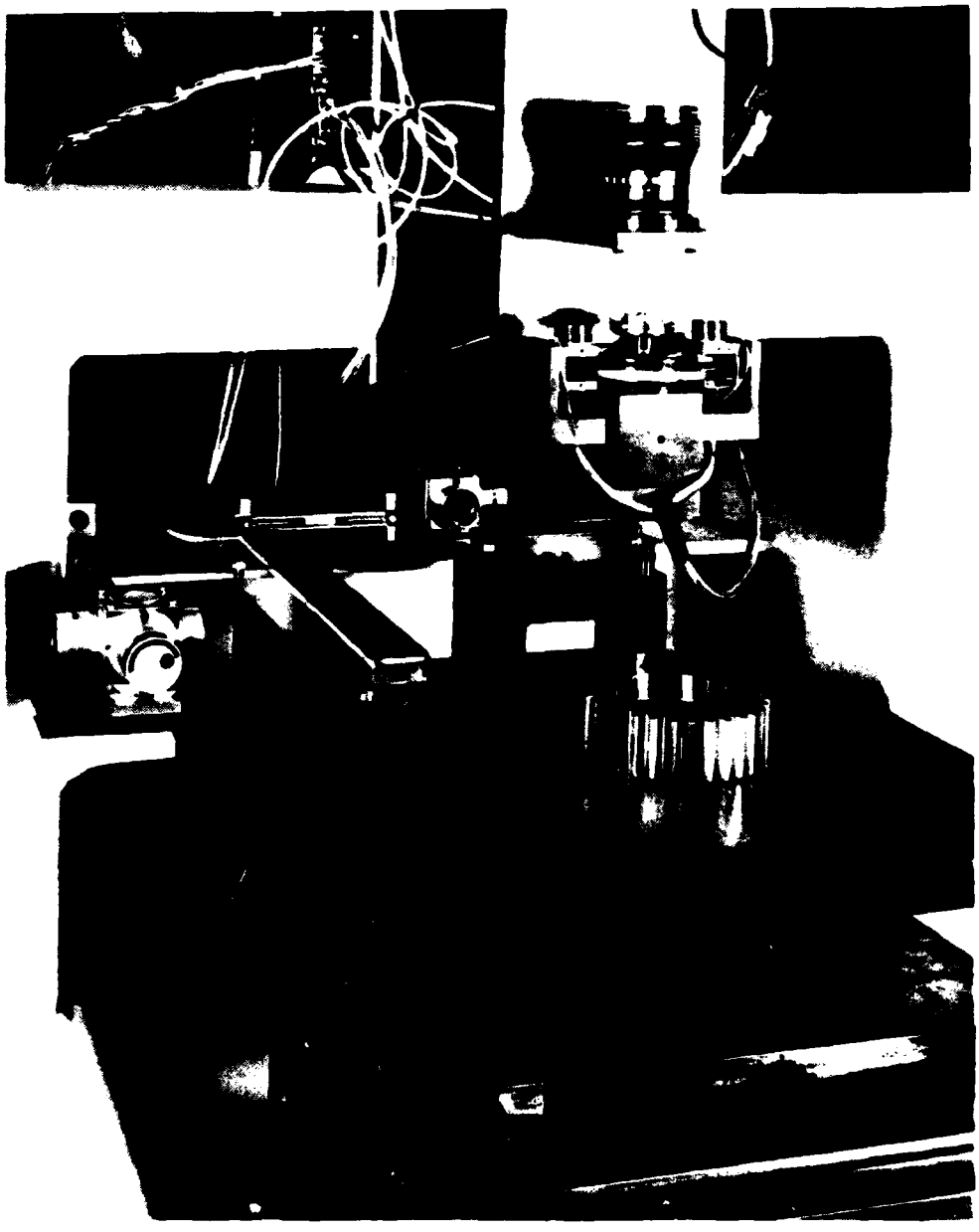

Figure 2.2 Phase I AGTCMD

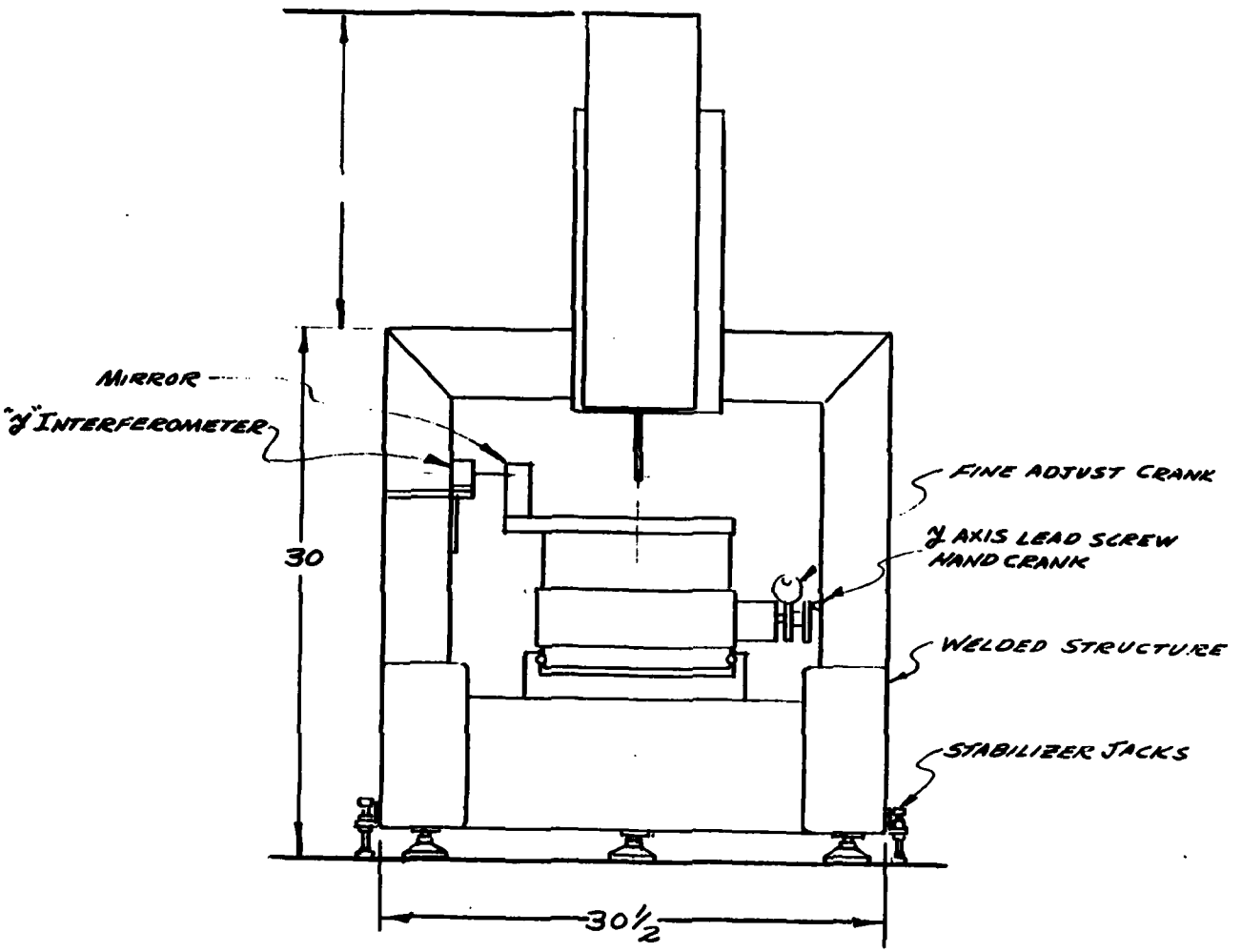

Figure 2.3 Front View — Phase I AGTCMD

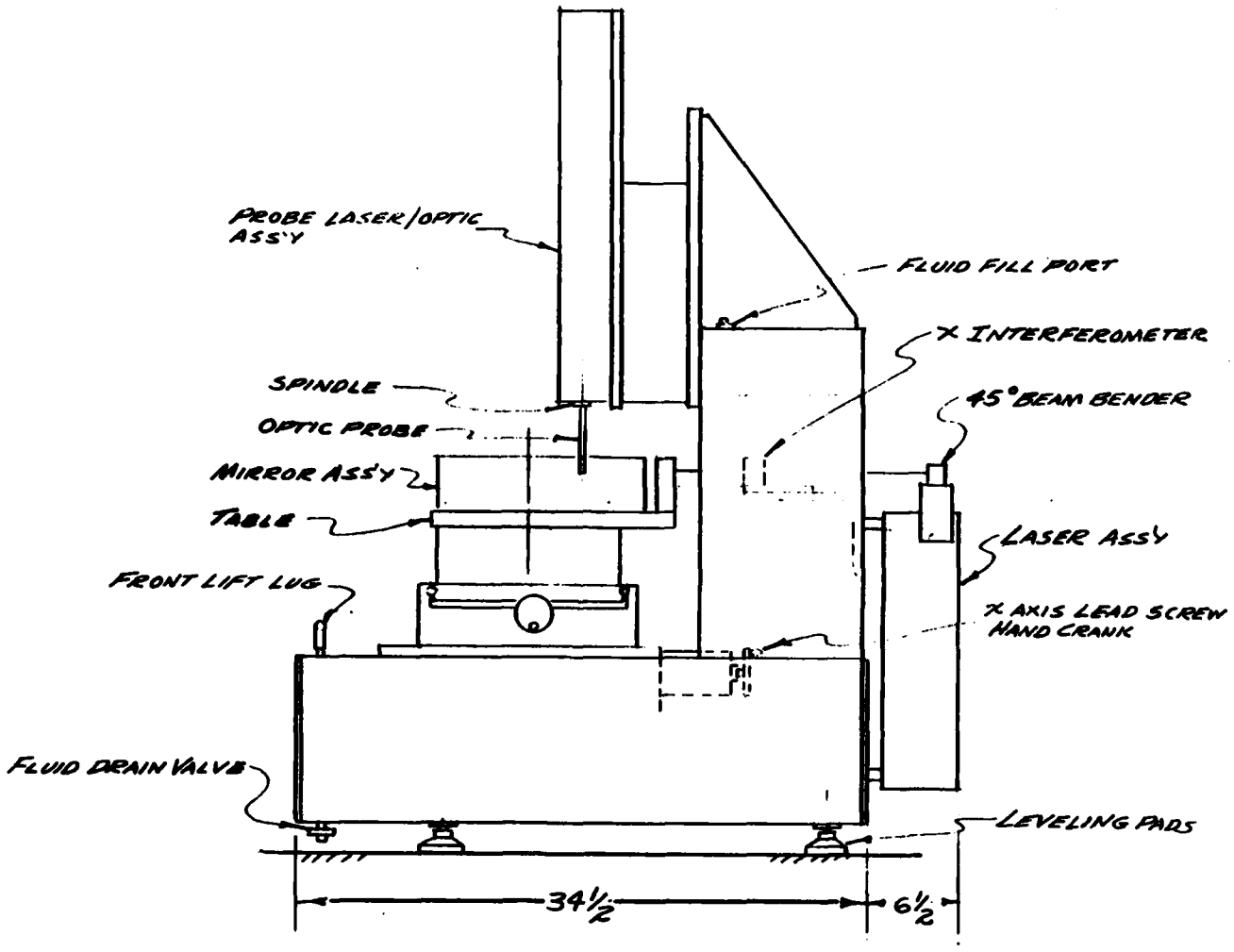

Figure 2.4 Side View — Phase I AGTCMD

Coordinate measuring machines having accuracy levels of 100 microinches or better are massive, multi-ton structures. Solid granite construction appears to be a popular choice among manufacturers. One of the goals of the AGTCMD is the design of a relatively lightweight portable machine. The methods used to achieve this goal are as follows:

a. The machine can be moved from one location to another without need for major set-up re-alignment of the elements of the machine. This is achieved by three point mounting pads and two torque calibrated auxiliary stabilization jacks. Accuracy degrading structural distortion due to mounting surface planarity is thus eliminated. Moreover, the machine configuration is such that mensuration accuracy is less dependent on geometric accuracy of the bearing ways. The reason for this is explained in Section 3.3.

b. Microinch level accuracy requires high thermal inertia, structural rigidity and dimensional stability. Granite is a good material for dimensional stability, and because it is used in large solid masses, it provides the desired thermal enertia. However, it is grossly inefficient in terms of weight/rigidity ratio. First, its modulus of elasticity is only 0.27 that of steel, but because its density is lower, the specific stiffness ratio favors steel by only a factor of 1.43. The large gain is derived from beam cross-sectional properties. Granite beams are solid whereas metal beams can be deep section, thin wall construction. Moment of inertia formulas say that beam stiffness increases with the cube of the cross-sectional depth. Thus, material in the area of the neutral axis can be eliminated without much reducing stiffness. A third advantage relates to joint construction. Granite beams are generally "simply supported" joints whereas a welded structure using thin wall deep section can approach the "fixed end" joints. This provides about a factor of 4 stiffness advantage. Thus, the lightweight, high rigidity structure shown in Figures 2.1 to 2.4 is a single piece, continuous joint weldment using deep section hollow steel tubing.

The high thermal inertia/low weight ratio is achieved by filling the hollow structure with a water soluable oil, such as is used for machine cutting coolants. Figure 2.3 shows the fluid fill port on the top of the bridge and a flex hose fluid drain valve at the front understructure. The advantage of fluid filling is that water has a

specific heat value that is 8.3 times greater than steel. The structure holds about 34 gallons for a fluid weight of 284 lbs. This alone provides an equivalent thermal mass of 2,355 lbs of steel. The final (Phase II) machine weight is estimated to be 857 lbs empty and 1,141 lbs fluid filled.

The machine structure was stress-relieved after welding to minimize long term distortion due to residual stress. While the long term dimensional stability of the weldment is not as good as granite construction, it will not produce errors during short term measuring cycles and the AGTCMD configuration is such that the geometric machine errors discussed in Section 3.3 are not affected by small long term structural creep.

The electronic/digital readout console is a stand-alone cabinet with cable connection to the machine. This isolates the major heat dissipation components from the machine structure. The cabinet contains the power supplies and electronics for the interferometer and the laser probe. The readout panel has seven digits plus sign displays for the x and y coordinate position, a six digit display for the probe angular position (β) and a 4 digit display for the calibrated probe radius (r). It has individual reset switches to zero out all displays. A single switch is provided to freeze the instantaneous readings of x, y, β and r. This allows time for manual data recording of a point measurement. Also included are a buzzer for probe contact, a power on/off switch a probe laser power on/off switch.

2.2 PHASE II SYSTEM

Reference is made to Aerodyne Proposal No. ARI-P-1358(A). The Phase II work, if funded, involves automating the prototype machine developed in Phase I. It will require the addition of the following elements:

a. Motor drives to the x-y slides that are closed-loop servoed with the x-y interferometers.

b. A z-axis slide with a linear incremental optical encoder. A motor drive that is closed-loop servoed with the z encoder.

c. An air bearing turntable with fixturing for mounting a variety of gear sizes according to Section 2.2.1 of this report.

d. A gear indexing servo motor drive with a rotary optical encoder.

e. A probe spindle servo motor drive.

f. A computing system according to Proposal No. ARI-P-1358(A).

g. Generation of a software package.

h. System electronics according to Proposal No. ARI-P-1358(A).

i. Console-mounted joystick controls for x, y and z slide drives, probe angle drive and gear index drive.

j. A probe radius and z axis calibration gauge.

k. Add to the control panel digital displays for gear turntable angle and z coordinate and various functional controls.

l. Safety interlock for probe protection.

2.2.1 Gear Mounting Method

A preliminary design of the gear mounting concept was performed in Phase I (ARI drawing J45-0003, included as Appendix A).

Gear parameter measurement must be referenced to the bore of the gear and since the desired mensuration accuracy is in the 10 to 30 microinch range, the mounting eccentricity would have to be less than 5 microinches. This presents a difficult, time-consuming requirement for the machine operator, particularly when one considers that the bore of the gear could have an out-of-roundness of 150 microinches. A better approach is to nominally position the gear on the turntable to within about 200 microinch runout and compensate for this mounting eccentricity in software. The method for software compensation is discussed in Section 3.5.3.

The gears to be inspected are mostly ring gears with bore sizes ranging from 1 to 10 inches in diameter and face widths of 1/2 to 3 inches. The gears should be mounted so that the face width centerline coincides with the interferometer beam; and so that the bore is concentric with the turntable within .0002 inches. The mechanism

for doing this (shown in drawing J45-0003) is based on an internal three-jawed chuck approach. Set-up for a particular bore size involves manual positioning of two jaws. Shop gauge blocks are used to set the radial position by referencing to the center pilot ring on the turntable. These jaws then remain fixed for all gear mounting of common bore size. The gear is set on the table and the third jaw is positioned on the bore to remove diametral clearances. Spacers are provided for positioning the different gear face widths at the correct z coordinate.

3. ANALYTICAL DISCUSSION OF SYSTEM ELEMENTS

3.1 X-Y TABLE MOTION SCALE

The table displacement transducer in the x-y plane is the Laser Interferometer. It uses the plane mirror interferometer which has a basic resolution of 1/8 wavelength ($\lambda/8$) without electronic resolution extension. So, fractions of the wavelength of a He-Ne laser are counted and displayed digitally. The internationally accepted standard for the wavelength (λ_{vac}) of a He-Ne laser in a vacuum is 2.4920921×10^{-5} in. Since the laser is operating in air, a compensation factor (C) must be applied. The relationship for table motion and displayed counts is then:

$$\delta_x = \delta_y = 2.492092 \times 10^{-5} \frac{D_c}{8M_c} C \qquad (3.1)$$

where:

$\delta_x = \delta_y$ = Absolute table displacement, inches

D_c = Digital display counts

M_c = Factor for electronic extended resolution

$C = \frac{\lambda_{air}}{\lambda_{vac}}$ = Environmental compensation factor based on air temperature, pressure and R.H.

The electronics allows for adjustable settings that give resolutions from $\lambda/8$ to $\lambda/120$. With the Phase I electronics, computer processing of the fringe counts was not included. This means that a displayed count is not an exact microinch unit. Selecting a resolution of $\lambda/24$ or $M_c = 3$, a console display count equals 1.0383717 microinches based on vacuum wavelength.

The compensation factor (C) will be determined automatically in Phase II. For now, a compensation factor handbook is used and the temperature, pressure and humidity of the air are recorded. The factor (C) has values like 0.999725 for $T = 21^{\circ}$ C.

and P = 770 mmHg. This value changes by about one PPM for increments of 1^{o} C or 2.2 mmHg or 30% R.H. Thus, over the range of ambient conditions, the first three digits to the right of the decimal point are always (.999).

It should now be noted that Equation (3.1) is valid only if there is no change in the environmental conditions during a measurement cycle. The measuring cycle is defined as the time interval between initialization and the last measurement recorded. Initialization involves zero reset of the digital display at the datum point of measurement. In measuring the length of a gauge block as an example, the stage is positioned so that the probe nulls to zero, at which time the interferometer is initialized by zero-reset. The stage is then positioned so that probe nulls at the other end of the gauge block and the counts are recorded. Since this takes only a few minutes, the ambient changes would be negligible. However, a 20-minute measuring cycle of a full gear could result in a significant change depending upon room air control. The foregoing discussion relates to what is called "deadpath"* error. The compensation factor (C) in Equation (3.1) corrects for the wavelengths of motion from zero datum, but does not account for the path length from zero datum back to the interferometer. This is labelled (L_D) in Figure 3.1. We can measure L_D and correct for deadpath error according to the more general equation:

$$\delta_y = \delta_x = \frac{D_c}{8M_c} \lambda_{vac} C + \left(\frac{C - C_o}{C_o}\right) L_D \qquad (3.2)$$

where

L_D = Deadpath length

C = Current compensation factor

C_o = Compensation factor at time of initialization.

It is noted that the value of L_D is a machine constant for the AGTCMD. It is independent of gear size because zero datum is the center of the gear which is always

*Deadpath: Linear distance from interferometer to mirror at the stage position when the probe is at the center of the gear. This is a constant for the AGTCMD.

located on the spin axis of the turntable. Thus, the second term of Equation (3.2) corrects for deadpath error via software.

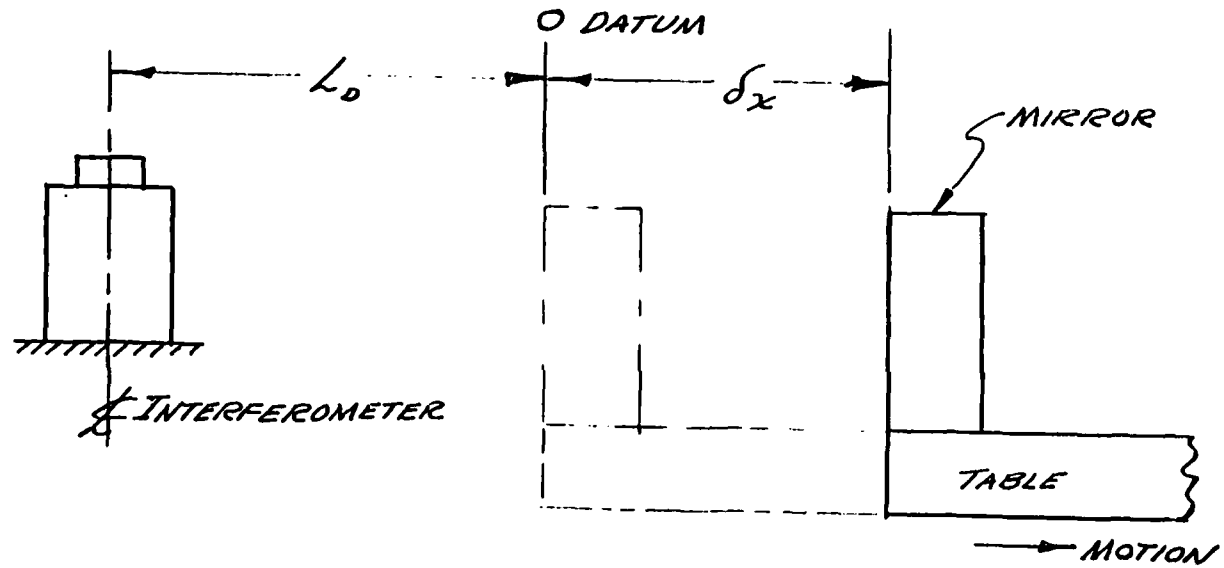

Figure 3.1 Laser Interferometer Deadpath Error

3.2 PROBE SPINDLE SCALES

The probe spindle has two scales, the primary linear scale (r) for sensing distance from the surface of the gear and an angular position scale (β) for orienting the sensing beam normal to the surface to be measured.

3.2.1 Angular Position

An optical incremental rotary encoder is used to determine angular position. It has dual read heads for extended electronic resolution and higher accuracy. The disc has 9000 divisions and with electronic multiplication, provides 360,000 counts per revolution. The digital display reads in degrees and decimals of a degree; for example, 289.362 degrees. Expressed in terms of arc seconds, this provides an angular positioning resolution of 3.6 arc seconds.

The probe rotates so that the laser beam is normal to the surface being measured. The following analytical discussion relates to these requirements.

Normality Requirements

During a surface scan, the probe is rotated to maintain the beam normal to the surface. The laser probe is relatively insensitive to small deviations in normality. As shown in Figure 3.2, surface points 1'and 2'could be measured with a constant β angle. Points 1 and 2 represent the calibrated center axis of the probe and by definition the distance $r_1 = r_2$.

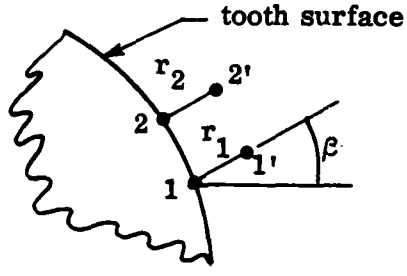

Figure 3.2

Coordinate Correction Factor

The x and y interferometers are zero referenced to the center axis of the probe. Scanning of surfaces at β angles with the axes of the x and y stages requires a correction factor.

For point 1 shown in Figure 3.3, the coordinates for the surface are:

$$x_s = x_p + r \; ; \tag{3.3}$$

$$y_s = y_p \; ; \tag{3.4}$$

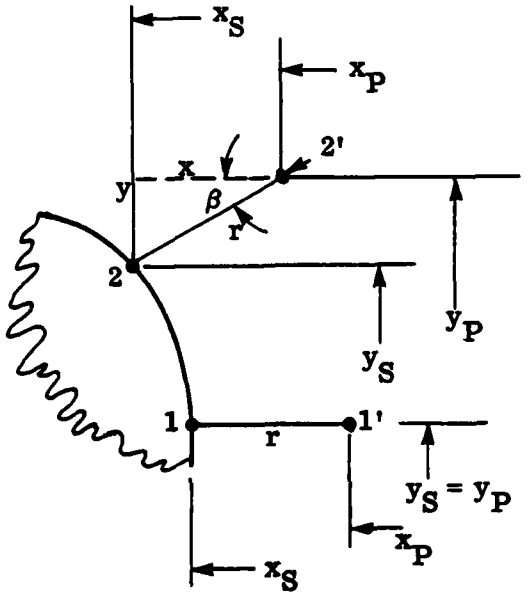

Figure 3.3

Subscript (S) represents the coordinate at the surface and subscript (P) is the coordinate at the center axis of the probe.

r = calibrated probe radius

For point 2, the coordinates for the surface are:

$$x_S = x_P + r \cos \beta \; ; \tag{3.5}$$

$$y_S = y_P - r \sin \beta \; ; \tag{3.6}$$

Correction Factor Error

While a small mismatch in the β probe angle with a normal to the surface produces a negligible error, an error in β as recorded by the positioning encoder is significant. The error Δx and Δy for an encoder error $\Delta \beta$ is derived as follows:

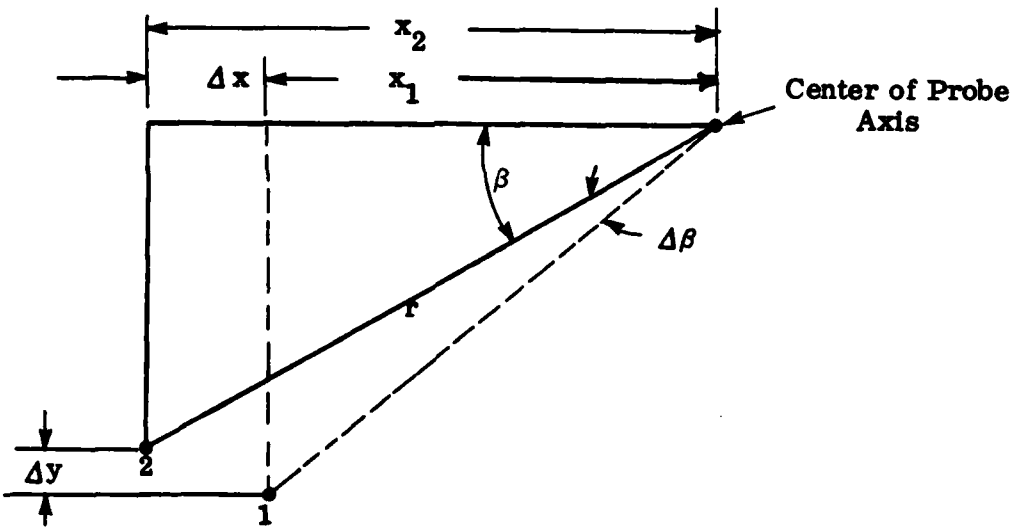

Figure 3.4

From Figure 3.4 we see that:

$$\Delta x = x_2 - x_1$$

where:

$$x_2 = r \cos \beta \qquad \text{and} \qquad x_1 = r \cos (\beta + \Delta\beta)$$

and substituting for x_2 and x_1

$$\Delta x = r\left[\cos \beta - \cos (\beta + \Delta\beta)\right] \tag{3.7}$$

In a similar manner:

$$\Delta y = r\left[\sin (\beta + \Delta\beta) - \sin \beta\right] . \tag{3.8}$$

The Teledyne Gurley encoder model number 8708 mounted concentric to the axis of rotation to within 0.1 mils is accurate to 5 to 7 arc seconds; and as mentioned earlier is designed with a positioning resolution of 3.6 arc seconds.

Selecting:

$\beta = 15^{o}$; $\Delta\beta = 7$ arc seconds; $r = 0.045"$

from Equations (3.7 and 3.8):

$$\Delta x = 0.045 (8.8 \times 10^{-6}) = 0.4 \text{ microinches}$$

$$\Delta y = 0.045 (32.77 \times 10^{-6}) = 1.47 \text{ microinches} .$$

We note that (Δx) approaches zero for small β angles while (Δy) becomes larger at small β angles. The worst case for (Δy) when $\beta = 0^{o}$ is:

$$\Delta y = r \sin (7 \text{ sec}) = 1.53 \text{ microinches.}$$

3.2.2 Linear Position

A four-digit display with ± signs is provided on the control panel of the console for the value of the probe radius (r). The output signal from the probe electronics is a function of the distance from the surface being measured and the axis of the probe. This signal can be adjusted to represent some even microinch increment.

3.3 GEOMETRIC MACHINE ERRORS

3.3.1 Slide Bearing Offset Error

Bearing offset error is seldom discussed by manufacturers of coordinate measuring machines. It is nevertheless a significant error source which must be considered. Principally, it relates to the differential displacement between the part measuring point and the slide position transducer. The transducer scale reads the length measurement, but due to slide bearing displacements, the measuring point motion is different. This is one important area where the AGTCMD has an advantage over the conventional x-y-z coordinate measuring machine. Slide bearings exhibit angular and parallel offset displacements. These are caused by a combination of the trueness of the machine ways and structural deflection due to translation of the table load. Perhaps the best way of illustrating the error relationship between slide motion anomalies and machine geometry is to first analytically describe the errors associated with a common bridge-type measuring machine (or jig borer) and then make comparison with the AGTCMD geometry.

Figure 3.5 shows this type of machine. The bridge has the y axis cross slide with the z axis slide mounted on the cross slide. The x axis slide is located on the machine base independent of the other axes. A bearing slide has six independent degrees of freedom: pitch, roll, yaw, axial positioning, vertical and lateral straightness of travel. The first three degrees of freedom are angular displacements of the slide about the ways centerline. Axial positioning bears no direct relationship with the type of geometry errors that we are discussing here, but does involve the cosine error, to be discussed in Section 3.3.2, and the basic accuracy of the scale. However, we include it because it is part of the overall measuring error. The last two degrees of freedom listed are parallel offset of the slide independent of angular motion.

In Phase I, the machine is operated in the x-y plane only and does not have the z axis slide, so the analysis holds z slide motion fixed and looks at the errors associated with the x and y slides only. Table 3.1 gives a list of symbols describing the various slide displacement errors.

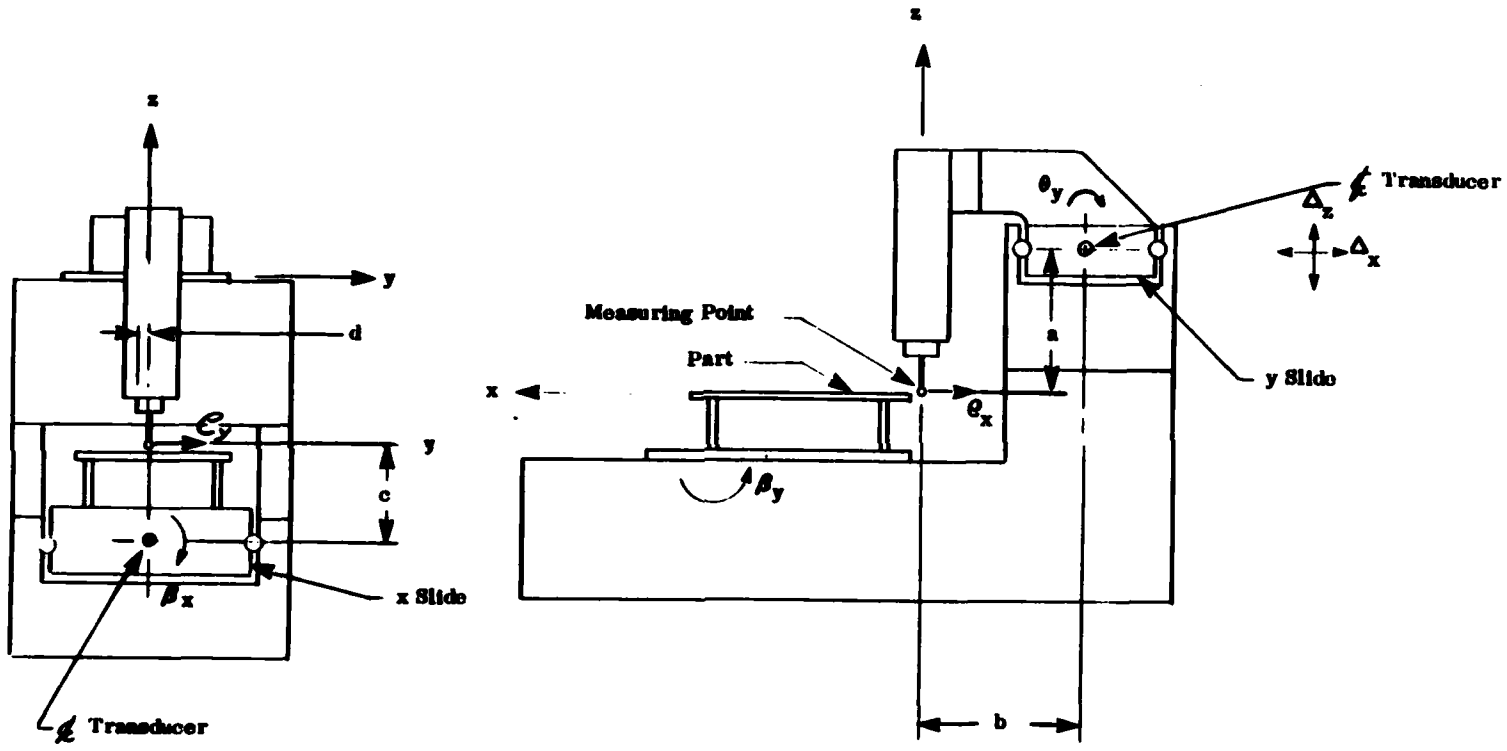

Figure 3.5 Geometric Machine Errors

Table 3.1 Slide Displacement Error Symbols

x slide	y slide	
β_x	θ_y	roll
β_y	θ_x	pitch
β_z	θ_z	yaw
δ_y	Δ_x	lateral straightness of travel
δ_x	Δ_y	axial backlash/transducer position error
δ_z	Δ_z	vertical straightness of travel

The symbols are shown in the diagram of Figure 3.5. Also shown are linear distances a, b, c and d from the machine scale to the point of measurement. These distances are what magnify the relative displacement between the scale and the point of measurement. For the small angular displacements of interest, the linear measuring error (ϱ) is best described with the angular excursion expressed in radians from the relationship:

$$\varrho = r\theta \tag{3.9}$$

Letting ϱ_x, ϱ_y, ϱ_z be the "part" mensuration error due to the six aforementioned degrees of freedom and from relationship (3.9), we can write the following equations for the x and y slides.

a. <u>y Slide Error</u>

$$\varrho_x = a\theta_y \pm \Delta_x \tag{3.10}$$

$$\varrho_y = a\theta_x \pm b\theta_z \pm \Delta_y \tag{3.11}$$

$$\varrho_z = b\theta_y \pm \Delta_z \tag{3.12}$$

It is noted that the term ($b\theta_y$) in Equation (3.10) and ($a\theta_y$) in Equation (3.12) are negligible for the small angles involved.

b. <u>x Slide Error</u>

$$\varrho_x = c\beta_y \pm d\beta_z \pm \delta_x \tag{3.13}$$

$$\varrho_y = c\beta_x \pm \delta_y \tag{3.14}$$

$$\varrho_z = d\beta_z \pm \delta_z \tag{3.15}$$

c. <u>Combined Slide Errors</u>

$$\varrho_x = a\theta_y \pm \Delta_x \pm c\beta_y \pm d\beta_z \pm \delta_x \tag{3.16}$$

$$\varrho_y = a\theta_x \pm b\theta_z \pm \Delta_y \pm c\beta_x \pm \delta_y \tag{3.17}$$

$$\varrho_z = b\theta_y \pm \Delta_z \pm d\beta_y \pm \delta_z \tag{3.18}$$

Since these errors are independent and of opposite signs, some statistical cancellation would result; the greater the number of terms, the less likely for all errors to be of the same sign. Another point to be made is the difference between repeatable and nonrepeatable (random) errors. For example, a slide straightness of motion error could consist of both types. The larger of the two would be the trajectory error, which would repeat itself and superimposed on this would be jitter due to slide anomalies, vibration or freedom of motion. This is an important distinction because the repeatable errors can at times be established as machine constants and be compensated for in the mensuration process. On the other hand, little can be done with the random errors. As a general rule, however, compensation of repeatable geometric error is not usually done for coordinate measuring machine usage

An examination of Equations (3.16, 3.17 and 3.18) reveals that geometric errors can be large when the measuring probe is far removed from the slide position scale, as indicated by the values of the factors a, b, c, d in the machine configuration shown in Figure 3.5. Since the slide displacements defined by θ, β, δ and Δ are

principally repeatable errors, the machine could perform with good repeatability or precision but with very poor accuracy. In other words, it would do a good job of measuring the part incorrectly every time. In this situation, the operator is unaware of the magnitude of the error in measurement and, on the basis of repeatability in his measurement, could construe that the accuracy of measurement is about the same as the machine repeatability error.

To place the magnitude of the error in perspective, the "worst case" error is calculated for a measurement along the y axis. The x slide will move only to clear the probe of the part and return to the same x coordinate. To do this, values are assigned to slide performance. For example, assuming that over a 2-inch measurement for the y slide,

$$\theta_x = \theta_z = 5\text{x}10^{-6} \text{ radians} = 1.03 \text{ arc seconds.}$$

Since the x slide was moved and returned to the same coordinate, the displacements are repeatability errors only and will be less than for the y slide.

$$\beta_x = 2\text{x}10^{-6} \text{ radians repeatability}$$

$$\delta_y = 10 \text{ microinches repeatability}$$

Also, for the machine configuration shown, let:

$$a = 12"; \quad b = 8"; \quad c = 5",$$

and substituting values in Equation (3.17),

$$\varepsilon_y = a\theta_x + b\theta_z + \Delta_y + c\beta_x + \delta_y$$

$$\varepsilon_y = 5\text{x}10^{-6}(12 + 8) + \Delta_y + 5 \text{ x } 2\text{x}10^{-6} + 10\text{x}10^{-6}$$

$$\varepsilon_y = 120 + \Delta_y \text{ microinches.}$$

So, the "worst case" geometric measuring error is 120 microinches to be added to scale error Δ_y. All error sources would likely not have the same sign and some cancellation would occur. By the same token, the assumed values for θ_x and θ_z were small and could have been larger if a heavy part were being measured. In any event, the same values will be used for comparison when calculating the geometry errors for the AGTCMD.

Refer to Figures 3.6, 3.7 and 3.8 when the AGTCMD geometric machine errors are discussed. These show the side, front and top views of the machine. The symbols used in the previous example also apply for this analysis.

It will be noted from the diagrams that the measuring point (probe) is fixed in the x-y plane and is located at the intersection of the x and y interferometer beams. The interferometers are also fixed so the relationship does not change. Therefore, mensuration takes place by moving the "part" in x and y. This means that the factors b, c and d of the previous example are now equal to zero and it can be seen which terms cancel by looking back at Equations 3.16, 3.17, and 3.18. These are the terms relating to angular displacements of the slides. Now, by mounting the x and y mirrors on the same plate as the inspection part, the errors associated with lateral straightness of travel (δ_y and δ_x) of the slides are eliminated. This is so because the y stage straight line motion errors are read by the x axis interferometer and can be corrected for by motion of the x stage; or it can be accounted for by software computation as a differential reading between the interferometer and probe. When correcting the error by motion of the other axis, the straight line motion is determined by the flatness of the mirror and this error is about 2 microinches compared to 40 microinches for a typical stage.

The offset factor not eliminated by the AGTCMD geometry is labelled "a" in the diagram. This factor relates to measurement in the z axis. It will be noted, however, that the magnitude of "a" is much smaller than the measuring machine of Figure 3.5 because the laser beam is centered at the mid range of z motion. Hence, for a 1/2 in. thick gear, "a" equals 0.25 inches up to 1.5 inches maximum for a 3-inch thick gear. The gear mounting fixture to be provided in Phase II sets the gear at the optimum height.

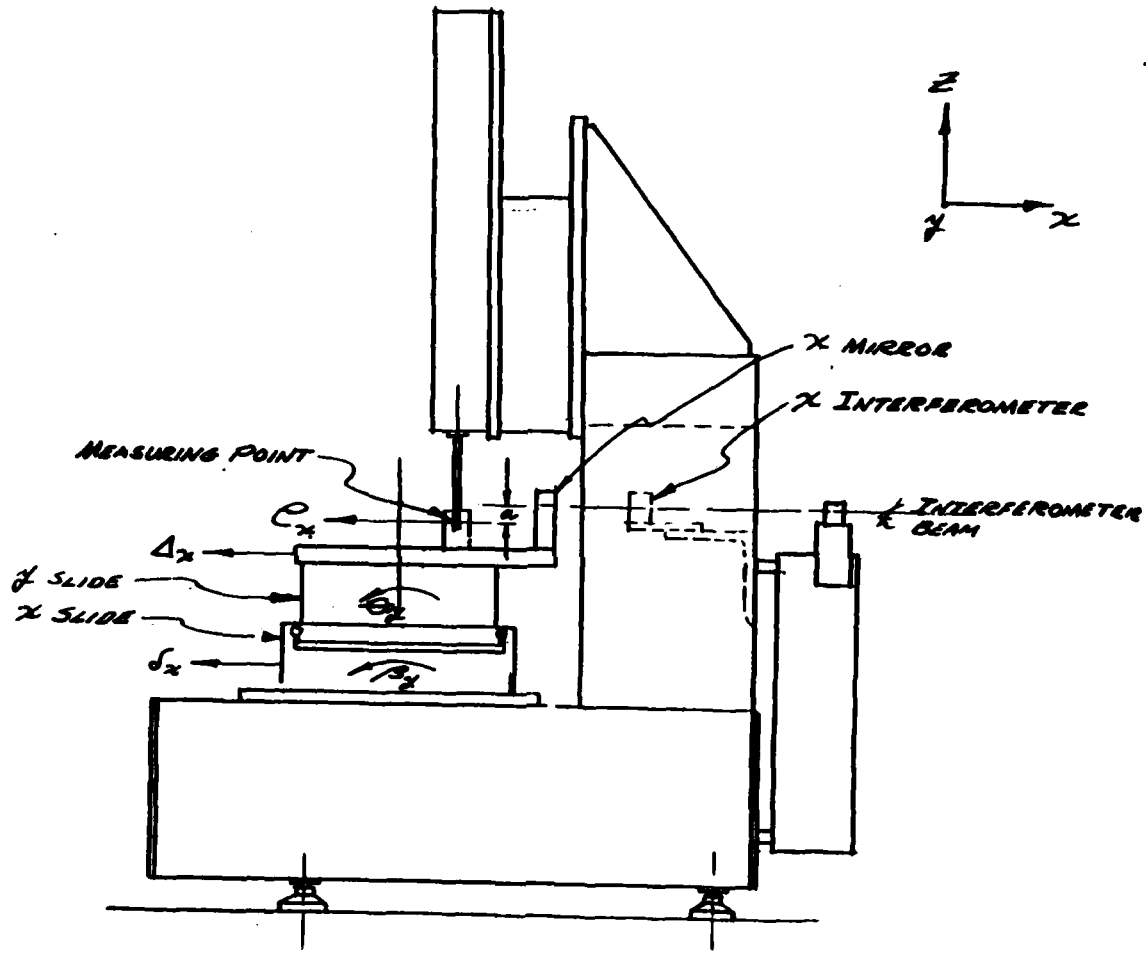

Figure 3.6 Side View — AGTCMD Geometric Machine Errors

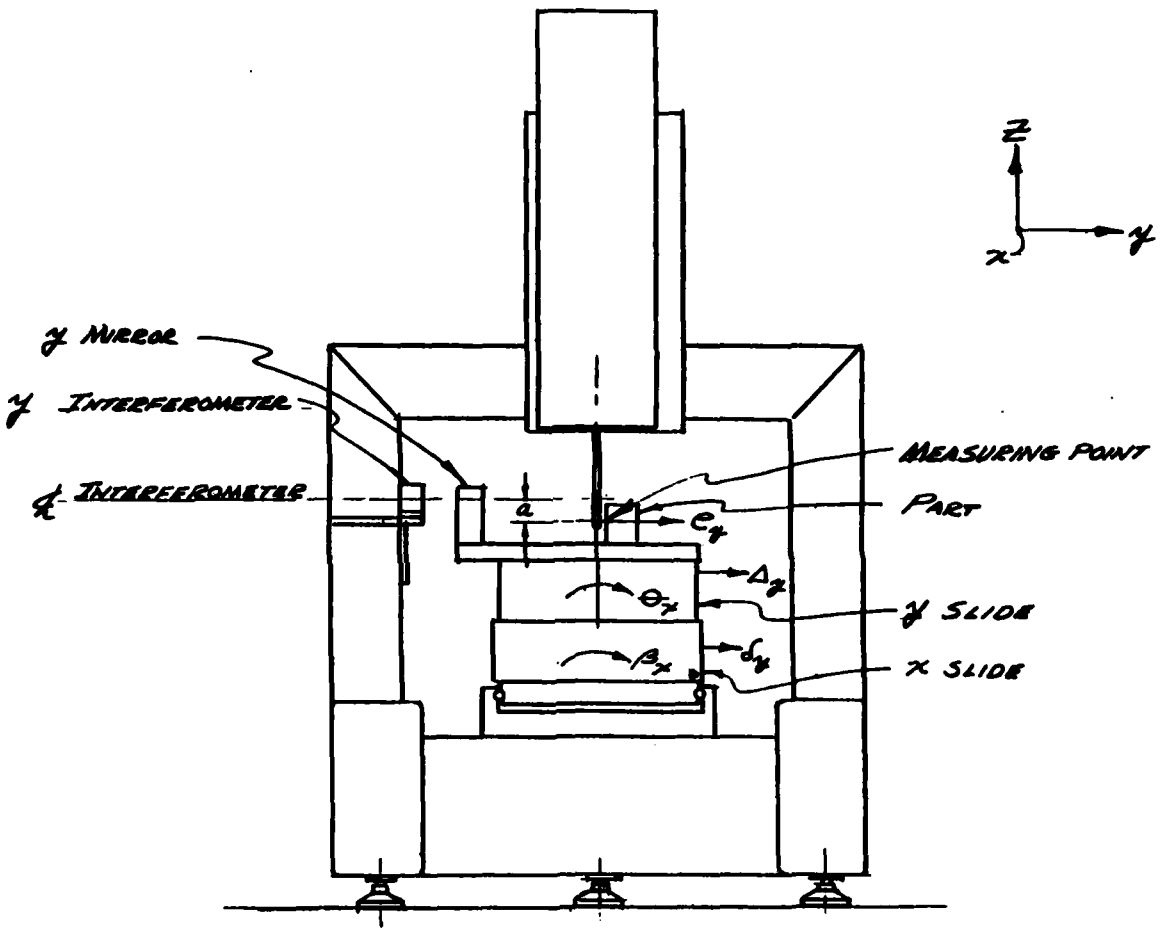

Figure 3.7 Front View — AGTCMD Geometric Machine Errors

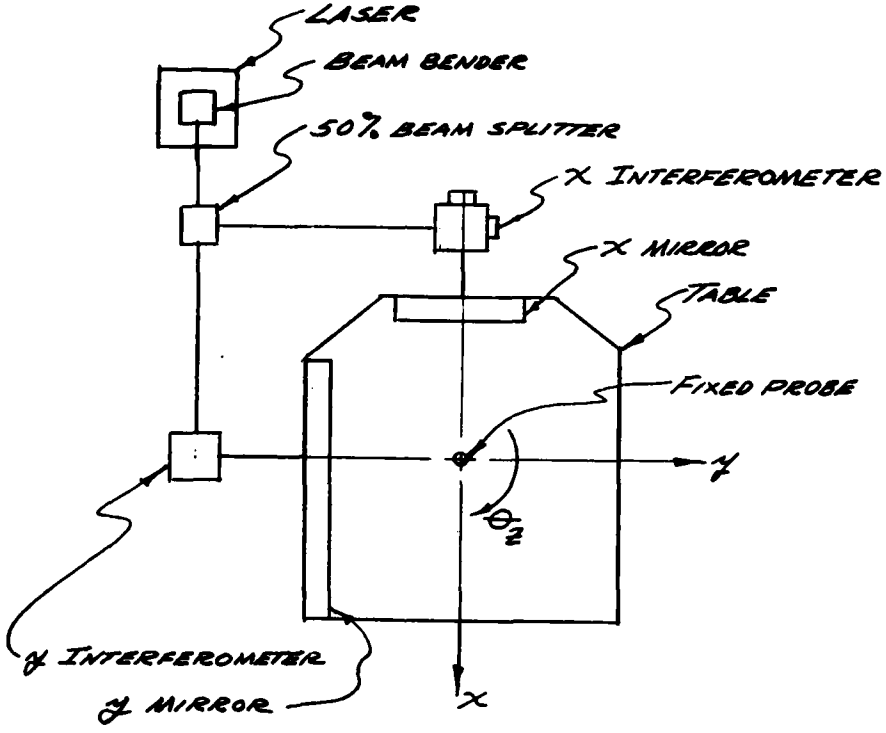

Figure 3.8 Top View — AGTCMD Stage Interferometer

Having described the geometry, the equations for the AGTCMD can now be written:

a. y Slide Error

$$\varrho_x = a\theta_y \tag{3.19}$$

$$\varrho_y = a\theta_x \pm \Delta_y \tag{3.20}$$

$$\varrho_z = \Delta_z \tag{3.21}$$

b. x Slide Error

$$\varrho_x = a\beta_y \pm \delta_x \tag{3.22}$$

$$\varrho_y = a\beta_x \tag{3.23}$$

$$\varrho_z = \delta_z \tag{3.24}$$

c. Combined x-y Slide Errors

$$\varrho_x = a\theta_y \pm a\beta_y \pm \delta_x \tag{3.25}$$

$$\varrho_y = a\theta_x \pm \Delta_y \pm a\beta_x \tag{3.26}$$

$$\varrho_z = \Delta_z \pm \delta_z \tag{3.27}$$

For a comparison of the errors between AGTCMD and bridge-type machines, the same slide performance is used for a measurement along the y axis:

$\theta_x = 5\text{x}10^{-6}$ radians

$\beta_x = 2\text{x}10^{-6}$ radians repeatability

and from Equation (3.26):

$$\varrho_y = a(\theta_x + \beta_x) \pm \Delta_y$$

$\varrho_y = 7a + \Delta_y$ microinches.

Hence, the geometric error ranges from 1.75 microinches for a 1/2-inch thick gear to 10.5 microinches for a 3-inch thick gear for the same conditions of the earlier analysis. The interferometer scale error (Δ_y) was discussed in Section 3.1.

Orthogonality*error in the x-y plane is governed by the squareness of the x and y mirrors and not the x-y slide. Fine adjust eccentrics are provided for setting the mirror orthogonality.

*Orthogonality: Accuracy of mutually perpendicular axes.

3.3.2 Cosine Error

This error source relates to alignment of the measurement axis with the axis of table motion. There are two elements to be considered regarding the measurement axis. These are the parts to be measured and the scale that records the measurement. We can illustrate better what is involved by the example shown in Figure 3.9.

For clarity, the cosine error (θ) is greatly exaggerated. In this example, the width of the channel in the part (dimension x) is to be measured. The fixed measuring probe nulls on the part of point 1 and the table moves to the left until the probe nulls at point 2. It can be seen that the illustrated horizontal motion of the table is the hypotenuse of the triangle. The part is x wide and the table has traveled δ_x. The error (ε_p) is the difference between the two dimensions, or:

$$\varepsilon_p = \delta_x - x,$$

and since $x = \delta_x \cos \theta_p$,

$$\varepsilon_p = \delta_x(1 - \cos \theta_p) \tag{3.28}$$

The part measuring error (ε_p) described by Equation 3.28 does not consider the scale alignment error in measuring table displacement (δ_x). There is an interaction between the two, where errors can sum or cancel for the mirror/interferometer scale of interest.

Referring to Figure 3.9, the mirror is shown perpendicular to the motion axis but the interferometer beam is misaligned by angle θ_s. The table displaced δ_x but the point on the mirror displaces δ_s along the beam path. In terms of δ_x, the scale error δ_s is

$$\varepsilon_s = \delta_x \left(\frac{1}{\cos \theta_s} - 1 \right) \tag{3.29}$$

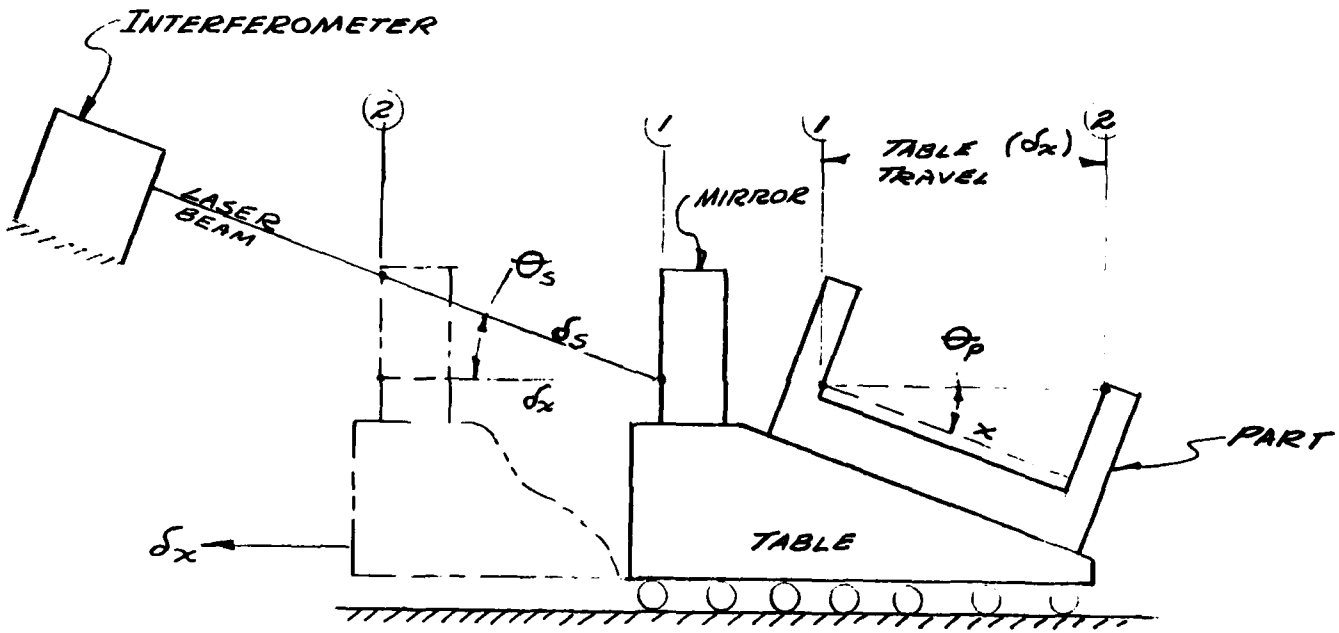

Figure 3.9 Cosine Error Diagram

and the total part measurement error is

$$\varrho_t = \delta_x \left[\left(\frac{1}{\cos \theta_s} - 1 \right) + \left(1 - \cos \theta_p \right) \right] \tag{3.30}$$

If the mirror surface were parallel to the side surfaces of the part, rather than perpendicular to the axis of motion as shown, the interferometer would measure short and would cancel the longer than true table displacement. For the case where the laser beam is parallel to the axis of motion, the cosine error is zero and is independent of small mirror angles. It is academic to go into other geometric combinations since it is only necessary to recognize that cosine error exists. This is true because the error is small in relation to angle θ; and the error can be made negligible by proper machine set-up. For a θ angle of 0.1 degrees, the cosine error is 1.52 microinches per inch of table travel. Assume that the machine table top is 12 in. long with a T.I.R. of 0.005 inches over the 12-inch travel. This is equivalent to an angle $\theta_p = 0.0239^\circ$ and from Equation (3.28), $\varrho_p = 0.087\,\delta_x$ microinches. Similarly, the interferometer laser beam can be aligned by an autocollimation technique from an optical square mounted on the table top.

In summary, the cosine error can be large if the sources contributing to it are disregarded, but given recognition, the machine can be set up so that the error is negligible.

3.4 THERMAL EFFECTS

It is well recognized that part size varies with temperature and that microinch level measurement must be done in a controlled environment. It could also be said that the magnitude of the error and factors contributing to it are not always fully appreciated, and are often disregarded by parts inspectors. Thermal errors are thus the cause of frequent disagreement between different inspection houses. The mensuration accuracy desired for the AGTCMD is such that thermal errors are a major contribution to the total error budget. It is important, therefore, to analyze thermal error in detail in order to compensate for its effects and to set guidelines for inspection procedures.

It was earlier mentioned that the size of a part must be measured relative to a reference temperature in order for the measurement to have any meaning. The international reference temperature is 68° F and if the environment, part and measuring equipment could be held to this exact temperature, thermal errors could be ignored. As this is not the case, consideration must be given to the fact that the machine will operate in a room having temperature excursions, where the greater the rate of change, the larger the error.

Other than the perfect environment, there are two basic conditions to consider:

a. Stabilized conditions at some constant temperature other than 68° F.

b. Thermal transients during the measurement cycle.

3.4.1 Stabilized-Steady State Condition

The most unwanted of the two is condition (b) where a change in temperature occurs during a measurement cycle, after the machine has been initialized.* This causes a shift in zero datum and possible structural thermal gradients. A measurement taken at a stabilized, constant temperature of, say, 72° F is preferred to a situation where the room temperature changes from 68° to 69° F during the measurement. This is true because the stabilized condition allows for compensation from known data—the expansion coefficient of the inspection part. The compensation of the laser wave-

*Initialization: Zeroing-out of the x-y-z position transducer with the rotational axis of the gear turntable.

length according to Equation 3.2 was discussed in Section 3.1. It was also noted that the compensation factor is only one microinch/inch per ^{o}C. Now, if the machine scale were a steel lead screw on linear glass encoder, it would be necessary to contend with compensation factors of about $11.7/^{o}C$, and $6.3/^{o}C$, respectively. Hence, with the laser interferometer corrected for the environment by an automatic compensator, an absolute linear scale with very small thermal error results. What remains, then, is the accuracy in measuring the temperature and certainty in the expansion coefficient of the part. The Phase II machine will have a sensor located on the table near the part to represent the part temperature and will communicate with the same automatic compensator that corrects for laser wavelength. With an input of the expansion coefficient of the part, the interferometer scale will measure a 72^{o} F part as though it were at a temperature of 68^{o} F. In other words, the scale has a built-in compensation much like the pattern maker who uses a special scale to allow for thermal shrinkage of castings; except that in this case, it shrinks and expands by the same amount as the part.

So, Equation (3.1) becomes

$$y = x = \frac{D_c}{8Mc} \lambda_{vac} \left[C - \alpha_p \left(T_p - 68 \right) \right] \tag{3.31}$$

where

α_p = Part material expansion coefficient/^{o} F

T_p = Part temperature, ^{o}F

$y = x$ = Absolute size of part inspected.

Equation (3.31) is valid for measuring a part under stabilized steady state conditions at temperatures other than 68^{o} F. The proposed Phase II machine will have the H.P. compensator which will automatically handle the terms in the bracket when

the material expansion coefficient (α_p) has been input. This is desirable since a room may not be available where the temperature can be held to 68° F. The temperature compensating feature allows measurement to an accuracy level where temperature offsets would otherwise cause relatively large errors. The mensuration error encountered when operating in a room having a constant temperature other than 68° F results from uncertainty in the value of the expansion coefficient of the material, but this is a small error.

3.4.2 Transient Conditions

The steady state conditon discussed in the previous section has limited usefulness because an environment that cannot be controlled to the 68° F reference temperature may also be one that has rapid unidirectional changes in air temperature, which is the condition that will be addressed in this section.

As already mentioned, it is under transient condition where the largest thermal errors occur. These effects are minimized by the following:

a. Provide a machine structure with a large thermal mass. Consistent with the portability concept, this is done by fluid filling the hollow machine, as was discussed in Section 2.1. This minimizes structural thermal gradients and bulk temperature changes and thus provides the thermal inertia that allows longer measuring cycles for a given thermal error.

b. Operate in a temperature-controlled room where the excursion is small. The air temperature can have rapid fluctuation so long as it is plus and minus about a nominal value. It is desirable that this be ± 1° F and since control means are needed for this, it is better to select 68° F as the nominal to reduce errors from uncertainty in the material coefficient of expansion. The structure, because of its large thermal mass, thus does not respond to the fluctuation in air temperature.

c. Minimize heat conductance into the structure from unstable heat dissipating components and allow a machine warm-up time interval (from cold start) prior to its use. The major heat generating components are located in the stand-alone console. The laser for the interferometer must be mounted on the structure and dissipates 15 watts. To reduce heat transfer to the structure, it is mounted vertically in a sheet metal channel conducive to convective heat transfer. The channel is insulated from structure by a thin wall stainless steel tubing mounting. This gives mounting rigidity while providing resistance to heat conductance. The 300 series stainless steel used has a conductance that is one-third that of carbon steel and the design calculations show that only about 10% of the laser heat is conducted into the structure.

d. Design the system so that it can be remotely operated as a means of minimizing heat input from the human body. Heat transfer from the body to the machine occurs by radiation and by conduction when hand-contacted. Since this heat load is transient by nature, it can produce large errors.

Thermal compensation could be considered for the structure but this would be of value only for a uniform bulk temperature change of the whole structure. Since transients cause gradients, it is not practical to attempt this. Rather, reliance is placed on the thermal stability of the machine after initialization of a measuring cycle. Even in a poorly controlled room, cycle times of around 5 minutes would result in small errors due to structural distortion. However, changes in air temperature pressure and humidity still affect the wavelength of the interferometer laser beam because this aspect has no thermal inertia. This was discussed in Section 3.1.1 and was described by Equation 3.2. So the final equation for environmental compensation of the machine and the part as an absolute measuring system is:

$$y = x = \frac{D_c}{8M_c} \lambda_{vac} \left[C - \alpha_p \left(T_p - 68 \right) \right] + \left(\frac{C - C_o}{C_o} \right) L_D \quad (3.32)$$

It should be noted that the part temperature (T_p) is being recorded by a sensor mounted to the table. As a result of this, a part placed on the table must be allowed to stabilize to equilibrium by conductive heat transfer. The time required for this is primarily a function of the mass of the part and its differential temperature. Minimizing the differential temperature is done by storing the parts to be inspected in the temperature controlled room near the inspection machine and keeping to a minimum the time that the part is manually handled during machine set-up.

3.5 MACHINE CALIBRATION/INITIALIZATION

There are three basic calibration functions that are required: the noncontact probe radius (r); the z axis straightness of motion, and the zeroing-out (initialization) of the x-y-z position transducers with the rotational axis of the gear turntable. The z axis straightness of motion is a machine constant which, once determined, should not require recalibration. The probe radius and slide position initialization would be done with each gear set-up. The sequence would first involve the probe radius and then the slide position.

3.5.1 Z Axis Straightness of Motion

In Section 3.3,the errors associated with angular and lateral displacement of the x and y slide were analyzed. It was stated that owing to the alignment of the interferometer beam with the measuring point, the x-y plane mensuration errors were either eliminated or reduced to negligible values. This cannot be done for the z slide as its motion produees x and orthogonality errors in the third dimension. These errors will be calibrated out with the same gauge used to calibrate the probe radius. For this purpose, the gauge will have two flat faces at right angles that are 3-1/4 in. long—one for the x component and the other for the y component. The face of the gauge will be scanned along the z axis and the displacement errors of the slide will be compared with the gauge face whose flatness is better than two microinches. The z axis slide will have a start of stroke "Home" position in the form of an encoder slit or optical switch. The "Home" position will be known relative to the gear face mounting on the turntable. Since the face width of the gear will be input data to the computer, the face width scan zone for a particular gear will be known relative to "Home" position. Therefore, the straightness of motion error determined by calibration can be compensated for in software. These errors will be stored in a software "look-up" table and applied as corrections at incremental z coordinates.

3.5.2 Probe Radius

The laser probe radius is calibrated on a fixed gauge cube whose absolute thickness is known in the x and y axis to one microinch. A thermal sensor attached

to the table will allow compensations for any small temperature changes. Holding z and y fixed, the probe will sense the gauge surface along the x axis, rotate through a β angle of 180^{o} and sense the other surface. The probe radius will then be:

$$r = \frac{\Delta x - t}{2}, \qquad (3.33)$$

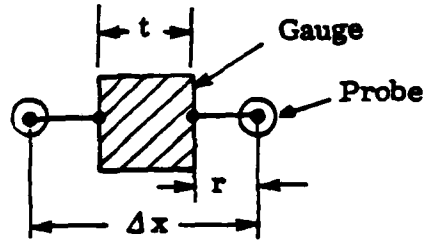

where Δx = x stage interferometer reading

t = gauge thickness.

This is repeated in the y axis so that runout error in the β bearing can be accounted for.

The probe is calibrated over its range of linearity for the purpose of machine operation in the Size or Surface Profile modes as well as for continuous fly scanning.

3.5.3 X - Y Coordinate Zero Datum Initialization

As mentioned earlier, the datum for measurement of all gear parameter is the bore of the gear. Gears to be inspected are mainly ring gears with bore sizes ranging from 1 to 10 inches in diameter. The bore diameter and roundness tolerances are expected to be large relative to the mensuration accuracy of interest, and since we have chosen to nominally position the gear on the turntable, the bore runout of about 200 microinches will be accounted for in software.

The first task is to initialize the x and y interferometers with the rotational axis of the turntable. A pilot ring permanently fixed to the turntable and with radial runout of less than 3 microinches provides the means for this calibration. The probe will be computed-commanded to move to the rotating ring for the calibration sequence. As shown in Figure 3.10, the probe moves from the start position (actually, the stage moves relative to the probe) along the x axis and seeks the high point of the ring. At this x coordinate, the probe moves along y until r = null, thus establishing y. The

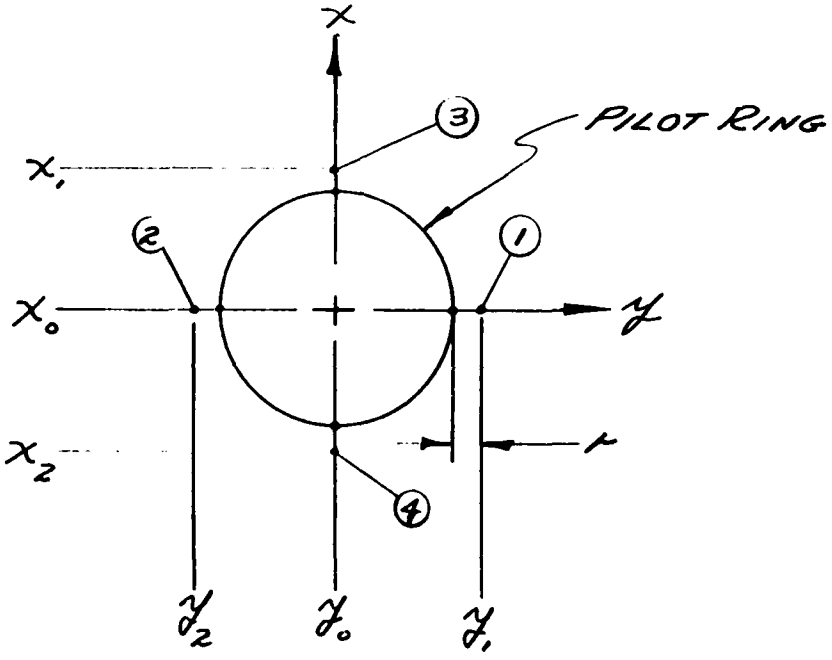

Figure 3.10 X-Y Coordinate Initialization

probe then rotates 180° and moves to position 2 at the same x coordinate and again moves along y until r = null and establishing y_2. The y datum (y_o) is then

$$y_o = \frac{y_2 - y_1}{2} \quad @ \quad r = \text{null} . \tag{3.34}$$

Since y_o is now known, the probe is commanded to move to point 3 at y_o. The sequence described above is then repeated for x_1 and x_2; whereby:

$$x_o = \frac{x_2 - x_1}{2} \quad @ \quad r = \text{null}. \tag{3.35}$$

Next, it will be necessary to probe the gear bore to determine its average bore axes offset. At coordinate y_o, the probe moves along the x axis until it nulls out on the rotating gear bore. While maintaining probe null, the x interferometer reads the runout which is a combination of mounting eccentricity and out-of-roundness. Data points can be taken at 5 degree increments to allow computation of a "best fit" circle by the least squares method. From this, the mounting eccentricity (E) is determined and the coordinate correction factors (Δ_x) and (Δ_y) for measurements taken at any gear rotation angle (θ) will be:

3.6 NONCONTACT OPTIC PROBE

3.6.1 Optical Element

The concept and elements of the Phase I optic probe are illustrated in Figure 3.11.

The light beam from a 7 mW helium neon laser is chopped by a set of oscillating blades at a frequency of 800 Hz. This permits exclusion of signals derived from other sources of light. Spatial filtering of the laser beam is done with a microscope objective focussing onto a pinhole aperture. This minimizes the signal instability by reducing the effects of variations in energy occurring over the area of the beam spot. The beam is then focussed onto the SELFOC lens by the relay lens. The SELFOC lens is a long, small diameter, graded refractive index glass rod. It transfers the image from one end directly to the other end. The exit end of the rod is fitted with a 45^{o} fold mirror for imaging normal to the surface of the gear tooth. The light reflected from the surface of the gear returns through the optical train and, by means of the beamsplitters, is focussed onto the two detector pinhole apertures. The beamsplitter shown near the detectors transmits 50% of the energy to detector (A) and reflects 50% to detector (B).

Now, one of the detector pinholes is set forward of focus and the other is set in back of focus. In this way, the spot diameter of the beam reflected from the gear surface overfills the pinholes. Only a fraction of the reflected energy is received by each of the photodetectors. When the laser spot is focussed onto the surface of the gear, the energy received by each sensor is equal and it is at this location that the probe is at "Null." When the probe is displaced from the gear surface, the light received by one detector increases while, at the same time, it decreases for the other. The signals derived therefrom are shown in the top diagram of Figure 3.12. These signals are fed into a difference and summing amplifier, where the output of the difference amplifier indicates the magnitude of probe displacement and the output of the summing amplifier accounts for variations in gear face reflectance. The difference signal (A-B) is shown in the lower diagram of Figure 3.12. The operating range is the linear portion of the curve indicated. The slope of the curve represents the sensitivity or resolution of the probe.

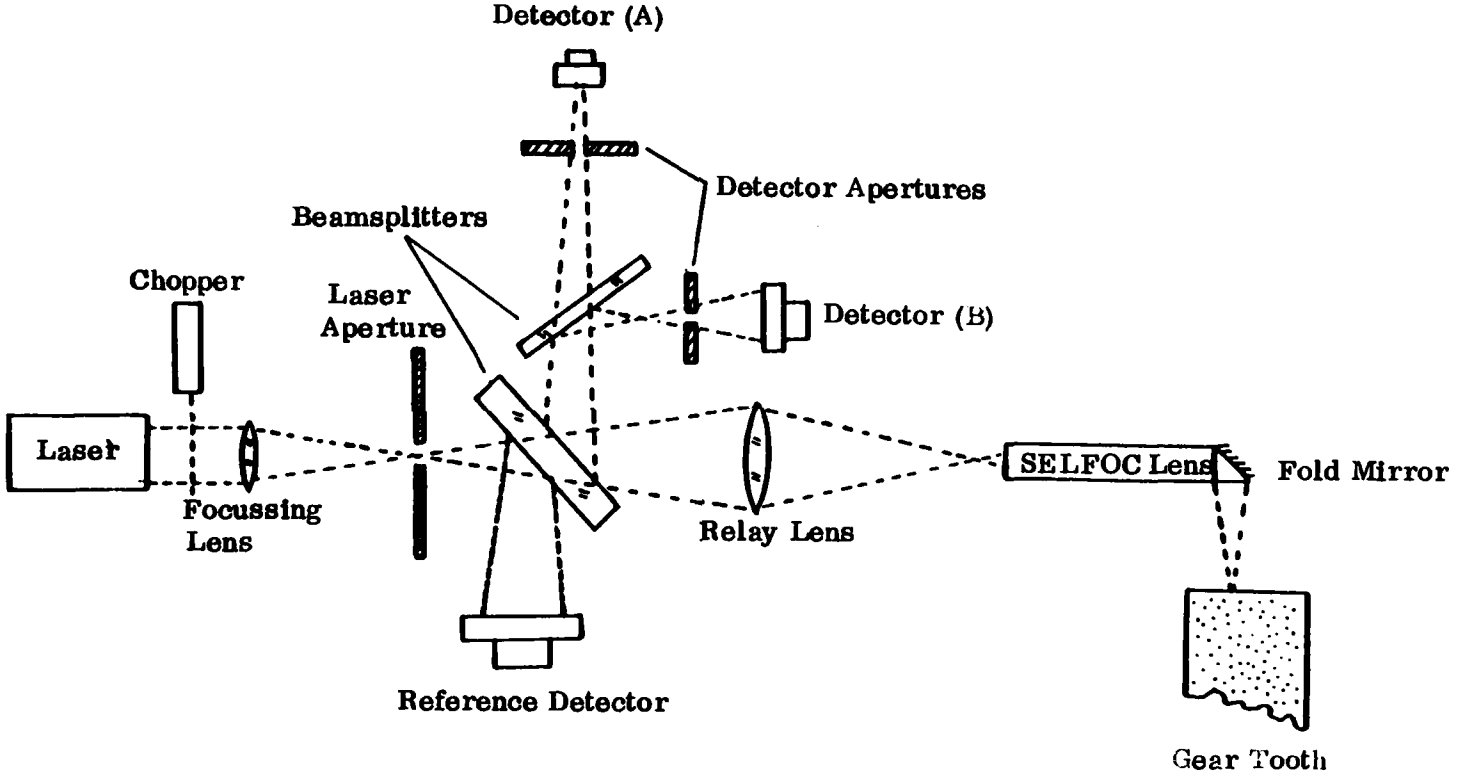

Figure 3.11 Optical Probe Design

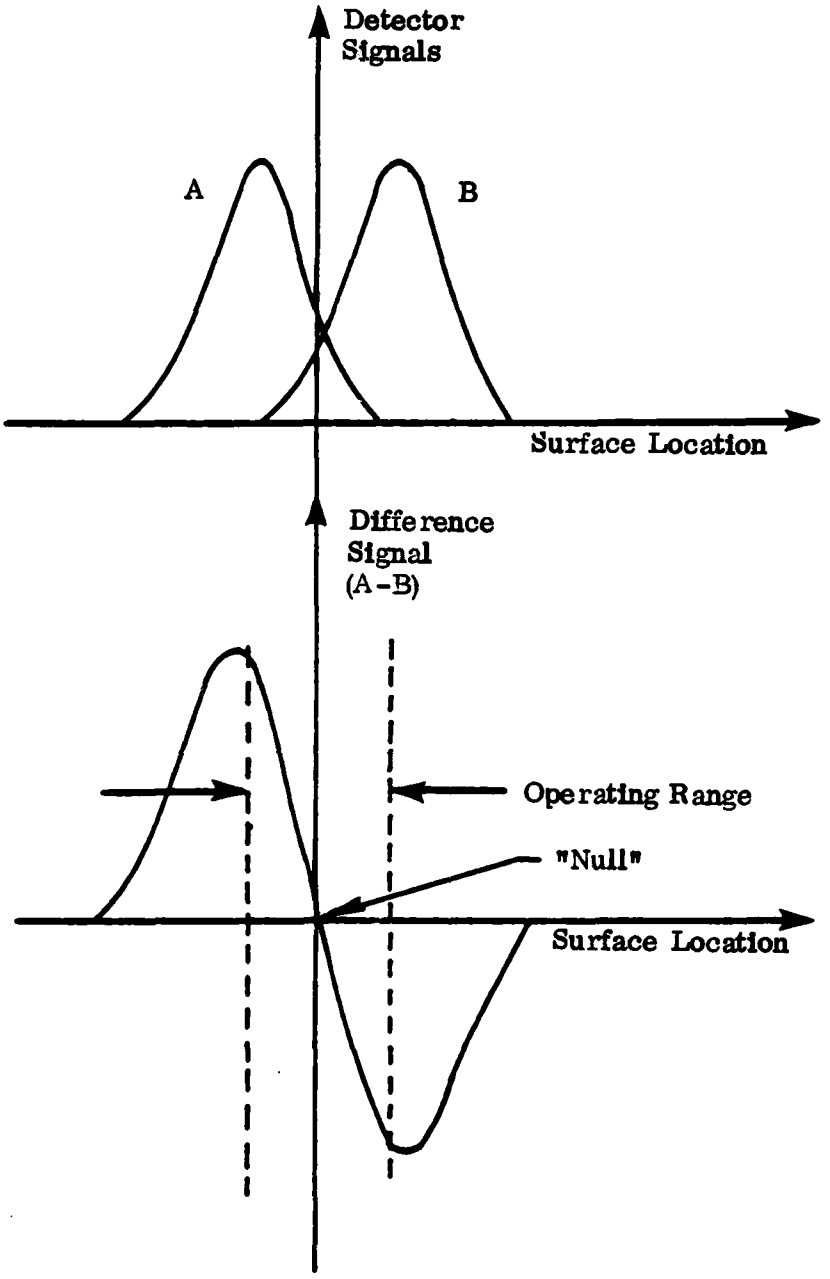

Figure 3.12. Probe Signals

Symmetry of the signal depends on how equal each of the detector pinholes has been set from focus as well as the accuracy of radial alignment with the optical axis. The sensitivity of the probe is a function of the magnitude of the offset of the pinholes from focus. It is also related to the f/number of the optical system. A low f/number is desired and the limitation is now at f/8 due to the N.A. of the SELFOC rod.

3.6.2 Processing Electronics

The processing electronics for the optical probe are illustrated in block diagram form in Figure 3.13. The electronics have been designed to process the signals from the two silicon photodiodes so as to eliminate the effects of variations in illumination level or variations in surface reflectivity, while at the same time maximizing the sensitivity to positional displacements of the target. Additionally, the processing electronics provide a high degree of immunity to variations in ambient illumination levels.

In order to minimize the effects of ambient illumination and to provide operation at an electrical frequency where I/F noise is not of significant concern, the laser illumination is "chopped" by a tuning fork type of modulator. The frequency of modulation is 800 Hz. The tuning fork type of modulator produces a quasi-square wave type of modulation with a frequency stability of about 1 or 2 Hz. The signal originating from the detector thus consists of an 800 Hz carrier and whatever additional modulation is present.

From the electronics block diagram, it can be seen that the following processing occurs. First, the photodiode signal is converted from current to voltage. The nominal gain is 10 million volts per incident watt. The nominal detector noise equivalent power is about 10 picowatts. It is desired to operate at signal-to-noise ratios of 1000:1 or better. Thus we are looking at a signal range of 100 to 1 microwatts which provides a preamp signal range of 0.1 to 10 volts. The active filter provides an electrical bandpass of 100 Hz, centered at 800 Hz. The gain amplifier, which in reality precedes the filter circuit, has a variable gain of between 1 and 10. Following the gain amplifier, the signal is full wave rectified by a synchronous detector and then low pass filtered to 50 Hz.

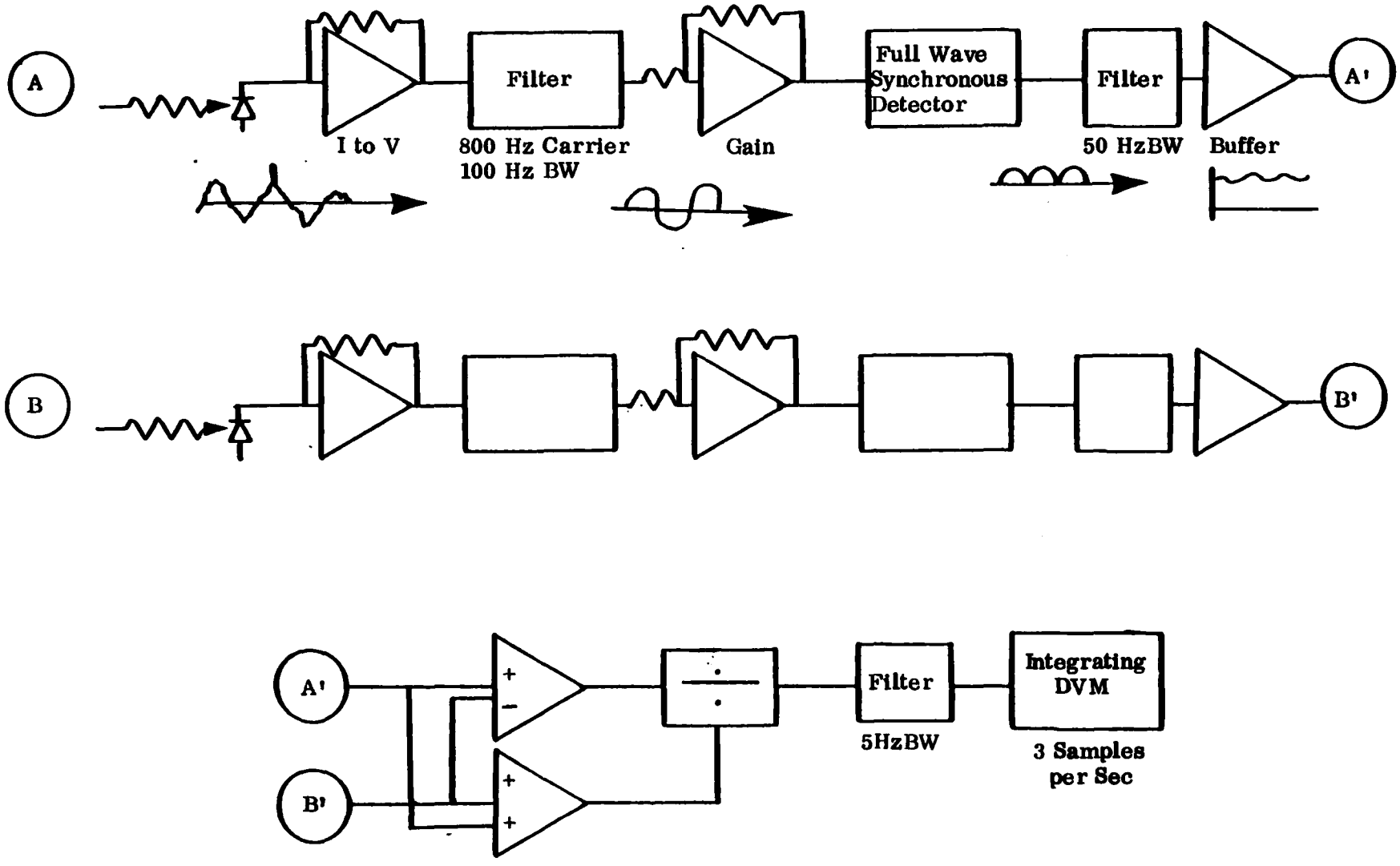

Figure 3.13 Probe Processing Electronics

At this point, the signals from both detector channels have been demodulated and are ready for differencing and normalization. The A and B signals are supplied to sum and difference amplifiers and then into an analog divider to provide the (A-B)/(A+B) signal which is the normalized difference signal.

Because of susceptibility to building and probe vibration, it was found desirable to include a final 5 Hz filter for breadboard testing. Following this filter, the final signal is sent to the digital panel meter which updates every 1/3 second.

4. PERFORMANCE TESTING/RESULTS

4.1 THERMAL STABILITY TESTS

Figure 4.1 shows the machine test set-up for the series of tests conducted to evaluate the thermal stability of the machine. A B&S Model 599-981 electronic indicator with one microinch resolution was clamped to the bridge structure. The measuring point on the part has a z offset of 1 to 1-3/8 inches for the various tests. This offset relates to the geometric errors that were discussed in Section 3.3.1.

The thermal stability tests involved zeroing-out the y interferometer count and the indicator meter at time (t_o) and then observing the readings from both sensors over some time interval.

The mensuration errors resulting from environmental effects were discussed in Sect. 3.1 for the interferometer scale and Sect. 3.2 for the machine. It was stated that laser wavelength changes with air temperature pressure and humidity, that the machine structure distorts from thermal gradients and that the linear dimensions of the part and machine change with temperature. All of these things occurred during the tests conducted. Since the stage was not displaced after initialization, the distance from the interferometer to the mirror is all deadpath (L_D) and the term $\left(\frac{C - C_o}{C_o}\right) L_D$ from Equations 3.2 or 3.32 applies for the changes in the interferometer scale. All tests for which the data are plotted in Figures 4.2 to 4.7 were conducted in an uncontrolled environment and without fluid filling the structure. Further, the data plotted are raw data, uncorrected for the change in the interferometer scale according to the preceding deadpath term.

By way of comparison, the test data of Figures 4.8 to 4.11 show the improvement achieved in thermal stability by fluid filling the structure and controlling room air temperature.

Figure 4.2 shows what happens when the machine is turned "on" from a cold start. The interferometer reading changed by + 80 microinches and the indicator reading by about - 30 microinches over a 160 minute interval. The (+) sign for the interferometer signifies an increase in the dimension (L_D) shown in Figure 4.1. The (-) sign for the indicator represents a motion of the stage to the left. Hence, the difference between

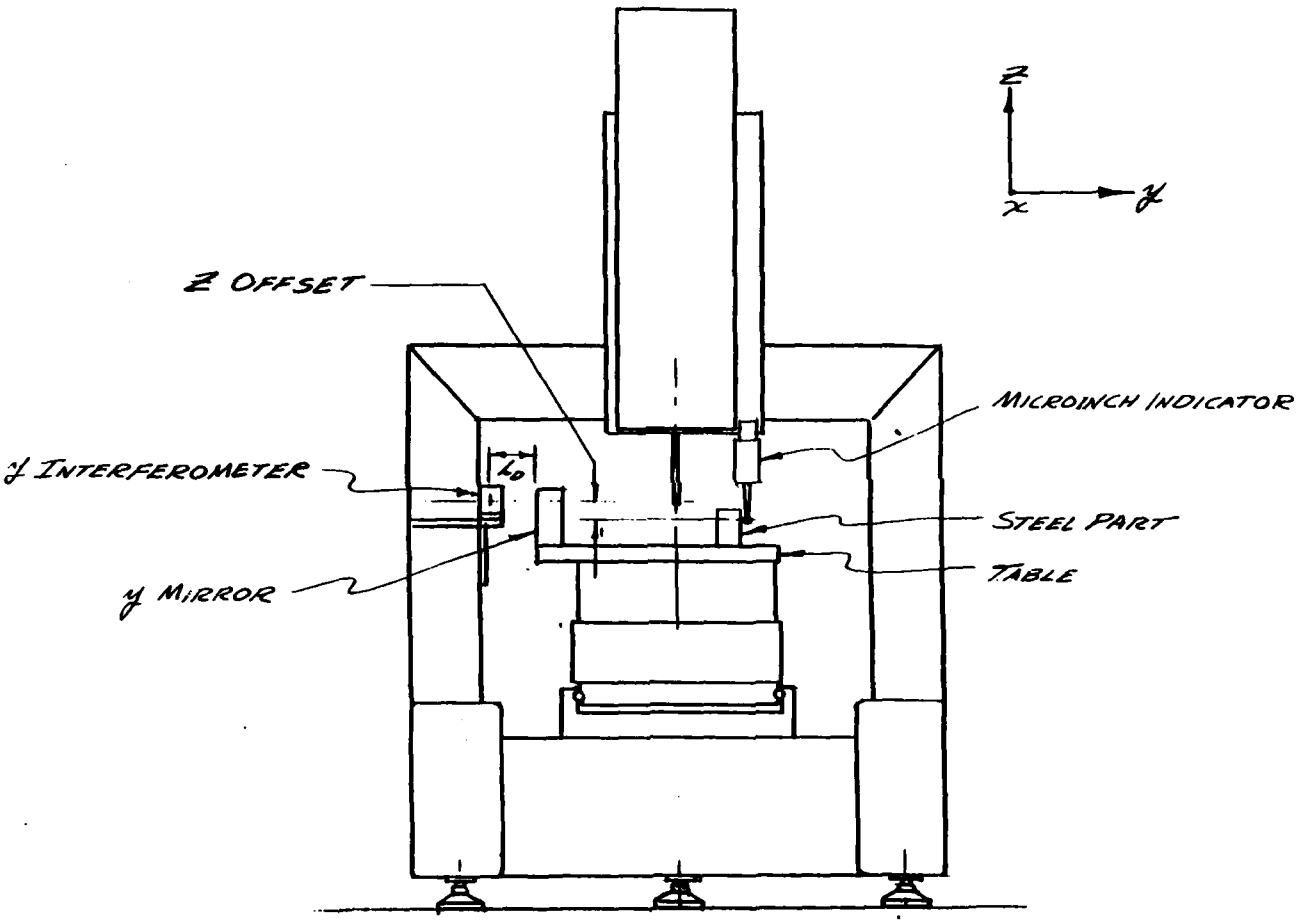

Figure 4.1 The Thermal Stability Test Set-Up

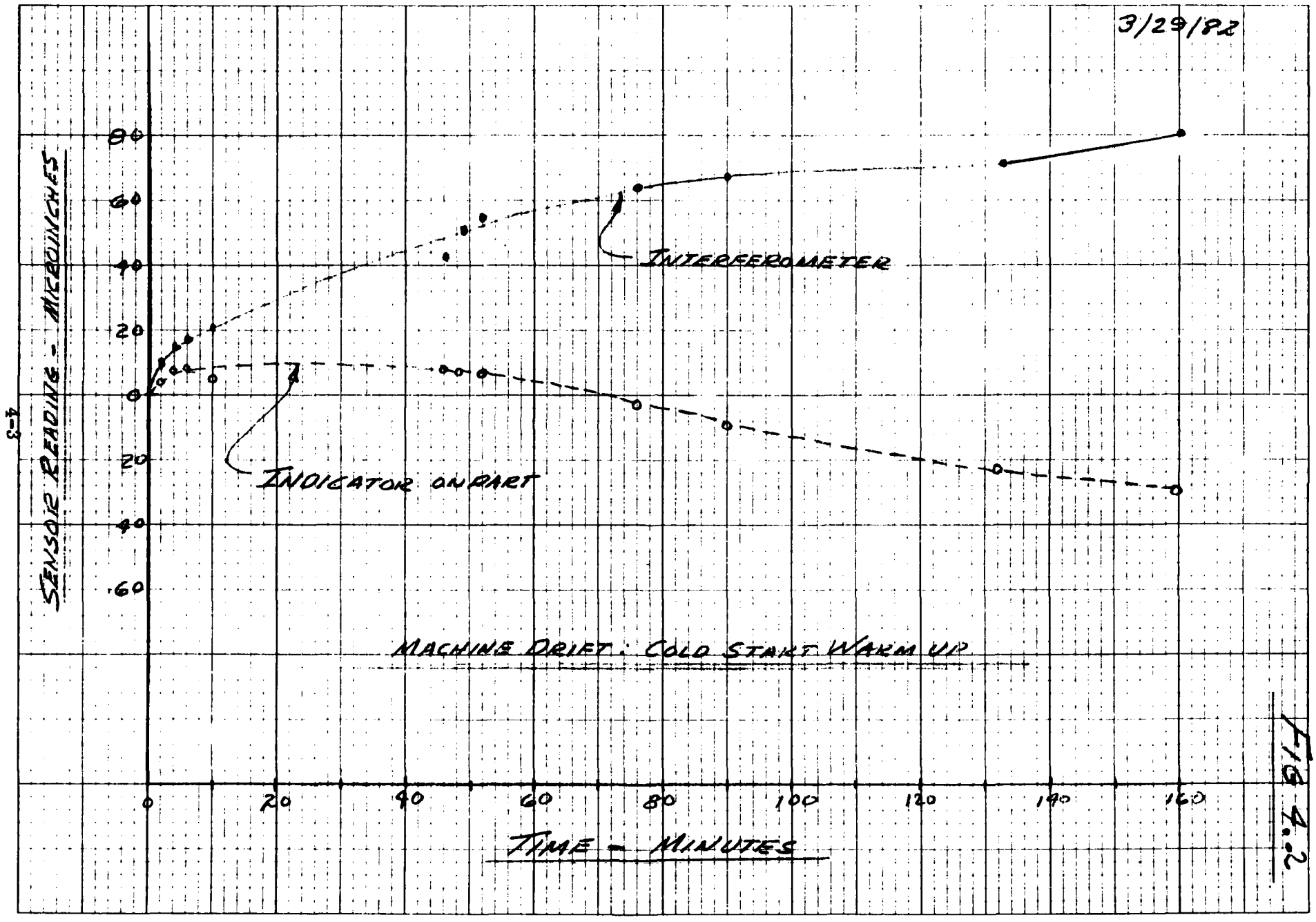

FIG 4.2

the two curves of Figure 4.2 is the mensuration error after initialization. For example, for a 40-minute measuring cycle, the last measurement would be in error by about 40 microinches due to environmental effects. In terms of the desired accuracy, this is a large error; but this is to be expected when the machine is first turned on. The system has to stabilize from the heat conducted from the laser and the placement of a part having a differential temperature. Figure 4.3 shows data recorded from the same test set-up but after about 4-hour machine warm-up. The mensuration error here, over a 40-minute measuring cycle, is about 7 microinches and stabilizing to 17 microinches; this is again the difference between the two curves. Also shown in Figure 4.3 is the unidirectional temperature change of 1^{o} C occurring over the 160-minute interval.

The interferometer scale change due to a temperature change from 23^{o} to 24^{o} C for a deadpath L_D = 4 inches is:

$$\left(\frac{C - C_o}{C_o}\right) L_D = \left(\frac{.999728 - .999727}{.999727}\right) 4 = 4 \text{ microinches}$$

hence, the major portion of the drift error is in the structure and part.

The test plotted in Figure 4.4 was run the next day with the machine power on overnight. It shows that drift continues after machine warm-up due to room ambient changes.

Most of the drift was in the indicator reading. Room temperature change was no greater than 2^{o} F over the test period. Up to the time interval of 102 minutes, the machine was left unattended and only two data points were taken. After that, the person recording the data was in close proximity of the machine causing body heat transfer to the machine.

The test plotted in Figure 4.5 was done specifically to determine body heat effects. Up to the 16-minute interval, the drift is due to changes in room ambient. It is noted that the difference between the probe and interferometer represents an error of only 2 microinches. The 10-minute interval from point (1) to (2) shows what happens when the hand crank support housing is hand-contacted. From point (2) to (3)

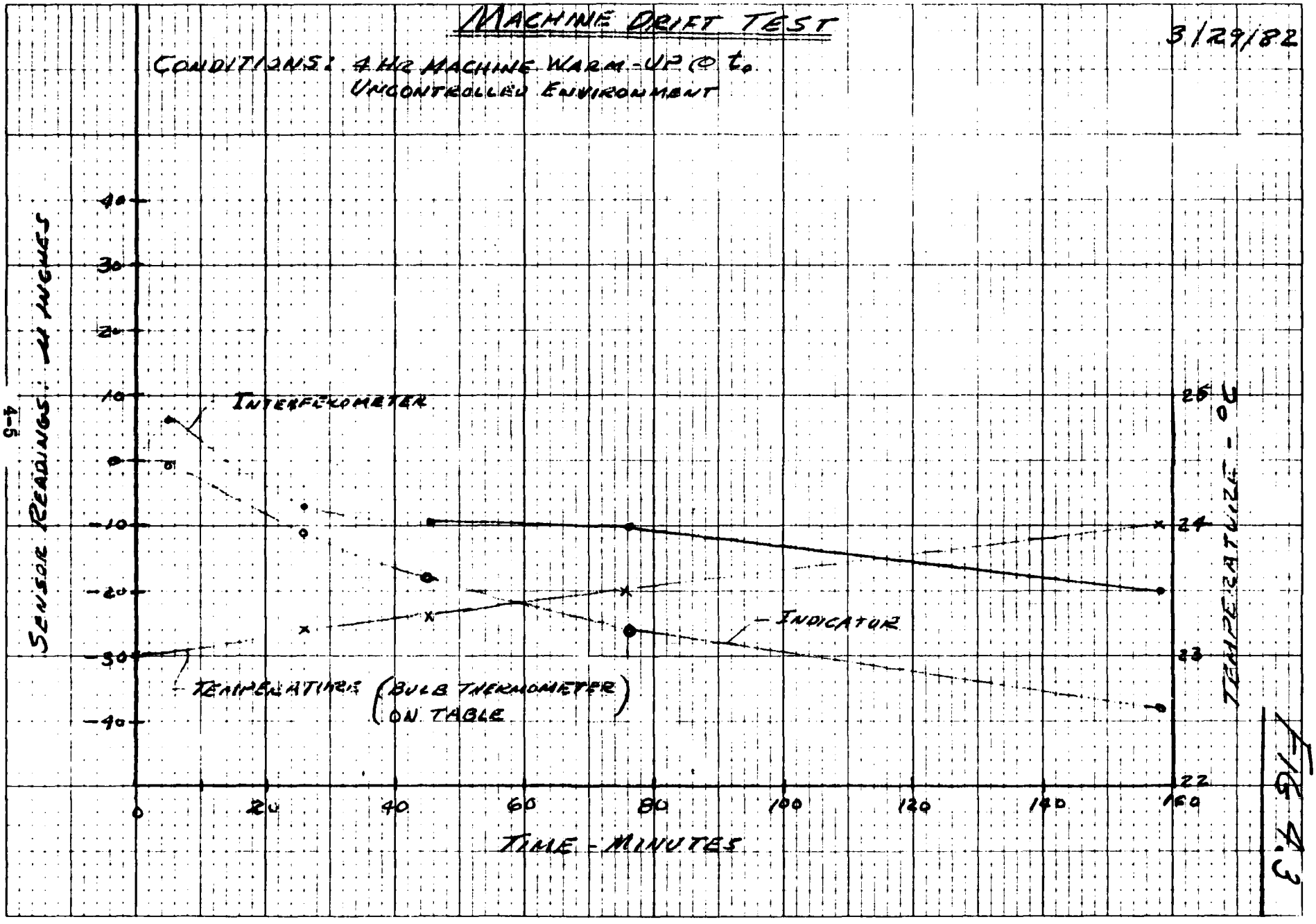

4-5

FIG 4.3

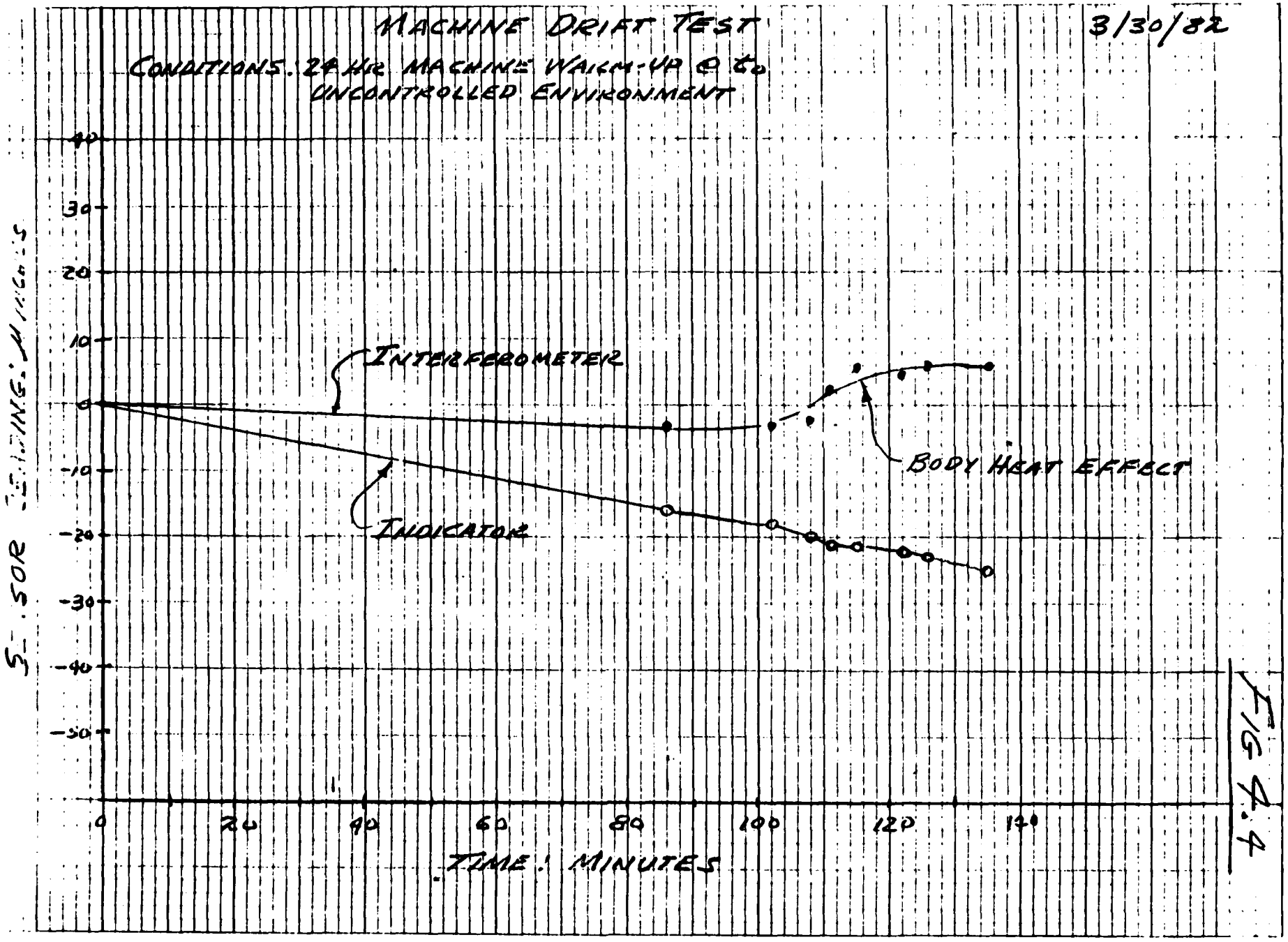
MACHINE DRIFT TEST
3/30/82
CONDITIONS: 24 HR MACHINE WARM-UP @ 60
UNCONTROLLED ENVIRONMENT
INTERFEROMETER
INDICATOR
BODY HEAT EFFECT
SENSOR READING: MICRONS
40
30
20
10
0
-10
-20
-30
-40
-50
0
20
40
60
80
100
120
140
TIME: MINUTES

FIG 4.4

FIG. 4.5

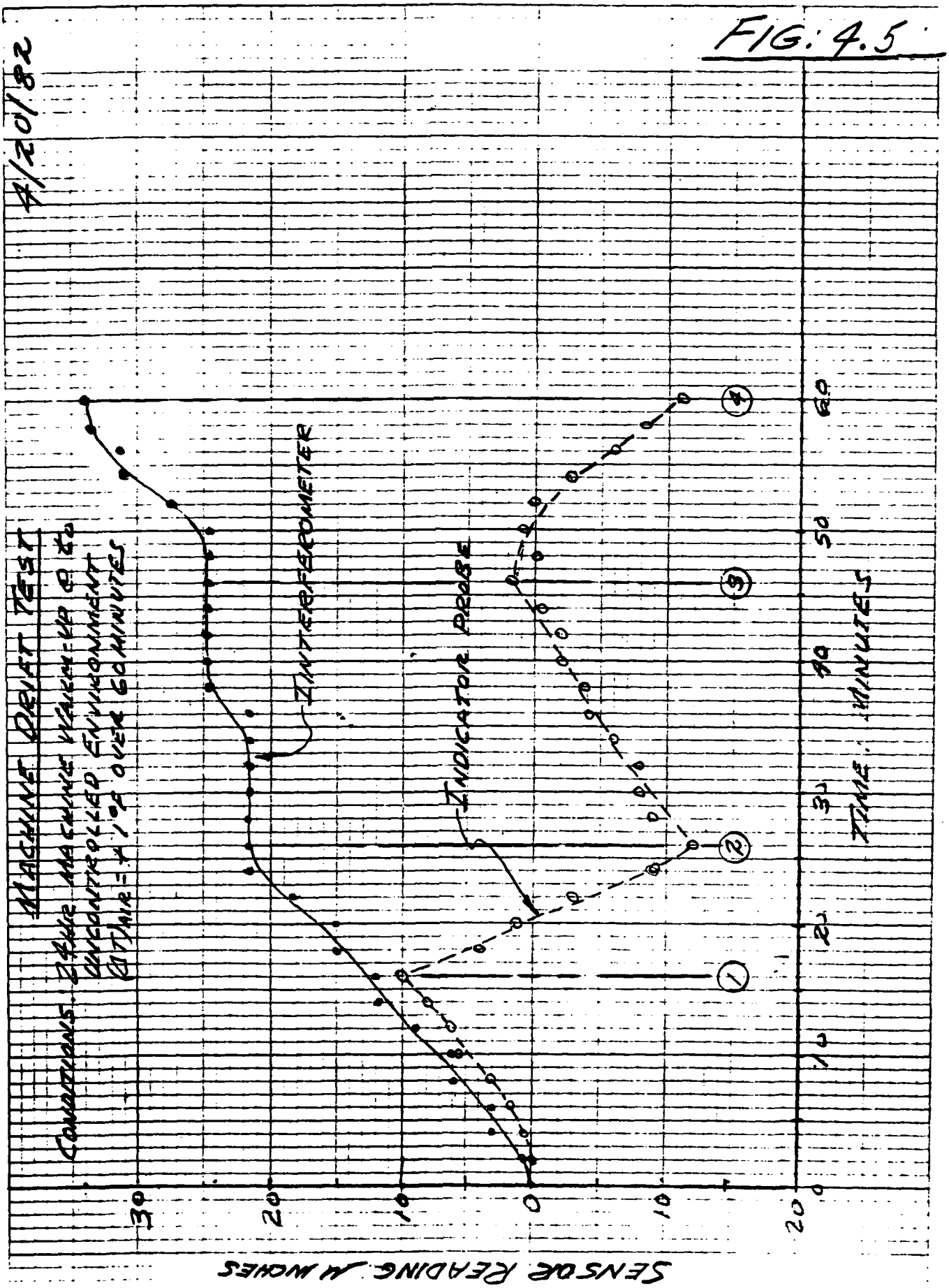
4/20/82
MACHINE DRIFT TEST
CONDITIONS: 4 HOUR MACHINE WARM-UP @ 4%
UNCONTROLLED ENVIRONMENT
CO IN AIR = 4.1 PPM OVER 60 MINUTES
INTERFEROMETER
INDICATOR PROBE
SENSOR READING IN MOLES
TIME IN MINUTES
30
20
10
0
10
20
10
20
30
40
50
60
1
2
3
4

data was taken from a distance of about 10 ft showing that the indicator reading is returning. Points (3) to (4) show drift just from standing close to the machine (without contact). As would be expected, the slope is not as steep. So the test data show that human body heat transfer by conduction and by radiation causes a significant mensuration error. This occurs because the heat input is a sudden change and the machine and part being measured have not stabilized to the input. Stabilized condition is the key solution to this problem. The Phase II machine is proposed to be remotely controlled from a console. Servo motors will be used to drive the x-y slide and the machine will stabilize from their heat input during the machine warm-up period. The change in heat dissipation from the motor during slide motion will not be much different from that of the "locked-rotor" condition because of the low power needs of slide translation.

Figure 4.6 shows a small drift of 5 microinches with both sensors having the same sign. So the maximum mensuration error is only 3 microinches (difference between the two sensors). For this test, the machine was on overnight, the air temperature changed less than 0.2° F and atmospheric pressure remained constant. Also, the deadpath (L_D) was reduced to 1.5 inches.

Figure 4.7 is just another thermal drift test showing a thermal error of about 9 microinches over a 45-minute interval. The air temperature was monitored with an accurate thermometer and showed a continuous rise of 0.3° F over the interval. Atmosphere pressure changed from 766 to 767 mmHg. After this test, Aerodyne moved to a new facility.

The test series shown in Figures 4.8 to 4.11 were done in the new facility where thermal excursions were less than the previous tests. Also, the structure was filled with fluid to provide a greater thermal inertia.

Figure 4.8 shows drift for the case where the room ambient increased 0.7° F over a 51-minute interval. Comparing this data with that of Figure 4.7, it can be seen that fluid filling provided significant thermal stability. Without fluid, the interferometer drift was 19 microinches for a $\Delta T = 0.3^{\circ}$ F compared to 3 microinches at a $\Delta T = 0.7^{\circ}$ F. Also, the mensuration error is less with fluid filling. This is shown better in Figure 4.9, where the difference between the interferometer and

FIG. 4.6

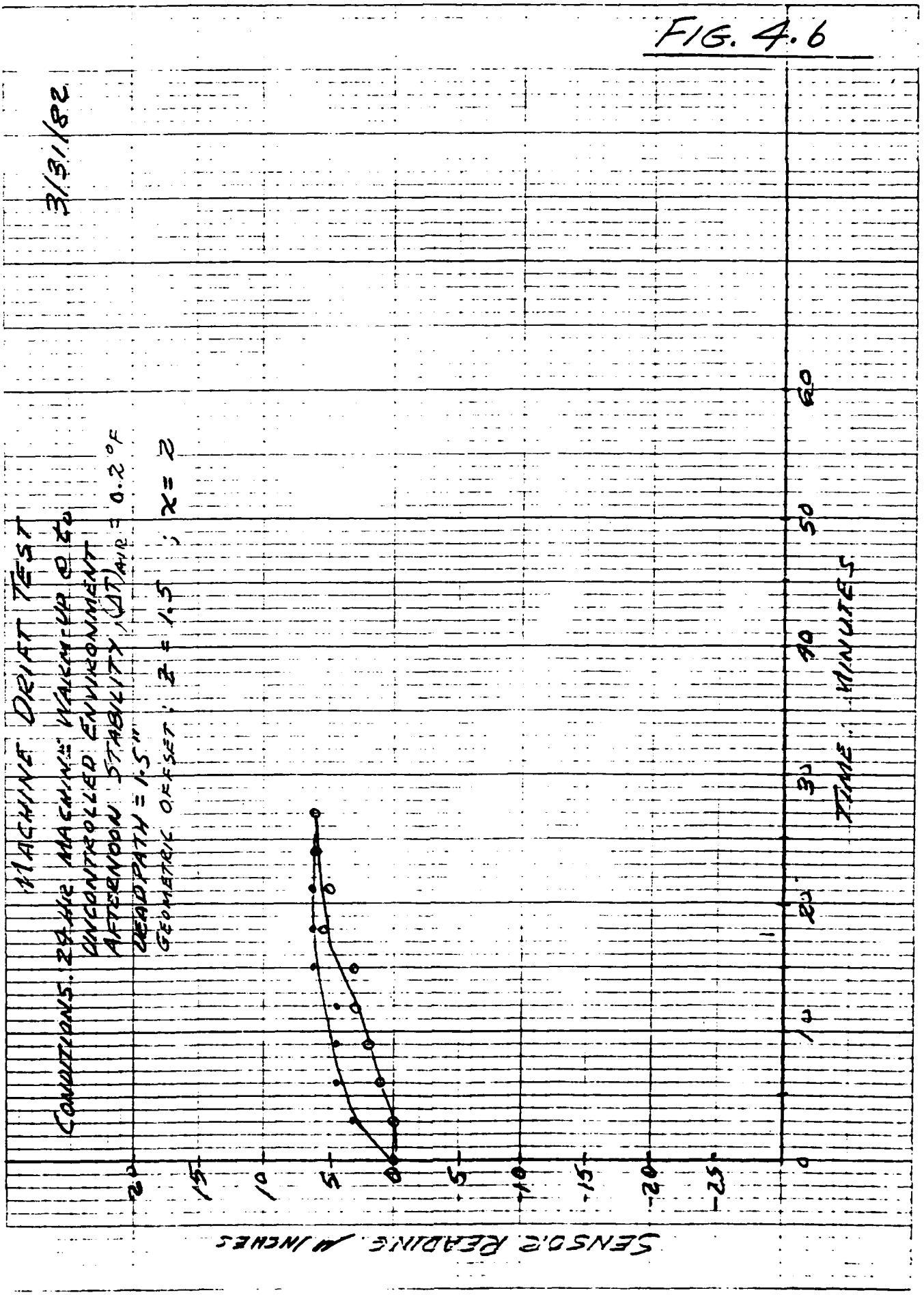
3/31/82
MACHINE DRIFT TEST
CONDITIONS: 24 HR MAGNETIC WALKTHROUGH
UNCONTROLLED ENVIRONMENT
AFTERNOON STABILITY, (ΔT)AIR = 0.2 °F
HEAD PATH = 1.5"
GEOMETRIC OFFSET; Z = 1.5 ; X = 2
SENSOR READING, MICRONES
TIME, MINUTES
20
15
10
5
0
-5
-10
-15
-20
-25
0
10
20
30
40
50
60

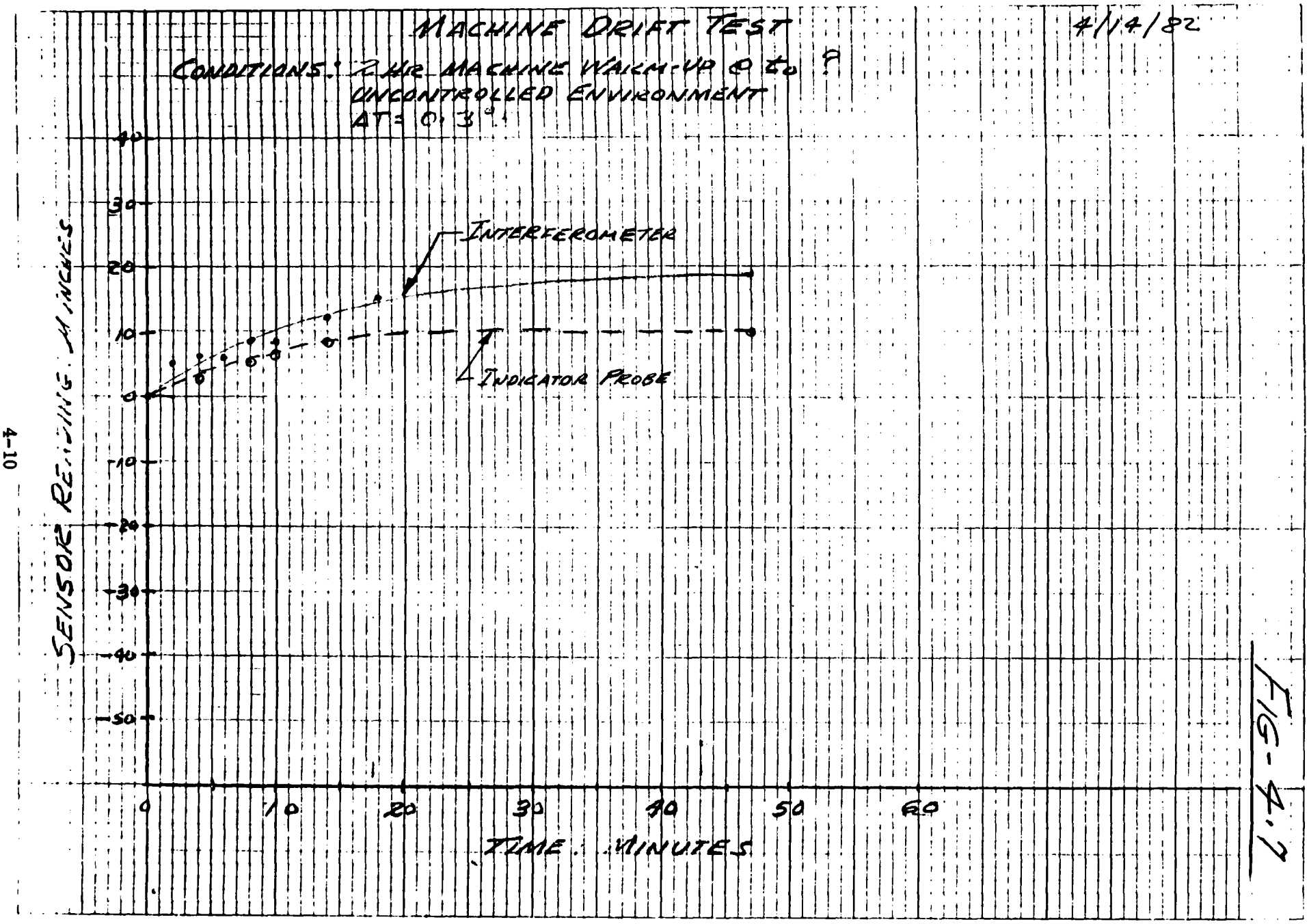
MACHINE DRIFT TEST
4/14/82
CONDITIONS: 2 HR MACHINE WARM-UP @ t0
UNCONTROLLED ENVIRONMENT
ΔT = 0.3°
INTERFEROMETER
INDICATOR PROBE
SENSOR READING, MICRONS
40
30
20
10
0
-10
-20
-30
-40
-50
0
10
20
30
40
50
60
TIME, MINUTES

FIG-4.4

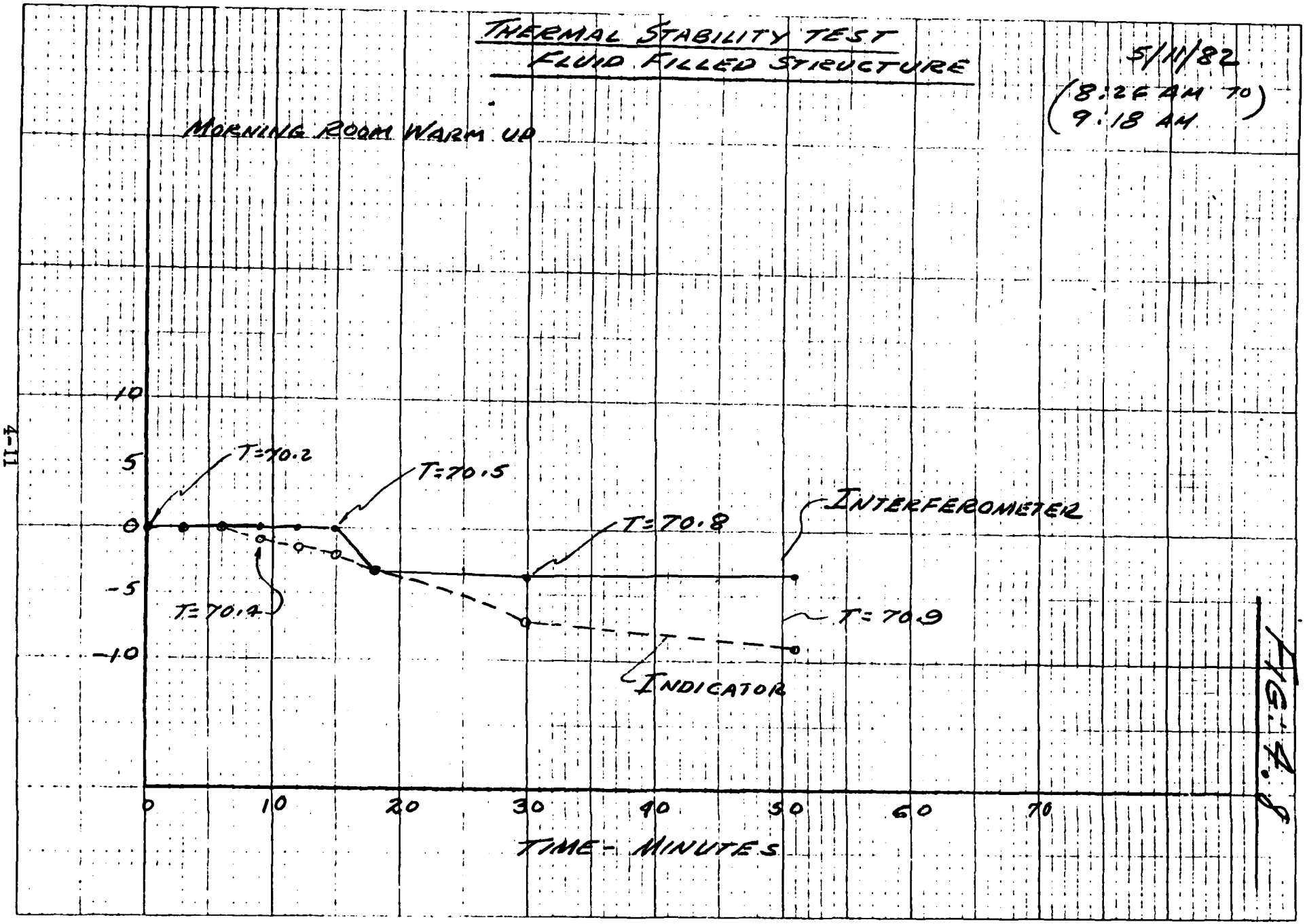
THERMAL STABILITY TEST
FLUID FILLED STRUCTURE
5/11/82
(8:26 AM 70)
9:18 AM
MORNING ROOM WARM UP
10
5
0
-5
-10
T=70.2
T=70.5
T=70.8
T=70.4
T=70.9
INTERFEROMETER
INDICATOR
0
10
20
30
40
50
60
70
TIME - MINUTES

FIG. 4.1

indicator is only 4 microinches for a $\Delta T = 0.2^{\circ}$ F. It is noted that the interferometer resolution is set at 3 microinches whereas the indicator has a resolution of one microinch. It was also observed that the interferometer occasionally jumps one or two counts. This is a sudden change, different from thermal effects. A count change due to thermal effects is characterized by intermittent cycling between count values before holding the next higher count. The count jump was later determined to be a problem in the electronic circuit controlling the digital display. This has since been corrected. The point at the three-minute interval in Figure 4.9 is due to this effect. Figure 4.10 shows drift for the stabilized condition (ΔT no greater than 0.1° F). This is the first test of the series where the absolute drift of each sensor is negligible and where the mensuration error is within the resolution of the sensor. Figure 4.11 is an unattended test over a longer time interval. Since the end of test points returned to zero, the five microinch differential at the 68-minute time could have been caused by someone entering the room, but more likely was caused by the electrical noise interferometer jump identified above.

Allowing for the known electrical noise jump, the test data of Figures 4.10 and 4.11 show that the thermal error is small for the stabilized, fluid-filled condition. Measurement cycles greater than one hour can be done providing thermal perturbations from personnel and room air are controlled.

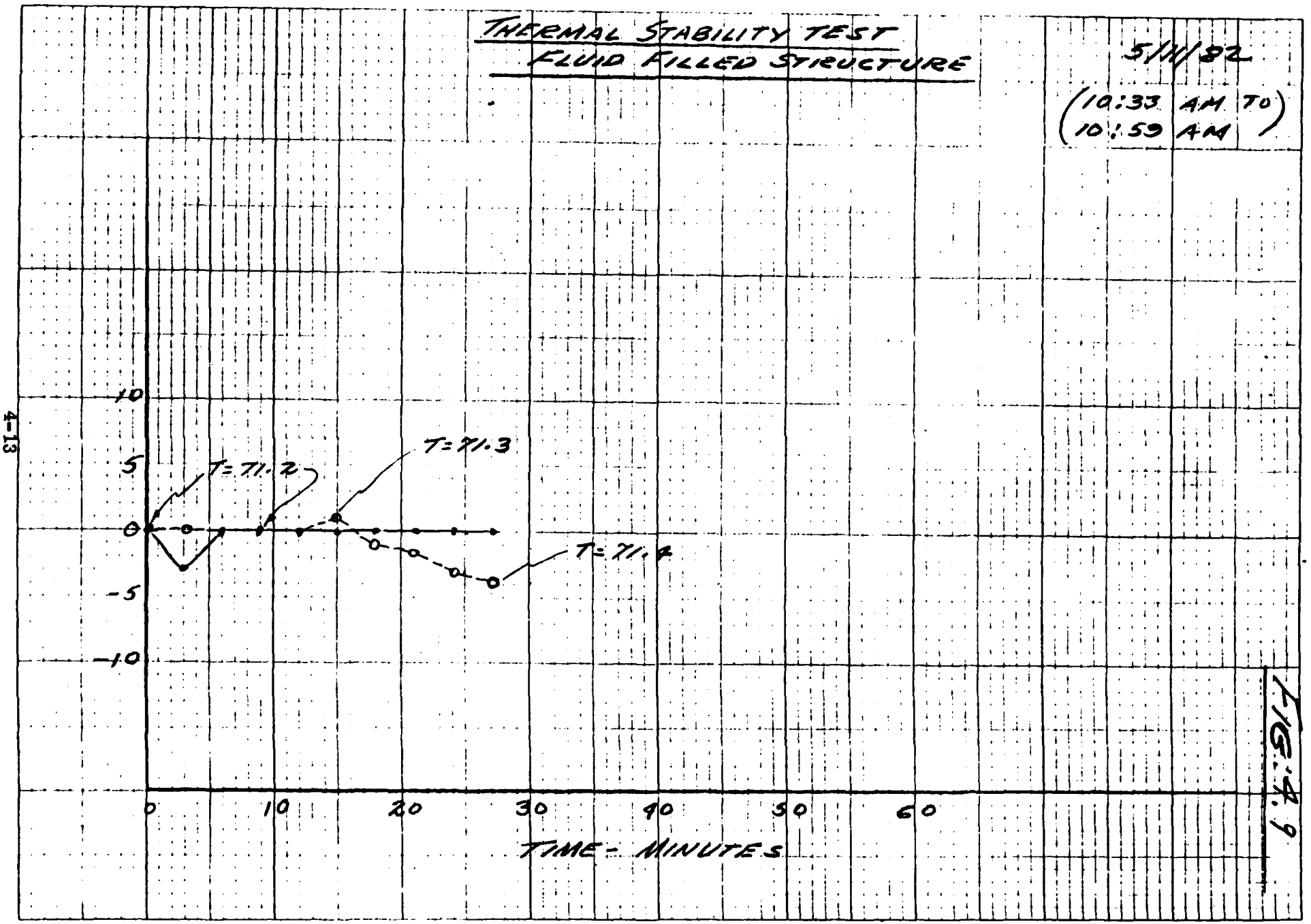
THERMAL STABILITY TEST
FLUID FILLED STRUCTURE
5/11/82
(10:33 AM TO
10:59 AM)
10
5
0
-5
-10
T=71.2
T=71.3
T=71.4
0
10
20
30
40
50
60
TIME - MINUTES

FIG. 4.9

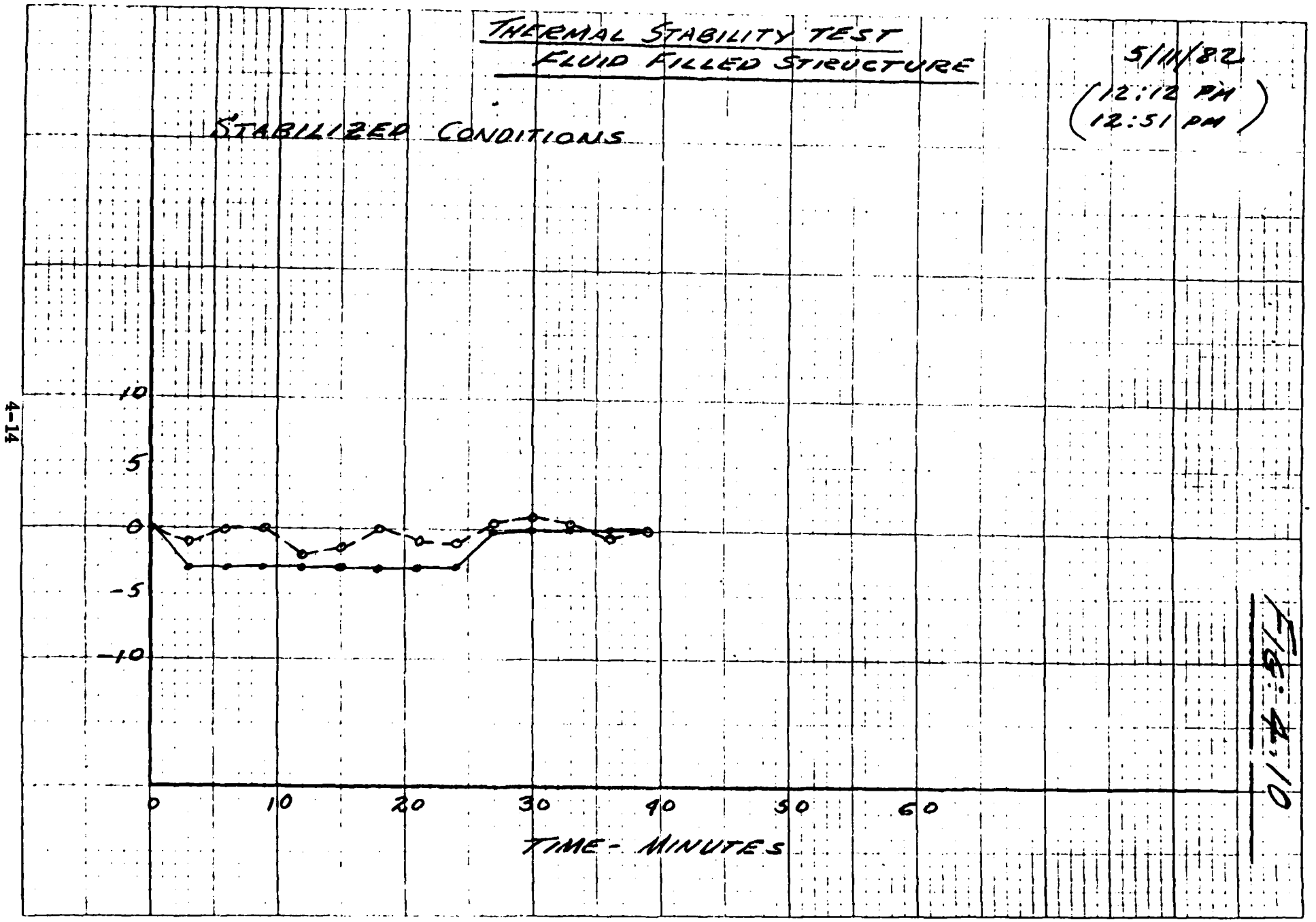
THERMAL STABILITY TEST
FLUID FILLED STRUCTURE
5/11/82
(12:12 PM
12:51 PM)
STABILIZED CONDITIONS
10
5
0
-5
-10
0
10
20
30
40
50
60
TIME - MINUTES

FIG. 4.10

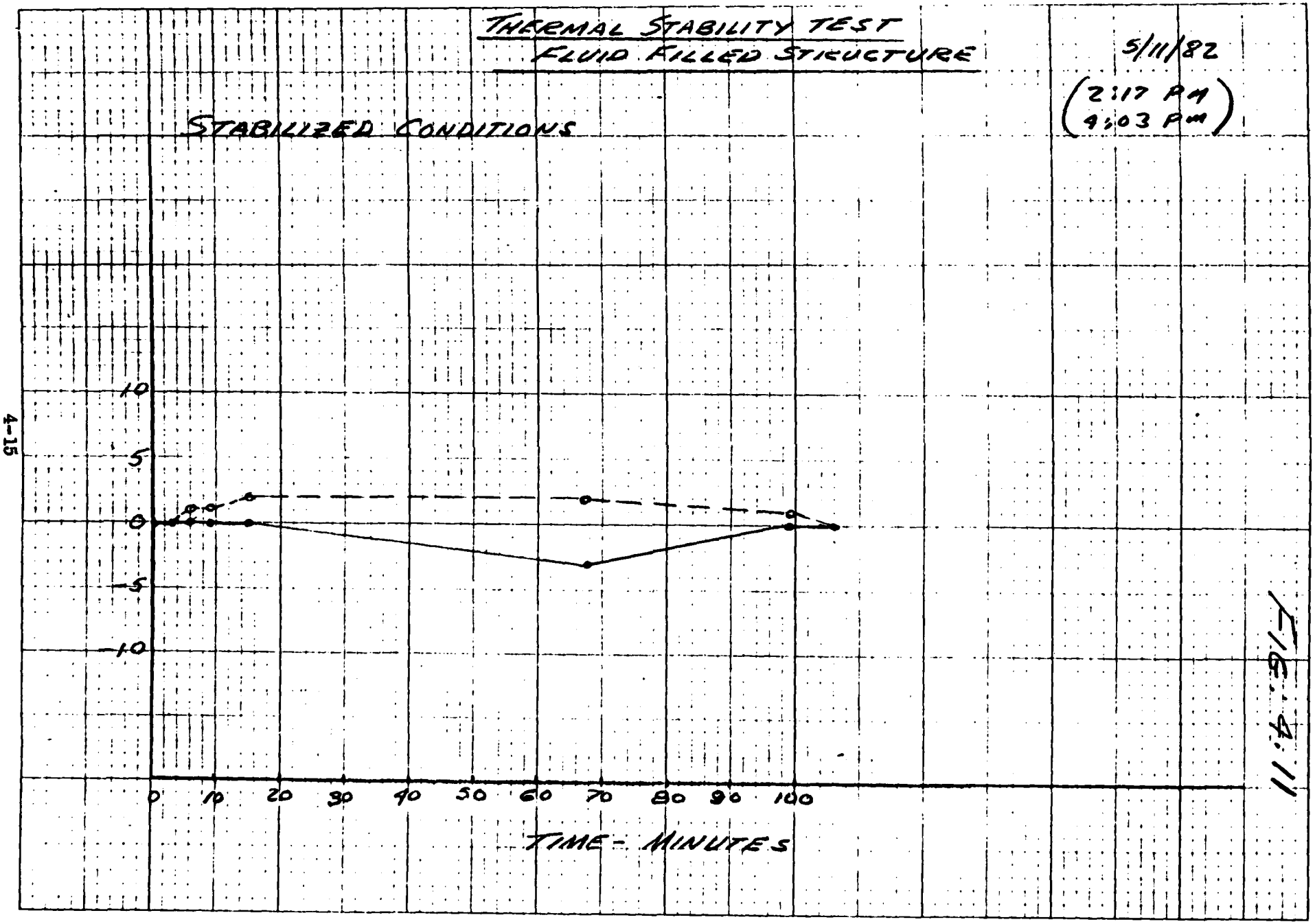
THERMAL STABILITY TEST
FLUID FILLED STRUCTURE
5/11/82
(2:17 PM
4:03 PM)
STABILIZED CONDITIONS
10
5
0
-5
-10
0
10
20
30
40
50
60
70
80
90
100
TIME - MINUTES

FIG. 4.11

4.2 SLIDE MOTION ACCURACY

This relates to the Geometric Machine Errors that were discussed in Section 3.3.1. As was shown by the analysis, a major advantage of the AGTCMD is that relatively large slide excursions have little effect on the mensuration accuracy of the machine.

Figure 4.12 plots the displacement of the mirror relative to the interferometer for a 7.2 inch travel of the x slide. The displacement shown is a combination of roll and lateral straightness of motion occurring at the z coordinate of the measuring point. Since the inspection part is mounted on the same table as the mirror, it displaces an equal amount at the z coordinate of the interferometer beam and thus does not result in a mensuration error.

The curve of Figure 4.12 does not show how much of the displacement is due to angular motion versus straightness of motion. The latter displacement cancels regardless of the z coordinate at which the measurement is made, but accuracy is affected by the roll motion. Refer to the analysis in Section 3.3.1. Equation 3.23 applies here:

$$\varrho_y = a\beta_x$$

where (a) represents the z coordinate from the laser beam—up to 1-1/2 inches for a 3" thick gear.

Acceptance test data for the x-y slide is shown in Figure 4.13. The straightness of travel is 45 microinches over a 9" travel and the roll is 3 arc seconds or $\pm 7.27 \times 10^{-6}$ radians. If the straightness of a part is inspected at a zero z coordinate, the error ϱ_y is zero. If the z offset is the maximum 1-1/2 inches, the geometric error calculates at:

$$\varrho_y = 1.5 \times 7.27 \times 10^{-6} = \pm 10.9 \text{ microinches over 9 inches of slide travel.}$$

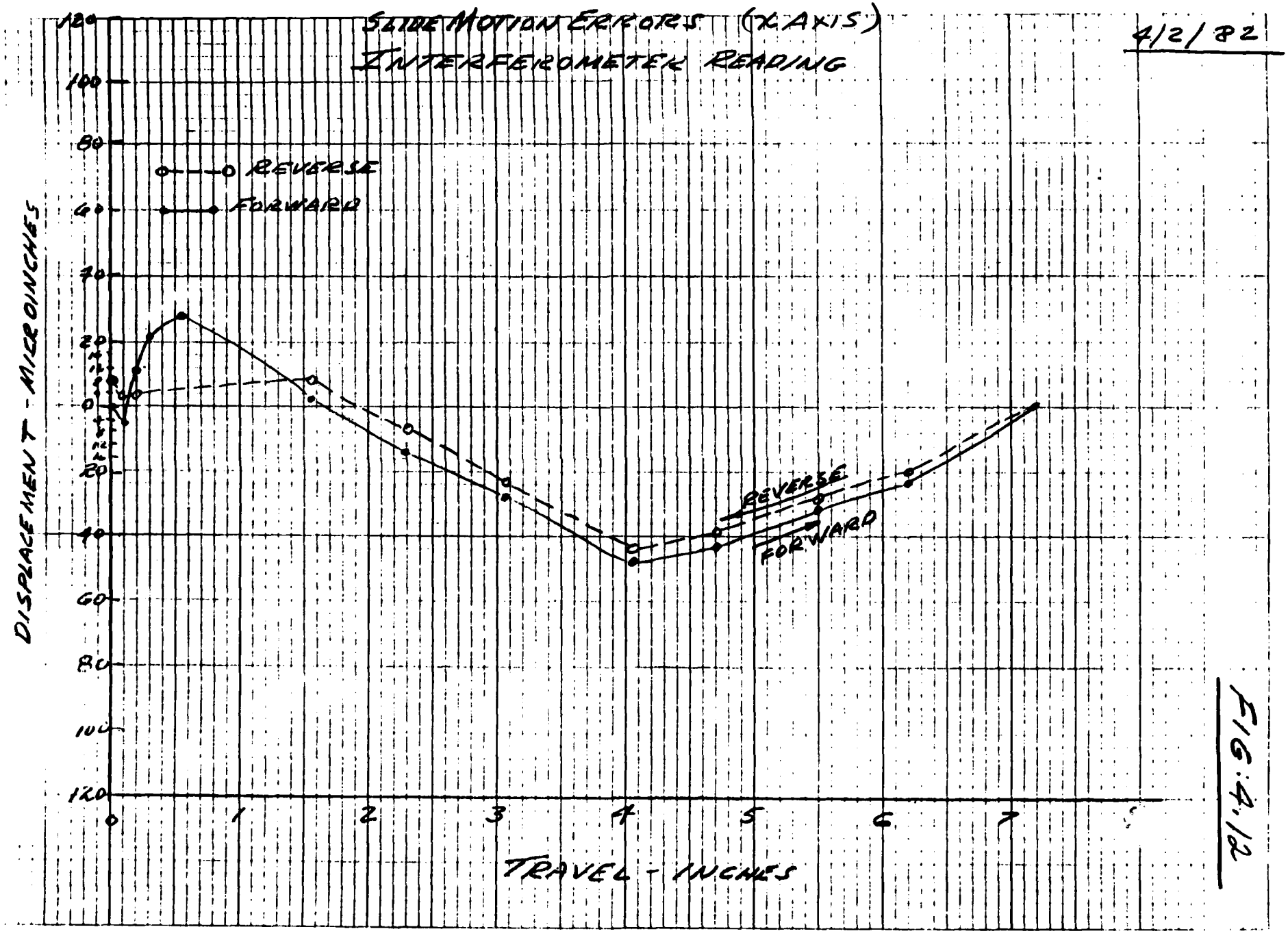
SLIDE MOTION ERRORS (X AXIS)
INTERFEROMETER READING
4/2/82
REVERSE
FORWARD
DISPLACEMENT - MICROINCHES
TRAVEL - INCHES
REVERSE
FORWARD

FIG. 4.12

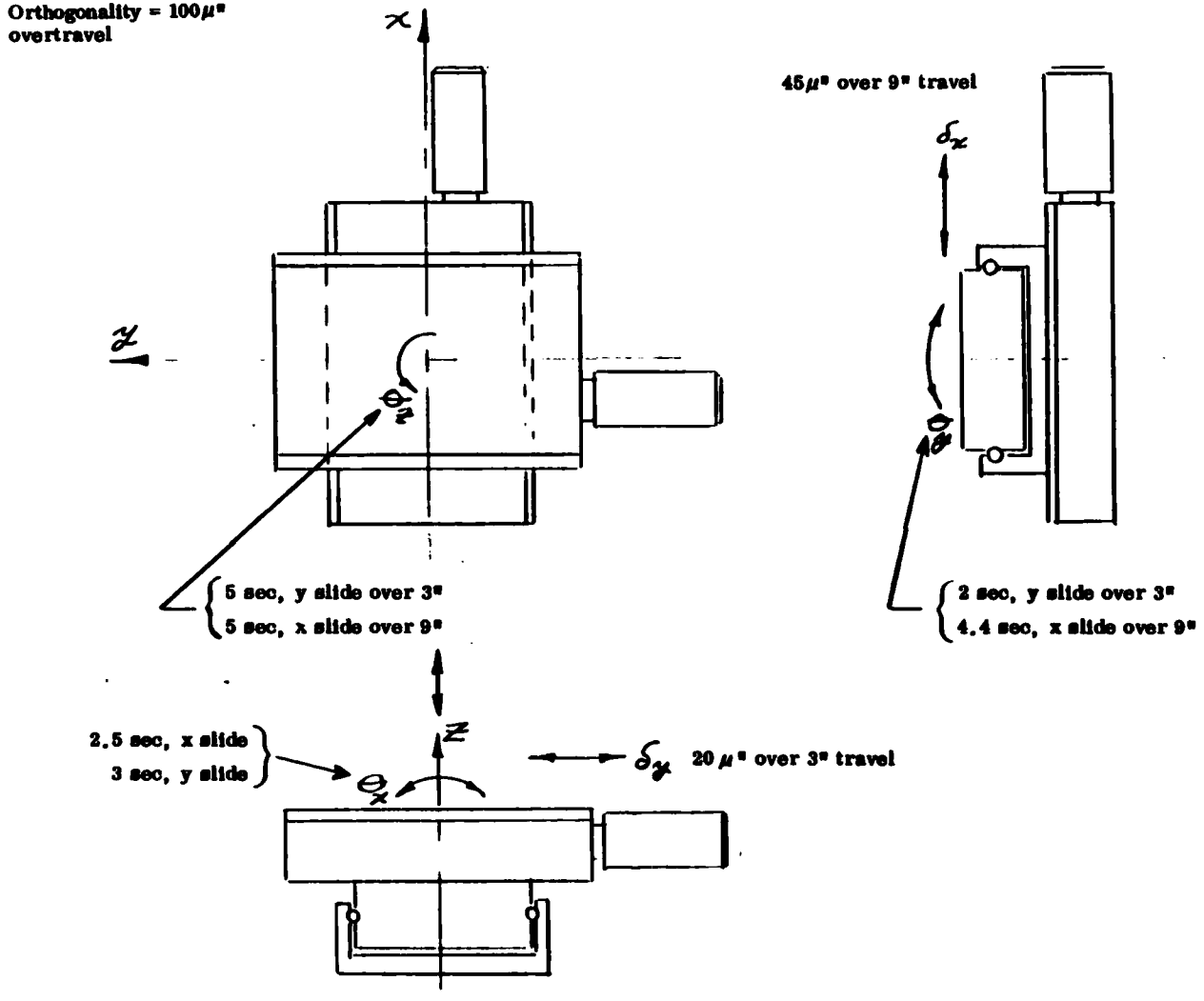

Figure 4.13 Geometric Errors over Travel of 9" x 3"

4.3 MENSURATION REPEATABILITY/PRECISION

The machine set-up shown in Figure 4.1 for thermal drift was also used for the machine repeatability test. The electronic indicator and interferometer were zeroed out at the start. The x slide was moved away from the indicator and then returned until the indicator nulled out on the part.

Figure 4.14 plots points representing slide positioning cycles to indicator probe null. Some of the approaches were unidirectional, while others involved an overshoot of null. The overshoot cycles did not require reverse return beyond null to reproduce the unidirectional approach, as is usually done to remove screw backlash in machine slide positioning. The interferometer was set at a resolution of about 3.1 microinches/display count for this test. The step rise in the curve is a thermal effect which is shown to increase by the resolution increment of 3.1 microinches after about four positioning cycles. Had the interferometer been set at 1.5 microinch resolution, the curve would have been smoother. If the thermal effect is discounted, the data of Figure 4.14 shows that the mechanical repeatability is as good as the resolution of 3 microinches.

Figure 4.15 is another repeatability test made four days later and shows similar precision in combination with the thermal drift effect. However, the drift rate appeared to be greater than that observed from the static thermal drift tests shown in Figures 4.3, 4.4 and 4.6. So, immediately after the repeatability test, a static drift test was conducted. It can be seen from Figure 4.15 that over an equivalent time period the drift differential between the interferometer reading and the indicator reading was only 3 microinches compared with 10.5 microinches for slide positioning cycles. This data supports the human body heat effect discussed in Section 4.1 and shown in Figure 4.5. Note that the Figure 4.15 test was performed one day earlier, before the body heat effect was fully appreciated.

Figure 4.16 shows mensuration repeatability for a 1.109 inch long part. These tests were also performed before body heat effect was known. The measurements were taken over a work day period where the room air temperature changed from 72.6° F to 75.6° F. The test set-up and part size computation is presented in the

FIG 4.14

4/15/82
PRECISION / REPEATABILITY TEST
INTERFEROMETER RESOLUTION = 3.1 μ"/COUNT
L0 = 3¼" ; 2 DOFFSET = ¾" ; 2 DOFFSET = 1
INTERFEROMETER READING — μ INCHES
20
10
0
5
10
15
20
25
CYCLES

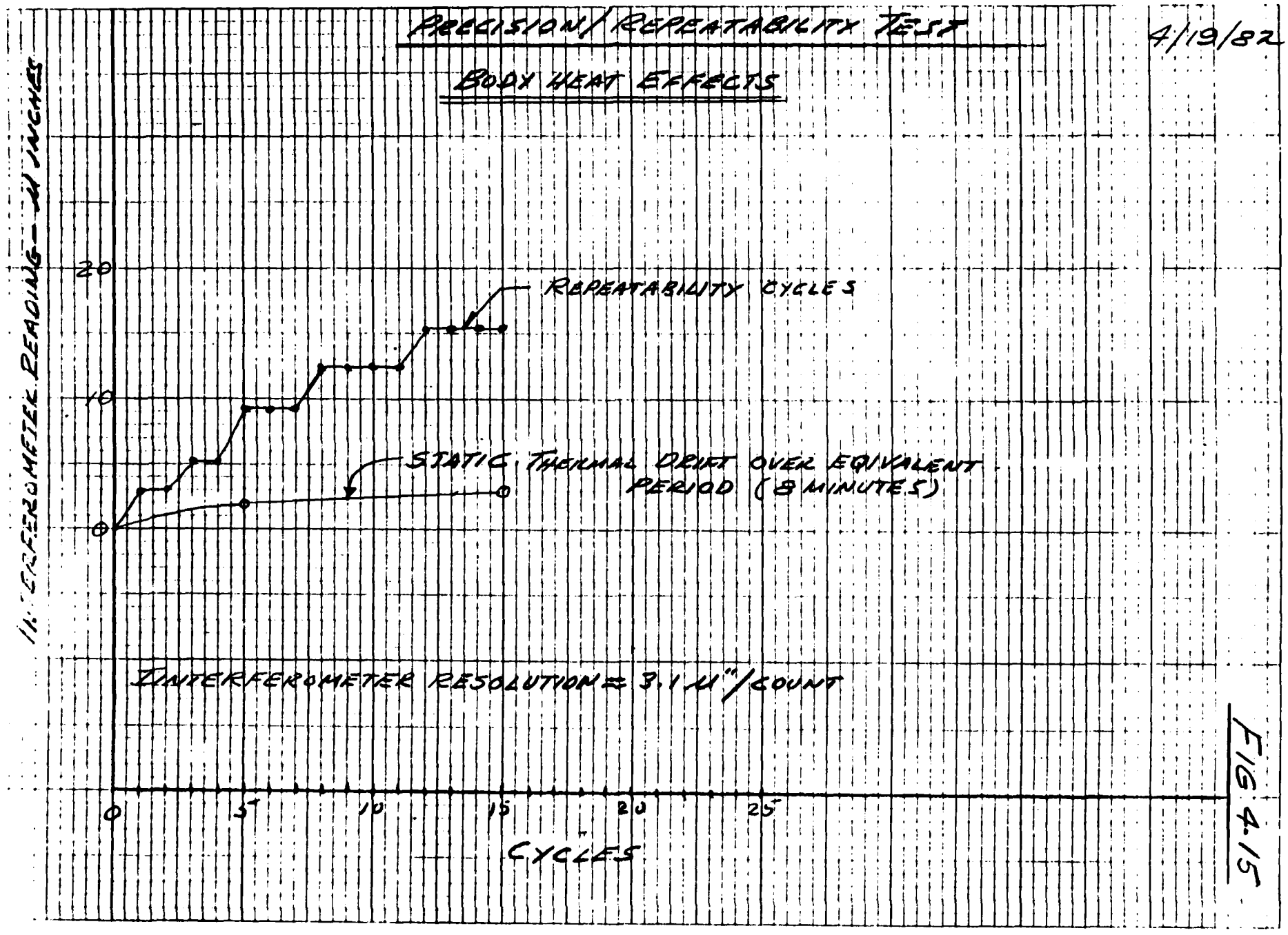
PRECISION/REPEATABILITY TEST
4/19/82
BODY HEAT EFFECTS
INTERFEROMETER READING - MICRO INCHES
20
10
0
REPEATABILITY CYCLES
STATIC THERMAL DRIFT OVER EQUIVALENT PERIOD (8 MINUTES)
INTERFEROMETER RESOLUTION = 3.1 MU"/COUNT
0
5
10
15
20
25
CYCLES

FIG. 4.15

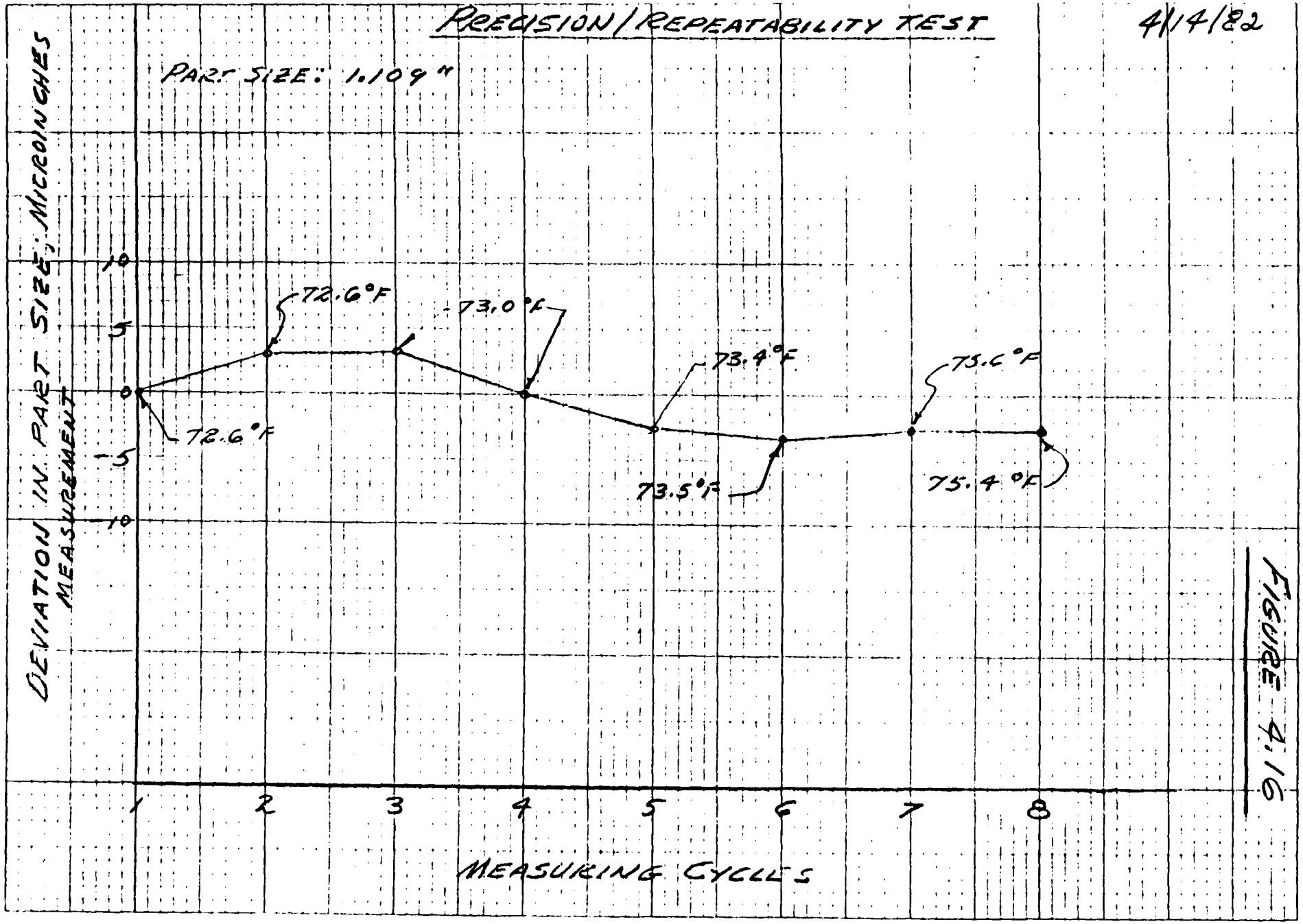

FIGURE 4.16

following section and was done using Equation 3.32. This was to evaluate machine repeatability as a temperature compensating measuring system in an uncontrolled environment. The points show a precision range of plus and minus 3 microinches for measurement of a 1.109 inch long part. This is excellent performance in view of the circumstances of the test. The interferometer resolution was set at 3 microinches in combination with a probe of one microinch resolution. Human body heat effects are included but each of the measurements were done in less than 2 minutes time. The temperature of the part was not measured directly and was assumed to be the same as the recorded air temperature, which rose by 3^{o} F over the day.

The mechanical repeatability or precision of the machine was shown to be within the combined 4 microinch resolution of the sensors for repetitive positioning cycles. Even more remarkable is the demonstrated precision as an environmentally compensated measuring system.

4.4 ABSOLUTE ACCURACY MEASUREMENT

These tests evaluate the system in the performance of its principal role and includes all of the error sources that were earlier identified and evaluated on an individual basis.

The test set-up is shown in Figure 4.17. Shop gauge blocks were "wrung" together as shown so that the unidirectional indicator probe could null-out on two surfaces. The basic dimension (y) measured was 1.109000 inches. The set-up was checked for cosine error along the z axis and the block face was indicated to be perpendicular to the y slide axis within about 50 microinches. The indicator was then nulled out at point (1) and the x and y interferometers were set to zero. The table was then moved along the x axis to clear the block step and returned to x_o. Next, the table was moved in y until the indicator nulled out at point (2) and the y interferometer counts were recorded. The travel path is shown in the top view in Figure 4.17.

In terms of geometric errors, the above described measurement is the kind that was analyzed in Section 3.3.1 concerning slide motion displacement errors. It involves the yaw and pitch excursion of the y slide and positioning repeatability errors of the x slide. The cosine error defined in Section 3.3.2 was reduced to negligible value by the alignment of the interferometer beam with the slide axis and the table top was aligned to within .001 inches with the slide axis. These are initial alignments of the machine and do not have to be repeated. However, the inspection part has to be checked for cosine error with each set-up.

Regarding thermal effects errors, the measurement cycle time is less than 2 minutes and we can refer to the thermal stability test data of Section 4.1. Since the lead screw hand cranks had to be manually operated during the measurement, the human body heat effects are the major contributor to thermal instability. Figure 4.5 shows that this can be as large as 8 microinches over 2 minutes but this is the drift rate upon initial introduction of the transient. The time spent in setting up the part allows some system stabilization with body heat load and 4 microinches is a better average to assume .

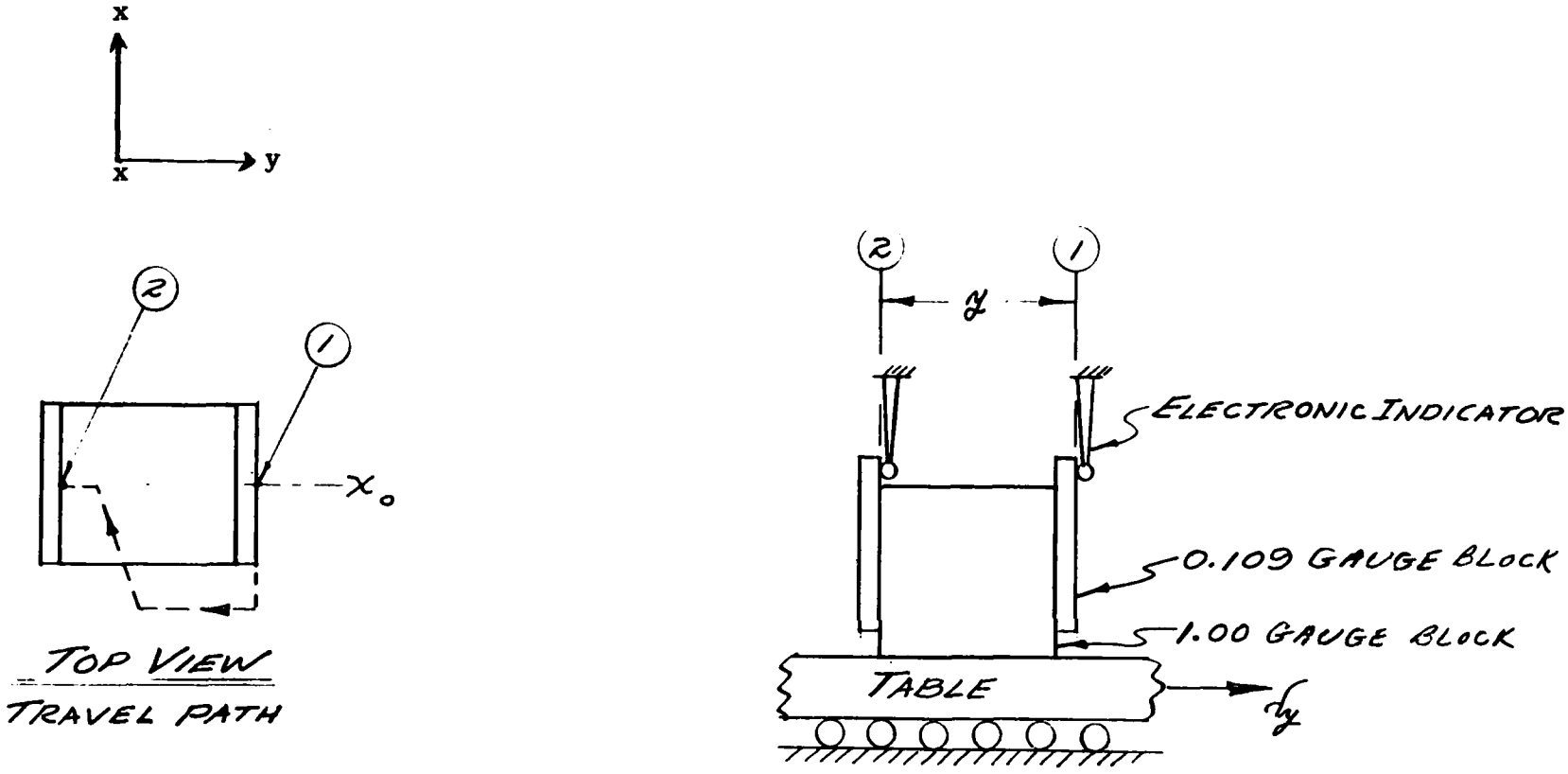

Figure 4.17 Test Set-Up — Absolute Accuracy Measurement

In Section 3.3 Equation (3.32) was developed for environmentally compensated measurement under transient conditions at temperatures other than 68^{o} F

$$y = \frac{D_c}{8M_c} \lambda_{vac} \left[C - \alpha_p \left(T_p - 68 \right) \right] + \left(\frac{C - C_o}{C_o} \right) L_D \qquad (3.32)$$

The Phase II machine, if procured, will have an automatic compensator that will handle the factor in the bracket and the last term will be handled in software. The instrumentation that was used for the following test was a bulb thermometer located just above the table to record air temperature and an absolute pressure gauge with a scale range from 0 to 800 mmHg. The relative humidity was not recorded and the interferometer scale compensation factor (C) was determined from the recorded air temperature and pressure at an assumed 50% R. H.

The machine table or part temperature (T_P) was not recorded and was assumed to be the same as the recorded air temperature. Further, in calculating the part size, the last term of Equation (3.32) is disregarded because the means for detecting the very small change in air temperature over a 1-1/2 to 2 minute measuring cycle was not available. This will not result in a significant error because even a change of 0.2^{o} F would involve only a 0.4 microinch compensation. Also, the interferometer was set at $\lambda/8$ resolution, so Equation (3.32) reduces to:

$$y = 3.115115 \times 10^{-6} D_c \left[C - \alpha_p \left(T_p - 68 \right) \right] \qquad (3.33)$$

a. Test Series 4/20/82

Room air ambient rising at a rate > 1^{o} F/hr.

Geometric offset: x = 0, z = 1", y = 2"

Table 4.1 Absolute Accuracy Test Data

Test No.	λ/8 Counts	T_{air} ^{o}F	Pair mmHg	Time	Comments
1	356146	79.8	775	1:49	Initial set-up
2	356146	79.8	775	1:52	Initial set-up
3	356147	80.1	775	2:10	Second set
4	356147	80.1	775	2:12	Second set
5	356119	?	775	2:20	Other side of block
6	356127	80.3	775	2:30	Center of block/correct
7	356128	80.3	775	2:32	Set-up
8	356129	80.3	775	2:34	
9	356130	81.1	775	3:06	Repeat test
10	356130	81.1	775	3:08	

Tests 1 and 2 (Table 4.1) show repeatability as do tests 3 and 4 taken about 20 mins. later. The change in counts represent about 3 microinches at an air temperature 0.3^{o} F greater. However, calculating the part size gives a dimension of 1.109049 or 49 microinches too large. The measurement was taken at the left edge of the block. It was decided to check parallelism by measuring at the right edge in test 5. This showed a parallelism error due to improper holding in a vise. The stack-up of the 3 gauge blocks shown in Figure 4.17 were off center from the vise clamp screw by about 1/4 in. The blocks were centered in the vise and lightly clamped; whereupon tests 6 through 10 were conducted with the measurement taken at the center of the block. The variation in counts during tests 6, 7 and 8 are likely thermal effects previously discussed.

Calculating the size for tests 6, 7 and 8:

$C = .999731 @ T = 80.3; \quad p = 775$ mmHg

$D_c = 356128$ avg counts

$\alpha_p = 6.5 \times 10^{-6}/^{o}$ F per gauge block manufacturer

$T_p = 80^{o}$ F assumed from air temperature and substituting values into Equation (3.33)

$$y = 3.115115 \times 10^{-6} \times 356128 \left[.999731 - 6.5 \times 10^{-6} (80-68) \right]$$

$$y = 1.1093797 \times .999653 = 1.1089947$$

or an error of -5.3 microinches from basic. This is excellent correlation in light of the thermal effects discussed earlier. Measurement was done in a poor environment at a temperature 12^{o} F higher than the reference temperature of 68^{o} F. The manufacturer of the gauge blocks (Do-All) gives a tolerance of + 4 and - 2 microinches for the set and where two blocks are stacked, the result is a + 8, - 4 microinch "worst case" tolerance on the part being measured.

An error of $1/2^{o}$ F in the assumed temperature of the part (T_p) represents 3.6 microinches.

If the vise clamp load were, say, 25 lbs., the blocks would be compressed by an amount:

$$\Delta = \frac{PL}{AE} = \frac{25 \times 1.109}{1 \times .8 \times 30 \times 10^{6}} = 1.16 \text{ microinches}$$

Repeating that same measurement 1/2 hour later at an air temperature of 81.1^{o} F, a size of 1.1089937 was computed from 356130 counts for tests 9 and 10. This is an error of - 6.3 microinches from basic size. Again, this is within the resolution of the system, part tolerance and recording equipment used.

b. Test Series 4/14/82

These tests were run before recognition of the effects of improper vise clamping and were taken at the edge of the gauge block. The gauge manufacturer is Helios and the stated accuracy of the set is + 6 and - 2 microinches. This gives a stacked "worst case" tolerance of + 12 and - 4 microinches. The data in Table 4.2 is for 8 measurements taken over a work day and shows that the average of the 8 measurements is 1.1096299 ± 3 microinches which is 29.9 microinches above basic size. The suspicion here is that the error is due to vise clamping effects which was shown to be the case in test series 4/20/82 above. The absolute dimension for each of the tests is calculated as was done in the 4/20/82 series. While the results cannot be used to demonstrate absolute measurement accuracy, they can be used to evaluate the precision of the machine in an uncontrolled environment. This data is plotted in Figure 4.16 in Section 4.3.

Table 4.2 Data Results of Test Series: 4/14/82

Test] No.	Interferometer λ/8 Counts	T_{air} °F	Pair mmHg	Time	Compensation Factor "C"	Part Size Inches	Repeatability Microinches
1	356123	72.6	766	9:00	.9997292	1.1090305	Base = 0
2	356124	72.6	766	9:10	.9997292	1.1090336	+ 3.1
3	356125	73.0	767	10:16	.9997290	1.1090336	+ 3.1
4	356124	73.0	767	10:30	.9997290	1.1090305	0
5	356124	73.4	768	11:30	.9997293	1.1090279	- 2.6
6	356124	73.5	768	12:40	.9997293	1.1090274	- 3.1
7	356129	75.6	770	4:46	.9997295	1.1090278	- 2.7
8	356128	75.4	770	4:51	.9997295	1.1090278	- 2.7

4.5 VIBRATION/STRUCTURAL STIFFNESS

All tests were performed with the machine mounted on a table having a steel base and a 2-1/4 inch thick wood top. The table stood on a concrete ground floor. The tests dated up to 4/20/82 were done in the Bedford building and subsequent tests were performed at the new Billerica building. The stabilization jacks were not used.

The machine did not appear to be sensitive to vibration under the conditions described above. Shock load from dropped objects or jumping near the machine resulted in an abrupt change of several microinches in the electronic indicator reading, but the observation is that machine performance was not degraded by the vibration associated with quiet ground floor buildings.

Measurements taken over the full capacity of the machine with heavy part loads should make use of the outrigger stabilization jacks. The structural stiffness was checked by recording relative motion between the bridge-mounted probe and the table-mounted part. Without the stabilization jacks, a 5-lb load at the exterior top corners of the bridge causes a 5 microinch indicator reading. At the exterior front corner, the reading is less than one microinch; the front has the two main supports. The 5-lb load on the top edge of the table causes an indicator reading of 24 microinches. It should be recalled, however, that this is not to be regarded as a direct mensuration error for the reasons explained in Section 3.3. Within the resolution and linearity error of the indicator, the interferometer was observed to read a displacement similar to the indicator, thus showing a cancelling out of some of the errors due to structural and stage displacements. The measuring point had a z axis offset of about 1-3/8" and according to Equation (3.17) the error would be 1.37 $(\theta_x + \beta_x)$. It would be better here to have measured the angular displacement of the stage rather than the linear motion of the part. Assuming a radius of 7 inches for an effective center of stage rotation $(\theta_x + \beta_x) = \frac{24 \times 10^{-6}}{7} = 3.43$ microradians and the error at a z offset of 1.37 inches = 4.7 microinches for a moment of 5.5x5 = 27.5 inch-lbs. As was explained in Section 3.3, the error is zero at a zero z axis offset .

The above load/deflection measurements show that the welded frame is much stiffer than the x-y stage. Use of the stabilization jacks would reduce the frame distortion to a negligible value providing that the machine mounting surface is rigid and stable. In Phase II, ways of reducing the x-y stage deflection will be considered.

4.6 LASER OPTIC PROBE

Testing has shown a probe sensitivity (resolution) between one to four microinches per count with a useful sensing range of four to eight mils. This sensitivity exceeds expectations since the goal had initially been set for a resolution of five microinches. However, these values do not now represent overall mensuration capability with the probe. The testing to date has revealed probe count instability and drift. The instability has varied, in a random fashion, to values of about ± 15 counts. This is multicausal and results from floor vibration and variations in the energy distribution in the laser beam. The drift is believed to be related to electronic processing of low signal levels. The following presents the test data and discusses the performance problems identified.

4.6.1 Optic Probe Resolution Range and Linearity

Figure 4.18 plots the digital count from the console panel vs the displacement of the probe. The displacement units represent one turn of the fine adjustment handwheel on the machine slide (833 microinches per turn). The solid line is motion in one direction while the dotted line reverses direction after five turns. The displacement between the two curves is about equivalent to the backlash in the handwheel. The curves for the tests show symmetry about null (zero count) and is the test where the best resolution was achieved. This is about one microinch per count. The range, for the point plotted, is 0.004 inches but could have a useful range up to 0.006 inches based on extension of the curves.

Figure 4.19 is another test with different optical parameter adjustments. Here, the resolution was 3 microinches per count with better linearity and a range greater than 0.006 inches. Also an attempt was made to remove handwheel backlash for the reverse stroke.

The above tests were done with the SELFOC rod. An earlier test was done without the SELFOC rod, where the part was located at the focal plane above the rod. The data for this test is shown in Figure 4.20. Similar results were achieved showing a resolution of 2.5 microinches per count with a range greater than .004 inches.

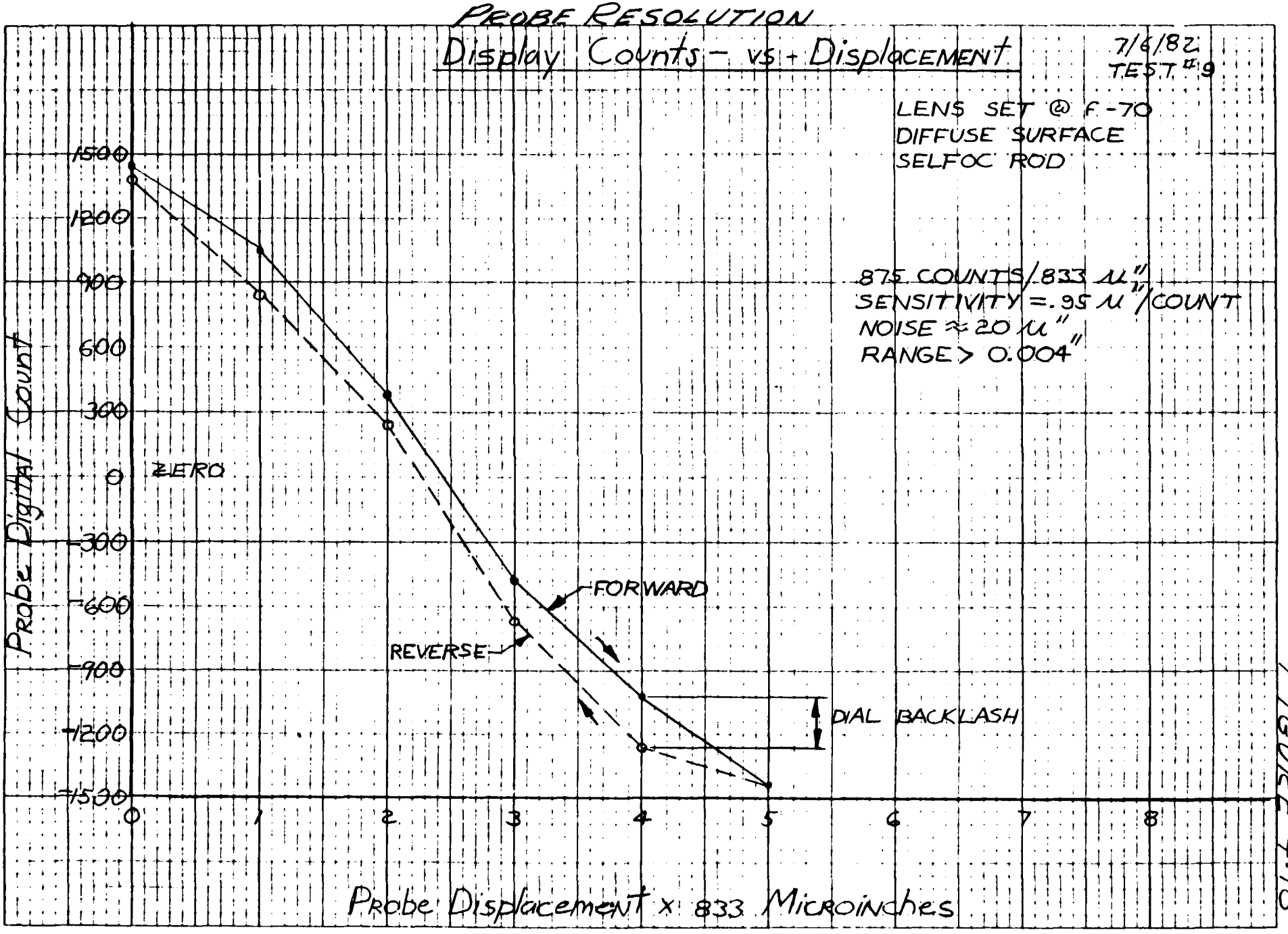
PROBE RESOLUTION
Display Counts - vs + Displacement
7/6/82
TEST #9
LENS SET @ F-70
DIFFUSE SURFACE
SELFOC ROD
875 COUNTS/833 μ"
SENSITIVITY = .95 μ"/COUNT
NOISE ≈ 20 μ"
RANGE > 0.004"
1500
1200
900
600
300
0
-300
-600
-900
-1200
-1500
ZERO
FORWARD
REVERSE
DIAL BACKLASH
0
1
2
3
4
5
6
7
8
Probe Digital Count
Probe Displacement x 833 Microinches

FIGURE 4.18

PROBE RESOLUTION

Display Counts – vs – Displacement

7/6/82
TEST #4
LENS SET @ F-1.1
SELFOC ROD

550 COUNTS / 1666 μ"
SENSITIVITY = 3.0 μ"/COUNT
RANGE > .006 INCHES

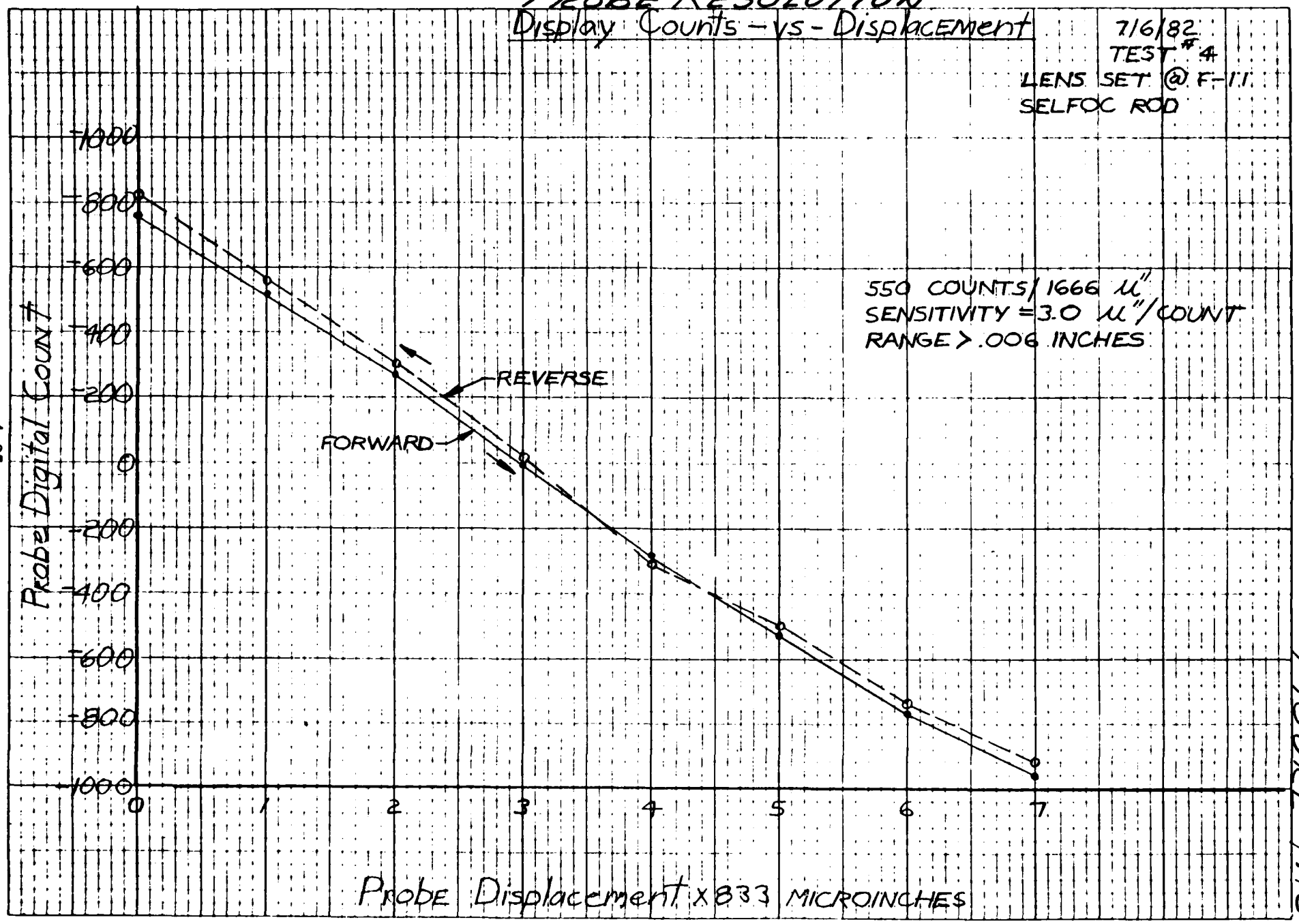

FIGURE 4.19

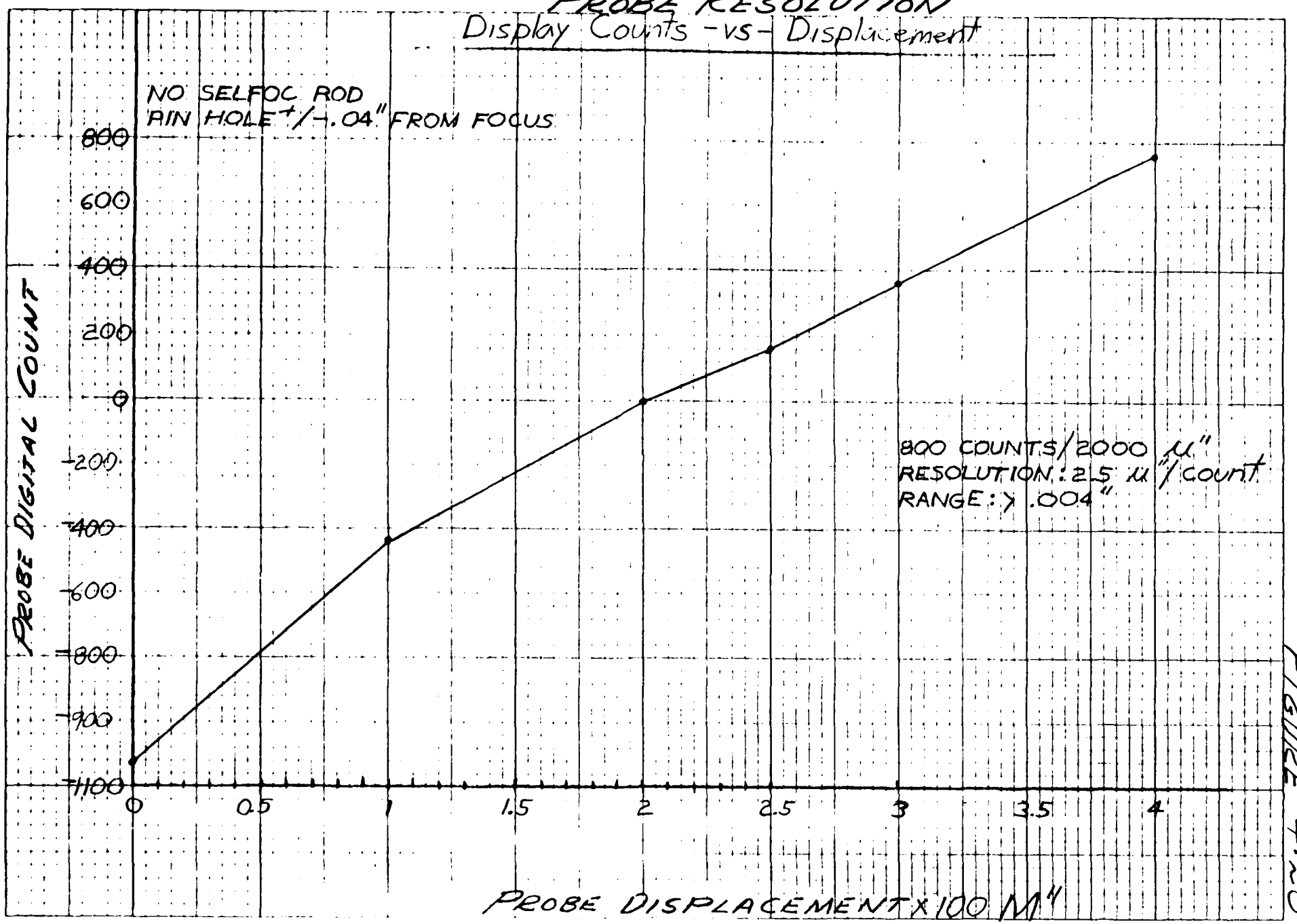
PROBE RESOLUTION
Display Counts -vs- Displacement
NO SELFOC ROD
PIN HOLE +/-.04" FROM FOCUS
800 COUNTS/2000 μ"
RESOLUTION: 2.5 μ"/COUNT
RANGE: > .004"
PROBE DIGITAL COUNT
800
600
400
200
0
-200
-400
-600
-800
-900
-1100
0
0.5
1
1.5
2
2.5
3
3.5
4
PROBE DISPLACEMENT X 100 M"

FIGURE 4.20

From the discussion in Section 3.6 regarding the setting of the detector pinholes, it can be appreciated that a variety of sensitivity curves can be achieved. The method used to determine the pinhole focus point involved the following.

A microscope was set up with a 45^{o} mirror located above the SELFOC rod. The microscope was adjusted to focus on the laser pinhole (refer to Figure 3.11 in Section 3.6). The cross hair of the microscope was also aligned with the center of the pinhole. This establishes the datum for setting the detector pinholes. Using care not to move the microscope, the detector pinholes are back-illuminated and moved axially until best focus of the spot is observed. The pinholes are then adjusted radially until aligned with the microscope cross hairs. This technique worked well for radial alignment to within 0.0001 inches but is not adequate for focus setting. The depth of focus of the relay lens is such that the range of uncertainty was about 0.05 inches axial motion. Front illumination resulted in about the same range.

With the optical configuration tested, a pinhole focus offset of .080 to .120 inches is believed to be the ideal range in terms of the resolution of the probe. Hence, the range of uncertainty is large by comparison and presented problems in achieving symmetry of the output signal. In the final system, this can be easily corrected by selecting a relay lens with a better focus resolution.

4.6.2 Vibration Induced Count Excursion

Figures 4.21 and 4.22 show the effects of vibration. Counts were recorded at about 3 second intervals. Data cycles (a) and (b) from Figure 4.21 represent the count excursion from all causes. Included in this is the pendulum affect of the probe with a heavy mirror at the end. Cycles (c) and (d) show what happens when the probe tip is structurally grounded with a block. It can be seen that the consecutive count jump is reduced from about 30 counts to less than 5 counts. This difference is quite clearly the probe mechanical vibration contribution to the noise aspect. However, it is also seen from cycle (d) that a large excursion still exists due to other causes.

Figure 4.22 also shows the vibration effect when testing was done without the SELFOC rod in the optical train. The part being measured was cantilevered from a

AD-A121 970 DEVELOPMENT OF AN AUTOMATED GEAR TOOTH CONTOUR MEASURING DEVICE(U) AERODYNE RESEARCH INC BILLERICA MA A R OUELLETTE 12 APR 82 DAAK50-81-C-0022 2/2

UNCLASSIFIED F/G 13/9 NL

END

FILMED

DTIC

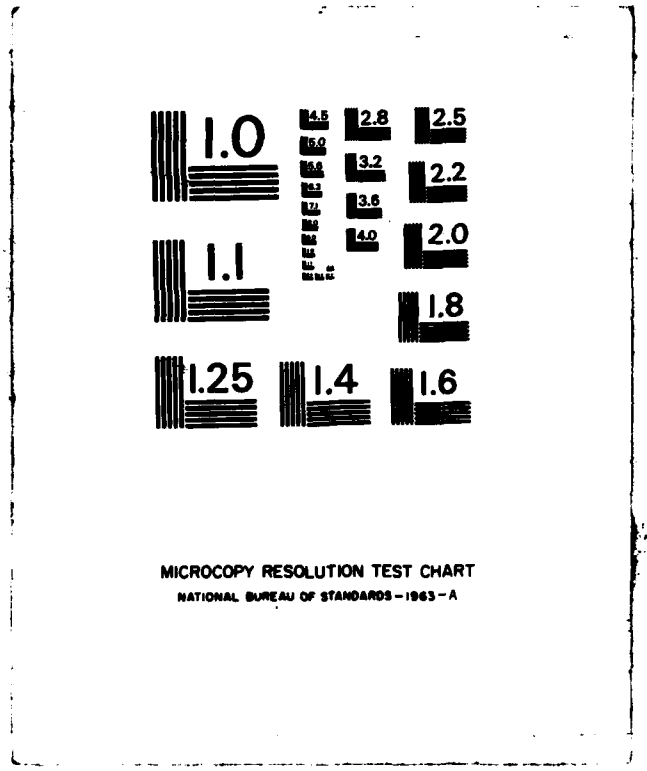
1.0
1.1
1.25
1.4
1.6
2.8
2.5
3.2
2.2
3.6
2.0
4.0
1.8
MICROCOPY RESOLUTION TEST CHART
NATIONAL BUREAU OF STANDARDS-1963-A

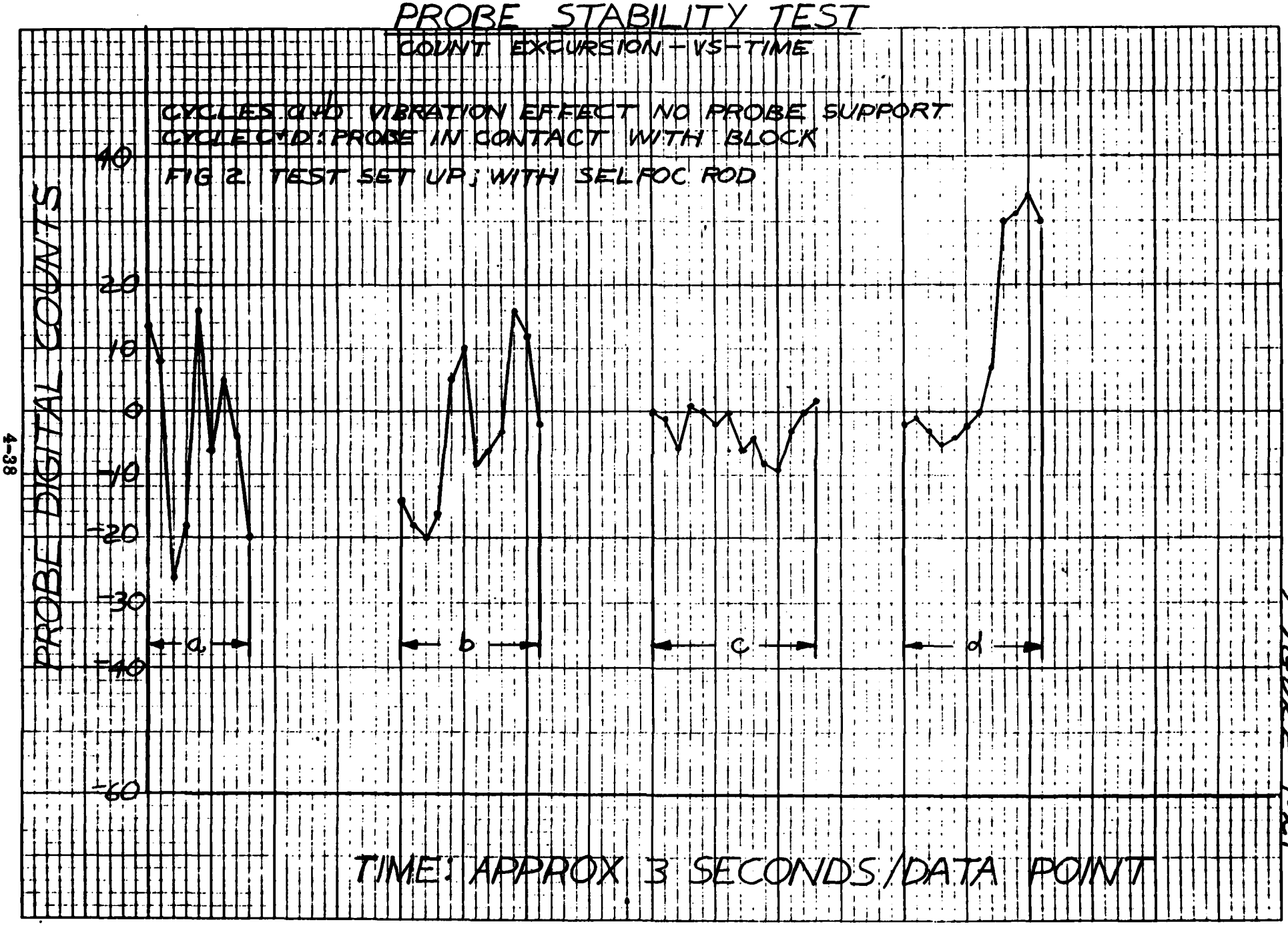
PROBE STABILITY TEST
COUNT EXCURSION - VS - TIME
CYCLES AND VIBRATION EFFECT NO PROBE SUPPORT
CYCLE C+D: PROBE IN CONTACT WITH BLOCK
FIG 2. TEST SET UP; WITH SELFOC ROD
PROBE DIGITAL STATUS
40
20
10
0
-10
-20
-30
-40
-60
a
b
c
d
TIME: APPROX. 3 SECONDS/DATA POINT

FIGURE 4.21

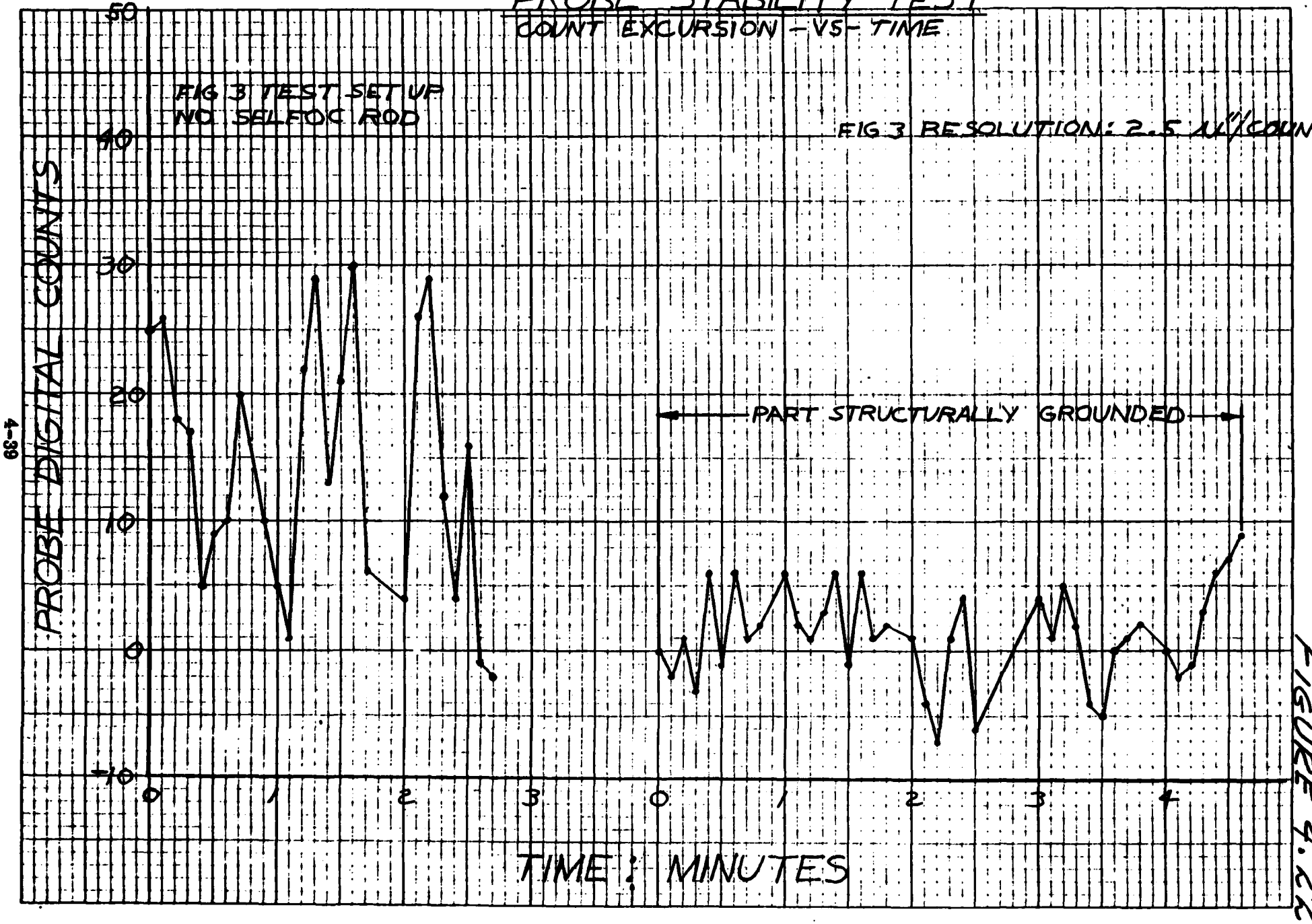
PROBE STABILITY TEST
COUNT EXCURSION - VS - TIME
FIG 3 TEST SET UP
NO SELFOC ROD
FIG 3 RESOLUTION: 2.5 μ"/COUNT
PART STRUCTURALLY GROUNDED
PROBE DIGITAL COUNTS
50
40
30
20
10
0
-10
0
1
2
3
0
1
2
3
4
TIME : MINUTES

FIGURE 4.22

standard optical x-y slide of poor rigidity. The plotted data to the right shows an improvement when the part was grounded by simply resting a small metal plate between the part and machine structure. Here again we can see the excursion occurring over a longer time period. Strip chart data have shown this excursion to be sinusoidal with periods ranging from 1 to 10 minutes. This effect will be discussed in Section 4.6.3 below.

The solution to the vibration problem is to mount the machine on a pneumatically isolated table. The need for this was recognized at the proposal stage, before development of the AGTCMD began. The floor vibration at the present facility is considerably higher than the previous location, where most of the machine performance testing was done.

4.6.3 Laser Beam Spatial Effects

A test was set up to try to isolate the cause of the long period, sinusoidal count excursion. The two detectors that generate the output of the probe position were removed from the optical train. They were mounted adjacent to each other, intercepting the diverging laser beam after the laser focussing lens and the beam chopper in the optical system. (Refer to Figure 3.11 in Section 3.6.1.) Figure 4.23 shows the normalized output from the detectors. The sinusoidal count excursion correlates with that observed in the fully assembled optical system. A spinning disc diffuser was then fabricated and placed in the path of the beam. Figure 4.24 shows the improvement in stability obtained by this device. This data tells us that spatial energy variation in the laser beam was the cause of the sinusoidal count excursion and that one of the solutions to the problem is the addition of a spinning disc diffuser. Other illumination methods offer alternate solutions.

The opacity of the disc used in the above test was too great to be used in the optical train of the operating system. It reduced the light level below processing limit when using the SELFOC rod.

A disc using a "trusite" glass material was used and this allowed sufficient transmission. However, the spinning disc diffuser device which was quickly fabri-

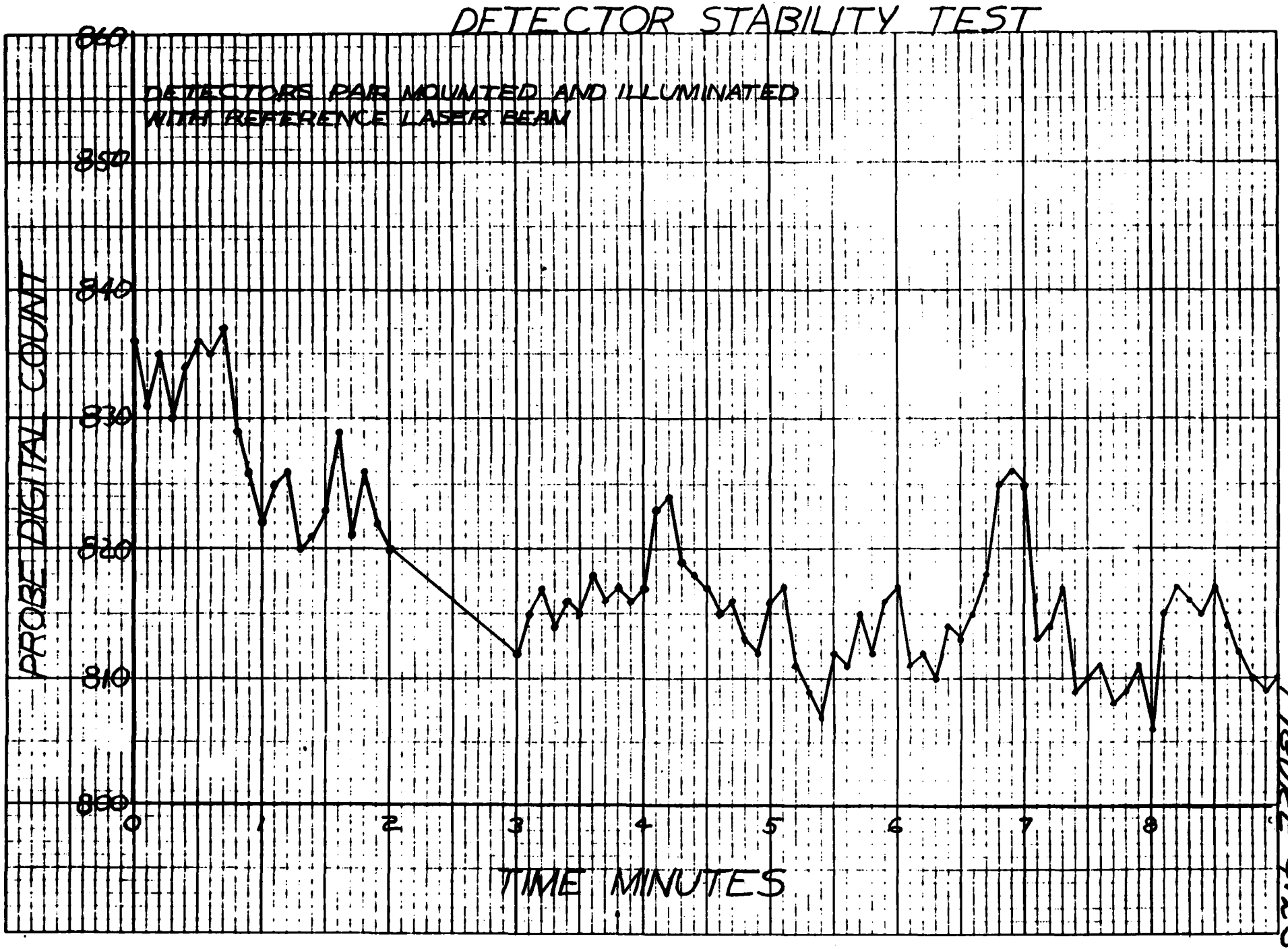
DETECTOR STABILITY TEST
DETECTORS PAIR MOUNTED AND ILLUMINATED WITH REFERENCE LASER BEAM
PROBE DIGITAL COUNT
860
850
840
830
820
810
800
0
1
2
3
4
5
6
7
8
TIME MINUTES

FIGURE 4.23

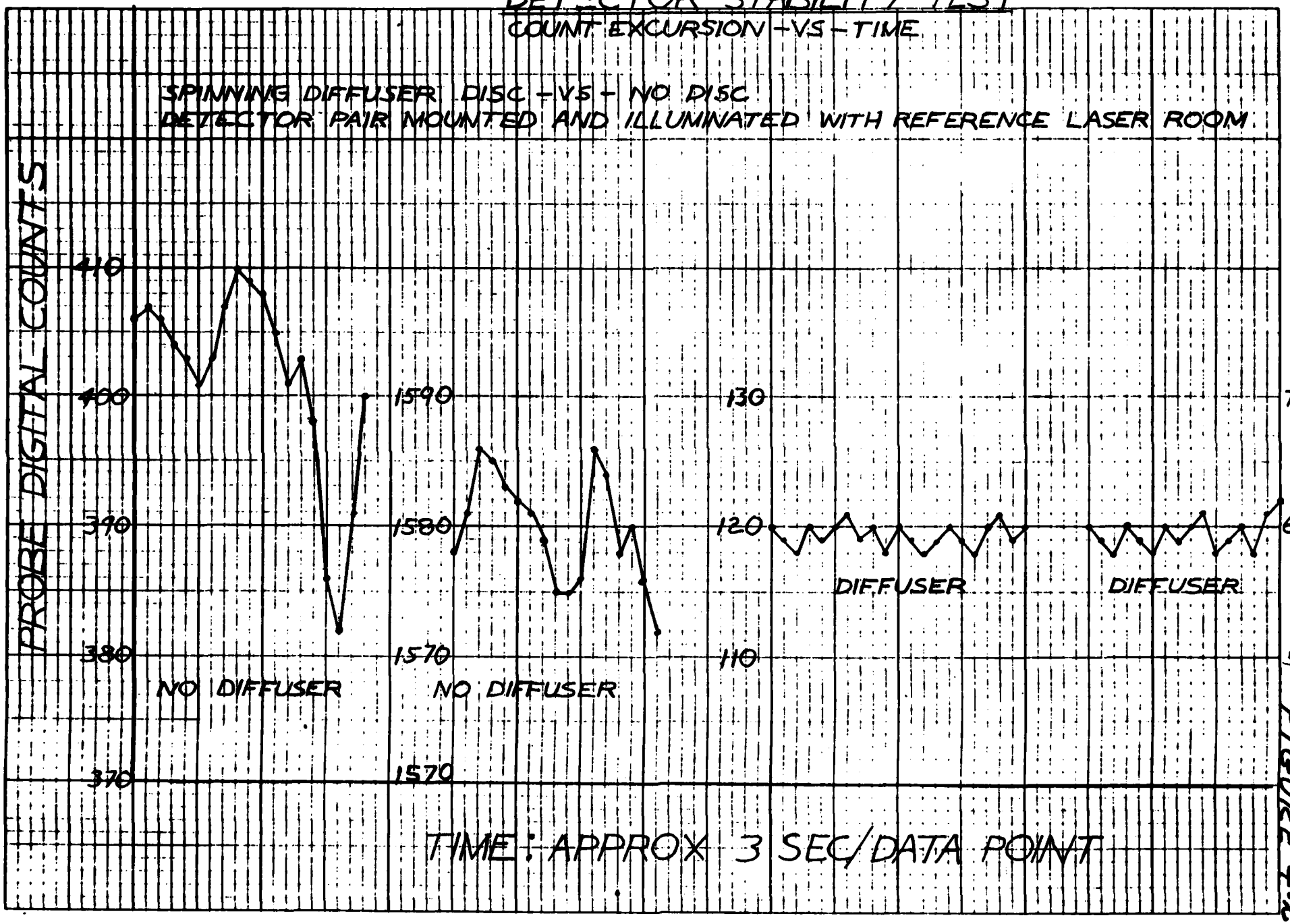
DETECTOR STABILITY TEST
COUNT EXCURSION +VS- TIME
SPINNING DIFFUSER DISC +VS+ NO DISC
DETECTOR PAIR MOUNTED AND ILLUMINATED WITH REFERENCE LASER ROOM
PROBE DIGITAL COUNTS
410
400
390
380
370
1590
1580
1570
1570
130
120
110
70
60
50
NO DIFFUSER
NO DIFFUSER
DIFFUSER
DIFFUSER
TIME: APPROX 3 SEC/DATA POINT

FIGURE 4.24

cated from available components caused problems of its own. The D.C. drive motor produced vibration and speed control was bad. It was determined by test that varying the speed of the disc caused a change in the probe count. The other dilemma was the diffusion characteristics of the trusite glass. While it permitted sufficient light transmission, it did not provide the desired amount of diffusion.

The spinning disc diffuser described above was located at the plane of the laser pinhole aperture shown in Figure 3.11 of Section 3.6.1. It replaced the pinhole and formed the light source object of the optical system. In spite of the poor implementation of the spinning disc diffuser, it was evident that it helped to reduce the sinusoidal count excursion.

A probe repeatability test was conducted using the above described spinning disc diffuser. The SELFOC rod focussed the laser beam onto a specular surface block mounted on the x-y interferometer table. With each cycle, the stage was displaced some arbitrary distance and returned until the optical probe nulled-out. The interferometer count was then recorded. The tabulated data below gives the results of three repeatability test series.

a. Repeatability at prove null (Series 1)

Probe Counts	Interferometer Reading (μinches)
+ 3 to + 2	0
+ 3 to - 2	+ 78
+ 1 to - 1	+ 53
+ 3 to - 3	+ 51
+ 4 to 0	+ 27
+ 2 to - 2	+ 84

b. Repeatability at probe null. Probe counts not recorded.

Cycle	Interferometer Reading (μinches)	
	Series 2	Series 3
1	0	0
2	+ 27	+ 28
3	+ 57	+ 50
4	- 4	+ 34
5	+ 39	+ 71
6		+ 82
7		+ 81
8		+ 73

Test series 1, 2 and 3 with the optic probe can be compared with the contact probe repeatability test data of Figures 4.14 to 4.16 in Section 4.3. While there is some thermal drift due to effects described in Section 4.3, the excursions tabulated are principally due to the optic probe. It represents the contribution from floor and disc motor vibration, spatial variation in energy distribution of the laser beam and electronic drift at the marginal signal levels associated with the numerical aperture of the SELFOC rod. Including drift, the repeatability over the test series is about ± 42 microinches. It is about ± 30 microinches without the electronic drift. Thus, the present probe repeatability is not much greater than the design goal repeatability of ± 10 microinches. Since the causes of the instability have been identified and solutions devised, attainment of the desired goal is feasible.

4.6.4 Surface Scan Sensitivity

In addition to sensing "size," the noncontact optic probe is required to operate in the "Surface Profile" mode in order to detect surface pits having diameters around 0.001 inches.

Surface scan tests reveal that the probe is now oversensitive to surface defects, i.e., the output signal indicates surface profile magnitude greater than absolute. This

phenomenon is associated with the uniform phase nature of the coherent laser light source. A laser source was chosen because of its intensity combined with low heat dissipation. However, the coherent aspect of the laser presents some unwanted "speckle" effects. The use of a spinning disc with adequate diffusion quality will produce a laser light with random (time average) phase wavefronts. Over finite sampling intervals the time averaged effect will be similar to using an incoherent light source.

Increasing the diameter of the laser spot would also help to desensitize the response to surface defects. At present, the spot diameter is 0.001 inches when in focus on the gear surface. This could be increased to, say, 0.003 inches and still allow detection of one mil surface pits.

Another alternative to the spinning diffuser and laser illumination is to use a bright incoherent source such as a mercury arc. With a mercury arc source, no spinning diffuser would be needed, but attention must be given to selecting the most efficient light coupling optics, i.e., using the highest practical numerical aperture in the final relay optics and then making sure that all other condenser and relay elements at least match or overfill. Experimental results indicate that a 100 watt Hg arc could provide light levels of 10^{-7} watt at the out-of-focus pinhole/detector elements.

4.6.5 Electronic Signal Drift/Dynamic Range

During the course of testing, difficulties were experienced in maintaining or reproducing a particular performance level achieved by optical alignment methods. Also, one or the other of the detectors would change signal strength or apparently go dead. It was later determined that, under conditions of high light levels, the photodiode detectors exceeded the saturation level of the preamp or the gain amplifier. In the breadboard, the problem was overcome by monitoring the amplifier output as a check that the output signal did not exceed the 15 volt supply limit. In the final system, this problem can be handled by incorporating a variable N.D. filter wheel which can be set from the control panel to accommodate the range of diffuse to specular surface reflectivities. Additionally, the control panel should include meters for indicating the

signal level of each detector. When operating the machine by joystick control, this will inform the operator that the probe is positioned in the operating range and that the reflected light from the gear surface is within the dynamic range of the electronics. In the automated mode, this would all be handled in software.

At low signal levels, typically associated with diffuse surfaces and the limiting N.A. of the SELFOC rod, it has been observed that the signal-to-noise ratio is such that larger count excursions occur along with a unidirectional drift of the probe count. This problem can be helped by scaling up the probe spot size and detector pinhole size.

The PHASE II AGTCMD will be pneumatically vibration isolated and this will permit elimination of the final 5 Hz output filter discussed in Section 3.6.2. This will aid in improving stability and will allow sampling at higher rates.

As was mentioned earlier, the problem relating to coherence of the laser light is solved by using a spinning disc diffuser. The electronics can be designed to optimize the effectiveness of this device. Specifically, it is desired that the random signal modulation on the 800 Hz carrier be smoothed relative to the disc spin frequency.

The basic electronic circuit, as now configured, gives the needed flexibility for optimization relative to final selection of optical parameters such as pinhole sizes, pinhole focus offset and illumination levels.

4.6.6 Phase II Implementation

The experimental testing with the breadboard noncontact optic probe has identified numerous performance problems, but has also provided the means for devising solutions to the problems uncovered. In accordance with the discussions of the preceding subsections, the following is a summary of the tasks envisioned for final development of the operational noncontact optic probe.

a. Convert the coherent laser light to an incoherent light source by designing and fabricating a spinning disc diffuser. The diffuser must be driven by a low vibration, constant speed motor. The diffusion characteristics of the disc must be optimized to system parameters. Since the disc plane is the light source object of the imaging system, the axial runout of the disc must be small.

The addition of this diffuser device will correct for the count excursions resulting from spatial variations in the laser spot and provide the random phasing needed to desensitize surface reflectivity effects. Attentive mechanical design of the spinning disc mechanism will eliminate the probe count noise that was contributed by vibration, speed variation and axial runout.

b. Select a relay lens which has a smaller depth of focus to improve upon the axial positioning accuracy of the detector pinholes. In combination with this, design and fabricate an axial and radial pinhole locating mechanism that facilitates the adjustment process. These features will aid in the optical alignment that determines the sensitivity, linearity and symmetry of the probe output signal.

c. Mount the machine on a pneumatically vibration isolated table. This will eliminate the count excursion contribution from building vibration.

d. In parallel with the SELFOC rod probe implementation, design and fabricate alternate probes. A set of microlenses fitted to a stepped diameter hollow tube is one such design that looks promising.

e. Add a variable N.D. filter wheel which can be set to accommodate the range of reflectivities for specular to diffuse surfaces.

f. Design the probe electronics for optimization with final optical parameters and for improved drift stability.

g. Add detector signal meters to the control panel for joystick operation of the AGTCMD. These will inform the operator of probe signal acquisition, probe sensing range and dynamic range of the system.

5. CONCLUSIONS

The Phase I development of the AGTCMD demonstrated the feasibility of meeting the mensuration accuracy goals of the AGTCMD in the final automated version. The test data for the two major developmental elements of the program showed an advancement in the state-of-the-art. The coordinate measuring machine measured to absolute accuracies well below 10 microinches and the noncontact probe showed resolutions of 1 to 4 microinches with repeatability of ± 30 microinches.

5.1 COORDINATE MEASURING MACHINE

Operating the machine manually with a one microinch resolution contact probe in combination with the interferometer set at a resolution of 3 microinches, resulted in the following system performance:

a. Absolute accuracy measurement of a 1.109" (+ 8, - 4 microinch) gauge block was within 6 microinches of the basic size in an uncontrolled environment at a temperature 12° F higher than the reference temperature.

b. System repeatability, under the influence of changing environmental conditions, was shown to be within ± 3 microinches for 8 measurements of a 1.109 inch gauge block taken over the span of a work day.

c. The machine appears to be insensitive to vibration levels associated with quiet, ground level floor mounting.

d. Given insufficient consideration, thermal effects can cause large errors, particularly for measurement cycles of long duration. Conductive and radiated heat transfer from human body heat have a significant effect on mensuration accuracy. To minimize this error source, the Phase II machine will be remotely operated from a control console. Unidirectional room air temperature change also causes significant errors for long duration measurements. It is noted that the measurement made for items (a) and (b) above were of about 2 minute duration and this interval was not long enough to result in significant thermal errors, even under the influence of body heat and changing air temperature. Operating the machine in the fluid-filled mode greatly

improved the thermal stability. This, in combination with a controlled environment, showed that measuring cycle times greater than one hour can be done without incurring significant thermal errors.

e. The stabilization jacks were not needed for the test conducted. However, their use would be beneficial when inspecting large, heavy parts.

5.2 NONCONTACT OPTIC PROBE

The breadboard was tested both with and without the SELFOC rod. Compared to currently available optic probes having resolutions of 75 to 100 microinches, the AGTCMD probe showed resolutions of 1 to 4 microinches. Regarding repeatability, available optic probes range between ± 150 to ± 200 microinches. Here, the AGTCMD probe showed repeatabilities of about ± 30 microinches but with electronic count drift when the SELFOC rod is used.

While the repeatability/stability goal of ± 10 microinches was not demonstrated in Phase I, the causes of the instability were identified and solutions devised. The implementation of these solutions are detailed in Section 4.6.6. They involve converting the present coherent light source to an incoherent light source, either by a spinning disc diffuser or using a mercury arc source. Optimizing the relay lens optics, detector pinhole size, spot size, mount adjustment mechanisms and processing electronics.

Additions required for Phase II are:

a. Control panel mounted meters indicating detector signal level and range for machine operation by joystick.

b. Pneumatically vibration isolated machine mount. This is needed to reduce the vibration of the 0.058 inch diameter x 3-1/4 inch long probe. As mentioned in the previous section, it is not needed when a rigid probe configuration is used.

c. An N.D. filter wheel settable from the control panel for the purpose of maintaining the detector signal level within the dynamic range of the processing electronics.

6. RECOMMENDATIONS

The development work accomplished in Phase I has produced a "building block" of a coordinate measuring machine and a breadboard model of a noncontacting optic probe.

With only minor modifications, the CMM can be expanded into the final AGTCMD. Since the machine performance was shown to exceed the requirements, the balance of the work in this area could be categorized as routine development.

On the other hand, the breadboard of the noncontacting optic probe served the function traditionally associated with the "breadboard" classification. It provided the vehicle for identifying problems, for investigating solution to the problems and for compilation of test data that lends a margin of comfort to the feasibility of meeting the program objectives. Based on the knowledge acquired in Phase I work, implementation of the tasks needed to provide a reliable, operational noncontact probe should proceed under a Phase II effort.

The performance level reported herein, for both the CMM and the noncontacting optic probe, signifies an important contribution to the field of metrology. The optic probe, in particular, is not application limited to measurement of the size and surface quality of spur gears. It offers the benefits of noncontacting means for general parts inspection with the accuracy and multiaxes/directional probing versatility only now obtainable with the electronic contacting probes.

APPENDIX A

ARI GEAR MOUNTING CONCEPT (PRELIMINARY)